Observational studies on long-period geomagnetic pulsations(Dissertation_全文)

AUTHOR(S):

Nose, Masahito

学位申請論文

能勢 正仁

主論文

Observational Studies on Long-period Geomagnetic Pulsations

Masahito Nosé

Dissertation for the Degree of Doctor of Science

Department of Geophysics, Graduate School of Science
Kyoto University

December 1997

Table of Contents

Table of Contents i

Abstract iii

1 General introduction 1
1.1 Geomagnetic pulsation 1
1.2 Outline of this thesis 2

2 Electron precipitation accompanying Pc 5 pulsations observed by the DE satellites and at a ground station 3
2.1 Introduction 3
2.2 Data 4
2.3 Observation and Analysis 4
2.3.1 Geomagnetic conjunction events of DE-1 and -2 . 4
2.3.2 Statistical analysis of Pc 5 and CNA observed at Syowa 6
2.3.3 Geomagnetic conjunction events of DE-2 and Syowa 7
2.4 Discussion 7
2.4.1 Electron acceleration mechanism 7
2.4.2 MLT distribution of Pc 5 and CNA pulsation occurrence 10
2.4.3 Magnetic field variations observed on the ground 10
2.5 Conclusions 10

3 ULF pulsations observed by the ETS-VI satellite: Substorm associated azimuthal Pc 4 pulsations on the nightside 12
3.1 Introduction 12
3.2 Experiment and Data Analysis 13
3.2.1 The satellite and magnetometer 13
3.2.2 Data coverage 13
3.2.3 Preparation of pulsation list 14
3.3 Statistical Results 14
3.3.1 Azimuthal Pc 5 pulsation 14
3.3.2 Azimuthal Pc 3 pulsation 15
3.3.3 Radial Pc 4 pulsation on the dayside 15
3.3.4 Azimuthal Pc 4 pulsation on the nightside 16
3.4 Discussion 16
3.4.1 Azimuthal Pc 5 pulsation 16
3.4.2 Azimuthal Pc 3 pulsation 17
3.4.3 Radial Pc 4 pulsation on the dayside 17
3.4.4 Azimuthal Pc 4 pulsation on the nightside 18
3.5 Conclusions 22

4 Dayside Pi 2 pulsations observed at low-latitude ground station 23
4.1 Introduction 23
4.2 Analysis 24
4.2.1 Preparation of Pi 2 list 24
4.2.2 Observational results 25
4.3 Discussion 26
4.4 Conclusions 27

A Automated detection of Pi 2 pulsations using wavelet analysis for substorm monitoring 28
A.1 Introduction 28
A.2 Application for Nowcasting of Substorm Onsets 28
A.3 Orthonormal Wavelet Analysis 28
A.3.1 Basics 28
A.3.2 Meyer wavelet 29
A.4 Detection of Pi 2 Pulsations by Wavelet Analysis 30
A.4.1 Example of wavelet analysis 30
A.4.2 Algorithm for Pi 2 detection 30
A.5 Operation at Mineyama Observatory 32
A.5.1 Pi 2 detection system 32
A.5.2 Detection results 32
A.6 Conclusions 33

Acknowledgments 34

References 35

Figure and Plate captions 40

Abstract

Long-period geomagnetic pulsations and associated effects on particles are studied by using data from satellites and ground stations. In chapter 2 of this thesis, we investigated interactions between Pc 5 pulsations and electrons, using data from a ground-based station and the polar orbiting Dynamic Explorer (DE) -1 and -2 satellites. DE-2 observed sinusoidal disturbances in the magnetic and electric fields in the upper ionosphere at the geomagnetic footprint of the high altitude region in which transverse Pc 5 pulsations were detected by DE-1. DE-2 observed electrons precipitating into the ionosphere with energies of several tens of keV These electrons were accelerated in the direction of the ambient magnetic field. When Pc 5 pulsations in the H-component and CNA pulsations were observed at Syowa Station, DE-2 which was in geomagnetic conjunction with Syowa Station also observed sinusoidal disturbances in the magnetic and electric fields. These sinusoidal disturbances are caused by small scale field-aligned currents each with width of 0.5°–1.4° invariant latitude. This suggests that Pc 5 pulsations have a small scale resonance structure in the radial direction. The resonance structure has a scale small enough to allow the finite ion gyroradius effects to play a role, then kinetic Alfvén waves having electric fields parallel to the ambient magnetic field can arise. Electrons accelerated by these kinetic Alfvén waves would cause CNA pulsations, the phase of which leads that of the H-component of the Pc 5 pulsations by 90° in the southern hemisphere. In chapter 3, the magnetic field data from the Engineering Test Satellite -VI (ETS-VI) have been analyzed to investigate the occurrence distributions of pulsations in Pc 3–5 frequency ranges in the magnetosphere. The observation of ETS-VI covered the invariant latitude (ILAT) range of 64.5°–69°ILAT near the geomagnetic equator (−10°–20° magnetic latitude) at all magnetic local time (MLT). From the occurrence distribution, we have found that azimuthal Pc 4 pulsations are observed frequently in the MLT range of 23–04MLT with an occurrence peak at 01–02MLT. They have continuous waveforms lasting for about 10 minutes. Although the azimuthal Pc 4 pulsations on the nightside start at almost the same time as substorm onsets, they are different from Pi 2 pulsations in the magnetosphere. We suggest that the azimuthal Pc 4 pulsations on the nightside are excited through coupling to the fast mode Alfvén waves which were launched at substorm onset. In chapter 4, we investigated statistical characteristics of dayside Pi 2 pulsations observed at Mineyama (25.5° geomagnetic latitude) from November 1994 through June 1996. We obtained the following results. (1) The ratio of the number of Pi 2 pulsations on the dayside (06–18MLT) to that on the nightside (18–06MLT) was about 31%. (2) The polarization of the dayside Pi 2 pulsations changed from right-handed before local noon to left-handed after local noon. (3) Wave power of dayside Pi 2 pulsations in the H-component has a peak around local noon and dips on both dawn and dusk sides. From these observational results, we proposed an excitation model of dayside Pi 2 pulsations, in which the H-component is ascribed to the cavity mode waves and the D-component is due to the westward propagating waves with $|m|\sim 2$.

Chapter 1

General introduction

1.1 Geomagnetic pulsation

Geomagnetic pulsations are oscillations of the earth's magnetic field with frequency lower than the local ion cyclotron frequency, that is, magnetohydrodyanmic (MHD) waves in the magnetosphere. The periods of geomagnetic pulsations range roughly from 10^{-1} to 10^{3} seconds. The amplitudes measured on the ground can range from 10^{-2}~10^{-1} nT for the short period events to about 100 nT for the long period events [*Jacobs*, 1970; *Orr*, 1973]. The notation and classification of geomagnetic pulsations were considered in some detail by the International Association of Geomagnetism and Aeronomy (IAGA) at the meeting held in Berkeley, California, 1963. Table 1.1 shows the notation and classification proposed by IAGA [*Jacobs et al.*, 1964]. Geomagnetic pulsations are divided into two main classes: those with regular and continuous waveforms which are denoted as Pc, and those with impulsive and irregular waveforms which are denoted as Pi. The first class (Pc) is further divided into five subclasses depending on the predominant period of pulsations. The second main class (Pi) consists of two subclasses covering the period ranges shown in Table 1.1. In addition to the classification above, IAGA decided to settle two new classes of pulsations in 1973; Pc 6 having a sinusoidal waveform with period longer than 600 seconds and Pi 3 having an irregular waveform with period longer than 150 seconds [*Saito*, 1978].

In terms of energy for excitation of geomagnetic pulsations, we can divide them into two main groups, although the energy is ultimately supplied by the solar wind, of course. The pulsations in the first group are excited by magnetospheric particles through a local wave-particle instability, such as Pc 1, giant pulsation (Pg) in the Pc 4 frequency band, poloidal Pc 4, and compressional Pc 5. These pulsations reflects states of particles in the magnetosphere. Pc 1 pulsations are thought to be excited by ion-cyclotron instability near the equatorial plane of the magnetosphere [*Cornwall*, 1966]. Excitation mechanism for Pg's is not still revealed, but they are estimated to be excited by internal excitation mechanism because they have large azimuthal wave number and preference of occurrence around L=6 [*Takahashi*, 1991; *Takahashi*, 1994]. Poloidal Pc 4 pulsations are thought to be driven by bounce resonance with energetic ions [e.g., *Anderson*, 1994]. Compressional Pc 5 pulsations are generated by drift mirror instability, which is driven by the pressure anisotropy of the ions [e.g., *Anderson*, 1994; *Takahashi*, 1996]. The second group consists of pulsations due to waves propagating into the magnetosphere which are produced at bow shock or magnetopause or magnetotail, such as compressional Pc 3, toroidal harmonic waves in the Pc 3-4 frequency band, toroidal Pc 5, and Pi 2. These kinds of pulsations have information of the dynamics and morphology of the magnetosphere. Compressional Pc 3 pulsations and toroidal harmonic waves show a strong dayside occurrence. Compressional Pc 3 pulsations are likely to be the results of transmitting of magnetospheric upstream waves into the magnetosphere, which are excited by the reflected ion beams in the earth's foreshock. Toroidal harmonic waves in the Pc 3-4 frequency band are excited by coupling to the compressional Pc 3 [*Yumoto*, 1986; *Anderson*, 1994]. This excitation mechanism is called field line resonance model [*Southwood*, 1974; *Chen and Hasegawa*, 1974], which was originally proposed to explain the occurrence of toroidal Pc 5 pulsations. The source of energy for excitation of toroidal Pc 5 pulsations are considered to be the Kelvin-Helmholtz instability on the magnetopause [e.g., *Kokubun et al.*, 1989]. Pi 2 pulsations are thought to be fed their energy by waves launched at substorm onset, but there are a

couple of proposed models for the generation and propagation mechanisms [*Yeoman and Orr*, 1989].

1.2 Outline of this thesis

This thesis mainly focuses on long-period pulsations classified in the second group (*i.e.*, pulsations excited by waves propagating into the magnetosphere), including associated effects on particles. We studied the following three phenomena. The brief descriptions of the research background and main results of our studies are also shown.

1. Electron precipitation accompanying transverse Pc 5 pulsations. There have been a number of observational and theoretical studies on modulation of particle flux by Pc 5 pulsations. Few studies, however, have shown observational results of electron precipitation associated with transverse Pc 5 pulsations. We investigated interactions between transverse Pc 5 pulsations and electrons, using data from a ground-based station and the polar orbiting Dynamic Explorer (DE) -1 and -2 satellites. The resonance structure of transverse Pc 5 pulsations was found to have a scale small enough to allow the finite ion gyroradius effects to play a role. This leads rise of kinetic Alfvén waves having electric fields parallel to the ambient magnetic field. We concluded that electrons are accelerated by the kinetic Alfvén waves in the parallel to the ambient magnetic field.

2. Substorm associated azimuthal Pc 4 pulsations on the nightside. There were few works which dealt with continuous pulsations on the nightside in Pc 4 frequency band accompanying substorm onsets, except for *Takahashi et al.* [1996] and *Saka et al.* [1996a, b]. *Takahashi et al.* [1996] proposed a change in magnetospheric convection during substorms for energy sources for this kind of pulsation. *Saka et al.* [1996a, b] presented a model in which plasma pressure generated in the nightside magnetosphere in association with energetic particle injections acts as an in situ sources of the pulsations. We investigated in detail the substorm associated azimuthal Pc 4 pulsations on the nightside, using data from the Engineering Test Satellite -VI (ETS-VI). We proposed an excitation mechanism that the azimuthal Pc 4 pulsations on the nightside are excited through coupling to the fast mode Alfvén waves launched at substorm onsets, which is different from the mechanisms by *Takahashi et al.* [1996] and *Saka et al.* [1996a, b].

3. Dayside Pi 2 pulsations at low-latitude. Previous studies have investigated dayside Pi 2 pulsations mostly from a viewpoint of simultaneous occurrence with nightside Pi 2 pulsations [*Yumoto*, 1986]. We studied statistical characteristics of dayside Pi 2 pulsations at low-latitude, and obtained some new results such as MLT dependence of wave power or phase difference between H- and D-components. We proposed an excitation model of dayside Pi 2 pulsations in which the H-component is ascribed to the cavity mode waves and the D-component is due to westward propagating waves with azimuthal wave number of about 2.

We organized this thesis as follows. Chapter 2 describes our study on electron precipitation accompanying transverse Pc 5 pulsations. Chapter 3 provided analysis of substorm associated azimuthal Pc 4 pulsations, including simple analyses and discussion for other kinds of long-period pulsations. Chapter 4 describes statistical analysis of dayside Pi 2 pulsations. Appendix A introduces an automated detection method of Pi 2 pulsations for nowcasting of substorm onsets, which was applied for Pi 2 pulsation study in Chapter 4.

Chapter 2

Electron precipitation accompanying Pc 5 pulsations observed by the DE satellites and at a ground station

2.1 Introduction

A number of observational studies have been made on the interactions between ULF waves and particles. There are some theoretical studies to explain the ULF wave-particle interaction mechanisms. Modulations of particle flux by Pc 5 pulsations have been investigated by many authors.

Kokubun et al. [1977] found flux modulations of energetic electrons and protons associated with transverse Pc 5 pulsations from Ogo 5 observations. They concluded that these modulations stem from the drift resonance, which is a special case of the drift-bounce resonance [*Southwood et al.*, 1969; *Southwood and Kivelson*, 1982]. *Cladis and Lennartson* [1986] explained that the rapid loss of the westward drifting ions in the ring current observed by ISEE-1 was through a bounce resonance interaction of the ions with the standing Alfvén waves. *Li et al.* [1993] studied analytically and numerically a loss mechanism for the ring current O^+ ions due to the combined effects of convection and corotation electric fields and interactions with radially polarized Pc 5 waves through a drift-bounce resonance.

Paquette et al. [1994] reported geomagnetic pulsations with long periods (100–1000 seconds) accompanied by pulsations in particle precipitation observed at South Pole Station. They found elevated levels of VLF activity and VLF modulation at pulsation frequency in some events, in which variations in particle precipitation begin several hundred seconds in advance of ULF pulsations. This observation suggests that magnetic pulsations indirectly cause precipitation pulsations by modulating VLF wave-particle interactions in the vicinity of the magnetic equator; this mechanism was presented theoretically by *Coroniti and Kennel* [1970]. *Sato et al.* [1985] examined quasi-periodic variations in cosmic radio noise absorption (CNA pulsation) with periods of 10–500 seconds obtained at Syowa Station. They found that CNA pulsations were accompanied by magnetic pulsations and quasi-periodic VLF emissions and concluded that the wave-particle interaction occurred near the equatorial plane in the outer magnetosphere. CNA pulsations and Pc 3–5 geomagnetic pulsations observed at Syowa Station and its three conjugate stations in Iceland were studied by *Higuchi et al.* [1988]. In order to explain the relative phase difference between the Pc 3–5 pulsations and CNA pulsations, they estimated the propagation time of hydromagnetic waves from the equatorial plane to the ground and concluded that particle modulation by hydromagnetic waves occurs near the equatorial region in the magnetosphere.

A prominent feature of the kinetic Alfvén wave, which is an Alfvén wave with a perpendicular wavelength comparable to the ion gyroradius, is that it has an electric field parallel to magnetic field lines [*Hasegawa*, 1976; *Goertz*, 1984]. *Hasegawa* [1976] suggested that the electrons which cause discrete auroral arcs are accelerated by kinetic Alfvén waves to energies of a few keV This acceleration mechanism can also explain the latitudinal scale size of auroral curtains. Recently, *Wei et al.* [1994] showed by a simulation study that the electron inertial Alfvén wave causes field-aligned potential drops of several kilovolts. They found that mode conversion to inertial Alfvén waves becomes important when the width

of the field line resonance narrows to about six electron inertia lengths.

The aim of this chapter is to identify the interaction mechanism between Pc 5 pulsations and electrons. Using data from satellites and a ground-based station, we investigated possible wave-particle interaction mechanisms.

2.2 Data

The Dynamic Explorer (DE) -1 and DE-2 satellites were launched together into polar orbits on August 1981. DE-1 had an orbit with apogee at 4.6 R_E geocentric distance and period of about 7 hours. The orbit of DE-2 initially had apogee at 1003 km and perigee at 299 km altitude, and period of about 1.5 hours [*Hoffman and Schmerling*, 1981]. The data used here are the magnetic field data obtained by the triaxial fluxgate magnetometer (MAGA) on board the DE-1 satellite [*Farthing et al.*, 1981]. Though the sampling rate was originally 16 vectors per second, we used the data averaged over spin period (6 seconds). Only the data obtained near apogee (where the magnitude of the main field is less than 1000 nT) were used to select transverse Pc 5 pulsations. We also used the data from the triaxial fluxgate magnetometer (MAGB) [*Farthing et al.*, 1981] and those from the vector electric field instrument (VEFI) [*Maynard et al.*, 1981] on board DE-2. The 0.5 second average data were used here, though the original data were recorded at the rate of 16 samples in each second. VEFI was designed for three axis measurements, but the z-axis antenna in the spacecraft coordinate (SPC) system did not deploy; so only two components of the electric field in the orbital plane were measured. Data obtained by the low-altitude particle instrument (LAPI) [*Winningham et al.*, 1981] on DE-2 were analyzed to investigate the relation between transverse Pc 5 pulsations and electron precipitations. Measurements of electrons from 5 eV to 32 keV in energy and from 0° to 180° in pitch angle were made by LAPI. The pitch angle 0° is defined as downward along the magnetic field, and 180° as upward apart from the direction of geomagnetic field.

Ground observations of geomagnetic field by a triaxial fluxgate magnetometer and cosmic radio noise by a riometer at 30 MHz with a sampling rate of 2 seconds have been carried out at Syowa Station (−70.0° geomagnetic latitude, 79.4° geomagnetic longitude) [*Kuratani and Igarashi*, 1984; *Fujii et al.*, 1985]. We used the H-component geomagnetic field data to investigate Pc 5 pulsations observed on the ground. The riometer data were utilized to find CNA pulsations which accompany geomagnetic pulsations.

Data from DE-1 and -2 are available for the period from August 1981 to February 1991 and the period from August 1981 to February 1983, respectively. However, the period in which the geomagnetic conjunction events of DE-1 and -2 were selected is from August to November 1982, because in this period DE-1 passed through the magnetic local time (MLT) region where Pc 5 events were observed frequently [see *Nosé et al.*, 1995, Figure 1]. The period of the data used here from Syowa Station is from April 1981 to February 1983.

2.3 Observation and Analysis

2.3.1 Geomagnetic conjunction events of DE-1 and -2

During the period from August to November 1982, we found several cases of geomagnetic conjunctions of DE-1 and -2 in which transverse Pc 5 pulsations were observed by DE-1. From visual inspection we identified Pc 5 pulsations which are dominant in the perpendicular magnetic field components, that is, transverse Pc 5 pulsations. The criteria for selection of conjunction events were as follows. (1) Invariant latitude (ILAT) ranges for observations by DE-1 and -2 are almost the same. (2) The difference between the magnetic local times (MLT) at the locations of DE-1 and -2 is less than one hour. (3) The time interval for observation by DE-2 is contained in the time interval during which DE-1 observed Pc 5 pulsation.

The DE-1 satellite observed fluctuations of the geomagnetic field on 20 October 1982 (DAY82293) as shown in Figure 2.1, where the data are plotted in the local magnetic coordinate (LMG) system. The top

panel ($\Delta B_{\parallel}$) shows variations in the tangential direction to the model magnetic field. The second and third panels show $\Delta B_{\perp 1}$ and $\Delta B_{\perp 2}$ components of variations in the magnetic field, respectively. The $\Delta B_{\perp 1}$ component is perpendicular to the model magnetic field and directed radially outward. The $\Delta B_{\perp 2}$ component is azimuthally eastward. These fluctuations are thought as temporal variations because DE-1 moved slowly near its apogee. The amplitude of fluctuations in the $\Delta B_{\perp 2}$ component is about three times as large as that in the $\Delta B_{\perp 1}$ component, and there are no clear fluctuations in the $\Delta B_{\parallel}$ component. The peak-to-peak amplitude has the largest value of 32 nT in the $\Delta B_{\perp 2}$ component at 0120UT. The period of fluctuations is approximately 5 minutes around 0100UT and decrease to 3 minutes near 0120UT. The fluctuations appeared in the ILAT range from 71.1° to 66.1° (*i.e.*, from 0053 to 0132UT) indicated by broken lines in Figure 2.1. We interpret this observation that DE-1 slowly passed the ILAT range in which transverse Pc 5 pulsation took place. This interpretation is consistent with the observation that the period of pulsation decreased as DE-1 moved to lower latitude.

Figure 2.2 shows the MAGB and VEFI data from DE-2 for this conjunction event. The top three panels in Figure 2.2 are the magnetic field perturbation in the SPC system, where the x-axis is in the direction of the satellite velocity and the y-axis is upward, with the z-axis completing a right-handed coordinate system. The lower two panels show the x- and y-components of the electric field data. The paths of DE-1 and -2 in the MLT-ILAT plane are indicated in Figure 2.3. This figure shows that DE-2 made an observation at the footprint of the region in which the transverse Pc 5 pulsation appeared. From Figure 2.2 we notice that there are sinusoidal disturbances in ΔB_z and E_x with an amplitude of 30–50 nT and 5–12 mV/m, respectively, in the ILAT range between two broken lines (66.1°–71.1°ILAT) where the transverse Pc 5 pulsation were observed by DE-1. There are no clear disturbances in the other components of the magnetic and electric fields within this range of latitude. The disturbances in ΔB_z and E_x have a good correlation. The correlation coefficient for the disturbances with spatial scales of 40–160 km was 0.92. Two general interpretations of these correlated disturbances are; (1) due to static structures in field-aligned currents [*Sugiura*, 1984] and (2) due to Alfvén waves [*Gurnett et al.*, 1984]. These interpretations are tested by the method of comparing the ΔB_z to E_x ratio with the height-integrated Pedersen conductivity or the inverse of Alfvén wave velocity. The observation by DE-2 in Figure 2.2 was interpreted as a spatial variation of pulsation at a specific phase of oscillation because the time interval in which DE-2 observed the disturbance was much shorter than the period of Pc 5 pulsation. The ΔB_z to E_x ratio calculated from the observation corresponds to 3–4 S, which is consistent with the value of the height-integrated Pedersen conductivity from the IRI90 model [*Bilitza*, 1990]. From the point of view discussed above, it seems reasonable to conclude that the sinusoidal disturbances in ΔB_z and E_x are caused by small scale field-aligned currents which have a latitudinal structure as shown in Figure 2.4. The small scale current system is expected to be rather uniform longitudinally, because ΔB_x has no clear disturbances. We see at least four pairs of small scale field-aligned currents each with latitudinal width of 0.7°–0.8°ILAT (84–96 km) in the observation by DE-2. The current density of this field-aligned current is estimated to be about 0.6–1.0 μA/m^2

Figure 2.5a gives the x-component of the electric field data in the same format as those in Figure 2.2 to be used in the comparison with the electron flux data. The LAPI electron data are shown in Figures 2.5b–2.5g. Figures 2.5b–2.5d and Figures 2.5e–2.5g give energy spectra of electron flux for two different pitch angles and pitch angle distributions of electron flux for four energies, respectively. Each pair of (b, e), (c, f) and (d, g) corresponds to the observation at one of the three epochs indicated by the arrows in Figure 2.5a. The electric field has northward peaks at 0108:47 and 0109:02UT, and a southward peak at 0108:53UT as shown by the arrows in Figure 2.5a. In Figures 2.5b and 2.5d (0108:46.73 and 0109:01.61UT), downward electron flux enhancements can be seen in the energy range from several keV to 27 keV We see in this energy range that electron flux with small pitch angle (4.8°–8.7°) is larger than or same as that with large pitch angle (42.3°–46.2°) except for the electron flux of 8.6 keV in Figure 2.5d. Pitch angle distributions in Figures 2.5e and 2.5g show an enhancement of electron flux with pitch angles less than 90° In Figure 2.5c (0108:53.11UT), however, there are no clear flux enhancement in high energy range (around a few keV), and electron flux with small pitch angle is less than or same as that with large pitch angle. Electron flux enhancement with small pitch angles cannot be seen in Figure 2.5f. It is also noted that the electron flux shown in Figure 2.5f are smaller than those in Figures 2.5e and 2.5g. These observational facts show that the electrons are accelerated to energies of several tens of keV in

the direction of the ambient magnetic field in the regions where the electric field has a northward peak. The accelerated electrons precipitate into the ionosphere at the height of 100 km, because the loss cone angle at the altitude of DE-2 (420 km) is about 68°

The ground data obtained at 6 stations in Table 2.1 were also utilized. These 6 stations have the values of ILAT which are contained in or close to the ILAT range of DE observations. Pc 5 and CNA pulsations were observed by a ground station (FYU), which is located in the same ILAT range as that of the DE-1 and -2 observations, 6 hours before DE-1 observed Pc 5 pulsation (Figure 2.6). A Pc 5 pulsation with a period of about 4 minutes are accompanied by a CNA pulsation which had the same period. These pulsations appeared around 08MLT. The top two panels of Figure 2.7 show Pc 5 and CNA pulsations observed at Syowa Station 6 hours after the observation by DE-1. The ILAT of Syowa Station (66.2°) was within the ILAT range of DE-1 and -2 observations of the transverse Pc 5 pulsation. The MLT range in which these pulsations appeared is 08–09MLT. The periods of both Pc 5 and CNA pulsations are about 4 minutes, and the Pc 5 pulsation lags behind the CNA pulsation by a phase difference of approximate 90° The amplitude of the Pc 5 pulsation is about 60–100 nT having a wave packet structure. There are no fluctuations in the ELF-VLF waves at 750 Hz and 1.2kHz with the same period as Pc 5 and CNA pulsations. In these frequency bands, electrons can interact with ELF-VLF waves. Other 4 stations (TIK, CCS, DIK, and TRO) observed Pc 5 pulsations clearly when they were in the MLT range of 08–09 hours (although not shown here). Since the value of the Kp index was high (Kp=3–4) during the time interval between the observations at Fort Yukon and Syowa Station, Pc 5 and CNA pulsations might have been present continuously in the region of 08–09MLT. Therefore we expect that the electron precipitation with energies of several tens of keV observed by DE-2 caused the CNA pulsation.

2.3.2 Statistical analysis of Pc 5 and CNA observed at Syowa

Pc 5 and CNA pulsations observed at Syowa Station were investigated statistically. We found 1340 events of Pc 5 pulsations (T=150–600 seconds) in the H-component during the period from August 1981 to February 1983, using an FFT analysis method. The average period of these pulsations was about 330 seconds. Fifty-five percent of the event had periods between 270 and 360 seconds. Figure 2.8a shows the MLT dependence of the occurrence time of Pc 5 pulsations. Pc 5 pulsations are observed frequently in the MLT range of 06 to 19 hours, and have an occurrence peak in the morning (07–10MLT). The average power density of the Pc 5 pulsations against MLT was also investigated statistically (Figure 2.8b). Pc 5 pulsations on the morning side (04–10MLT) have larger power densities than those in other MLT regions.

We scanned the riometer data visually to select clear CNA pulsations which appeared simultaneously with the Pc 5 pulsations detected above. Out of 1340 events, 73 events of Pc 5 pulsations with clear CNA pulsations were found. The wave power density of the 73 Pc 5 pulsations accompanied by CNA pulsations was $10^{-1.42}\mathrm{nT}^2/\mathrm{Hz}$ on the average, which is much greater than the average power density of Pc 5 pulsation events shown in Figure 2.8b. Figure 2.9 shows an example of the event in which both Pc 5 and CNA pulsations appeared. Pc 5 and CNA pulsations with periods of about 4 minutes appeared around 07–08MLT. The amplitude of the Pc 5 pulsation is changing with time between 50 and 160 nT. Although the Pc 5 pulsation starts at 0530UT, CNA pulsation can be seen from 0620UT approximately. The phase difference between Pc 5 and CNA pulsations for the time interval 0630 to 0704UT was about $-84°$, indicating that the Pc 5 pulsation was preceded by the CNA pulsations by this amount. The MLT distribution of these 73 events is indicated in the top panel of Figure 2.10, which shows that CNA pulsations associated with Pc 5 pulsations occur most frequently on the morning side (06–10MLT). The number of events decreases suddenly after 11MLT, although a considerable number of Pc 5 pulsations appeared after this MLT according to Figure 2.8a. The bottom right panel in Figure 2.10 gives statistical results on the phase differences between Pc 5 and CNA pulsations. We see that there is a large peak around $-90°$ in the phase difference distribution. This result indicates that the phase of Pc 5 pulsations in the H-component lags behind that of CNA pulsations approximately by 90° in most cases.

2.3.3 Geomagnetic conjunction events of DE-2 and Syowa

Out of the 73 events of Pc 5 pulsations followed by clear CNA pulsations discussed above, several events were observed by DE-2 on magnetic field lines close to the one which passes through Syowa Station. Figure 2.11 shows a geomagnetic conjunction event of DE-2 and Syowa Station on 30 May 1982 (DAY82150). The orbit of DE-2 and the location of Syowa in the MLT-ILAT plane for this event are shown in Figure 2.11a. Pc 5 and CNA pulsations whose periods are 4 minutes appeared on the morning side (06–08MLT) as shown in Figure 2.11b. Pc 5 pulsation with amplitude of 50–100 nT continues to appear in the whole time interval shown in Figure 2.11b, while CNA pulsation starts from about 0630UT. A weak modulation of ELF-VLF activity at 750 Hz can be seen in the time interval from 0710 to 0730UT, which is much shorter in duration than those of Pc 5 and CNA pulsations. Figure 2.11c shows an observation of ΔB_z and E_x by DE-2, where both data are high-pass filtered with a cut-off period of 25 seconds because the raw data of this event were influenced by the nutation of the DE-2 satellite with a period of about 30 seconds. A good correlation between ΔB_z and E_x is noticed. The correlation coefficient for the disturbances (40–160 km in spatial scale) is 0.78. The sinusoidal disturbances whose amplitudes are 20–30 nT in ΔB_z and 5–6 mV/m in E_x appeared in the ILAT range from 69.2° to 65.8° (0731:12–0732:06UT). The ratio of ΔB_z to E_x corresponds to 3–4 S, which is comparable to the height-integrated ionospheric Pedersen conductivity. The model of small scale field-aligned currents shown in Figure 2.4 can account for the sinusoidal disturbances, as is the case with the DAY82293 event. There are some pairs of small scale field-aligned currents each with a latitudinal width of 0.5°–1.0°ILAT, that is, 60–120km in length.

A conjunction event of DE-2 and Syowa on 19 December 1982 (DAY82353) is presented in Figure 2.12 in the same format as in Figure 2.11. At Syowa Station, Pc 5 and CNA pulsations were observed in the early morning (04–06MLT). The Pc 5 pulsation which appeared from 0330UT precedes the CNA pulsation which began at 0410UT by about 40 minutes (Figure 2.12b). Both pulsations have the same period of 4 minutes. ELF-VLF activity at 750 Hz shows a sudden enhancement around 0500UT, but this may not be related directly to the ULF wave-particle interaction because the modulation of ELF-VLF lasts only about 10 minutes. There is no clear enhancement in ELF-VLF activity at 1.2 kHz. From Figure 2.12c we see that the variations in ΔB_z and E_x are correlated well. Disturbances with 64–240 km in spatial scale have a correlation coefficient of 0.80. There are sinusoidal disturbances in ΔB_z and E_x in the ILAT range 66.4° to 72.7° (0527:10–0528:49UT); their amplitudes being 50–120 nT and 7–16 mV/m, respectively. We derived the height-integrated Pedersen conductivity of about 5–6 S from the ΔB_z to E_x ratio for this case. The small scale field-aligned current model can be adopted for the interpretation of this event in the same way as the two previous observations of DE-2. The current pairs with latitudinal width of 0.6°–1.4°ILAT (72–168km) were found in 5–6 pairs.

2.4 Discussion

2.4.1 Electron acceleration mechanism

We have investigated electron precipitation phenomena associated with transverse Pc 5 pulsations. From the observations of the DE-1 and -2 satellites, it was found that the electrons with high energies from several keV to 27 keV were precipitating into the ionosphere in the region where transverse Pc 5 pulsations appeared. These electrons were accelerated in the direction of the ambient magnetic field line.

The ULF wave-particle interaction by the drift-bounce resonance [*Southwood et al.*, 1969; *Southwood and Kivelson*, 1982] has been reported observationally by *Kokubun et al.* [1977] and *Cladis and Lennartsson* [1986], and numerically by *Li et al.* [1993]. *Kokubun et al.* [1977] studied the resonance between the particles and the radial component of the magnetic field variations of Pc 5 pulsations. *Li et al.* [1993] showed that some particles whose initial state satisfies the resonance condition gain energy in the presence of radially polarized Pc 5 waves but with no stationary electric fields (convection and corotation electric fields). However, the transverse Pc 5 pulsation investigated here had small amplitude in the $\Delta B_{\perp 1}$ (radial) component, which is essential to the drift-bounce resonance. Thus the drift-bounce resonance may not be suitable for the ULF wave-particle interaction mechanism for the events treated

here.

Coroniti and Kennel [1970] presented a wave-particle interaction mechanism in which compressional ULF waves can modulate the growth rate of the VLF waves and lead to electron precipitation pulsations indirectly through equatorial VLF wave-particle interactions. *Sato and Kokubun* [1980] and *Sato et al.* [1985] found a good coherency between VLF emissions and magnetic pulsations in the D-component observed at ground stations. They concluded that these observations strongly suggest interaction between VLF waves and compressional hydromagnetic waves in the outer magnetosphere. However, the DE-1 satellite did not observe fluctuations in the $\Delta B_{\parallel}$ component in the DAY82293 event (Figure 2.1). Besides, we do not recognize any obvious modulation of the ELF-VLF activities at 750 Hz and 1.2 kHz in the DAY82293 event, although Pc 5 and CNA pulsations appeared (Figure 2.7). Therefore the theory of *Coroniti and Kennel* [1970] cannot explain this event. The DAY82150 event shows a weak modulation of the ELF-VLF activity at 750 Hz around 0720UT (Figure 2.11b). The duration of ELF-VLF modulation, however, is shorter than that of CNA pulsation. The CNA pulsation accompanied by a Pc 5 pulsation appears in the time interval 0740 to 0820UT, in which there are no ELF-VLF modulations. In Figure 2.12b (DAY82353 event) we can see a strong modulation of ELF-VLF waves with a much shorter duration than the durations of the Pc 5 and CNA pulsations. It may be difficult to explain these two events by the Coroniti and Kennel's theory because the duration of ELF-VLF waves is much shorter than that of CNA pulsations. However, there remains a possibility that VLF waves modulated by compressional ULF waves in the magnetosphere were not observed at Syowa Station due to propagation of VLF waves along the duct or reflection on the ionosphere.

It was found from the DE-2 observation that the sinusoidal disturbances in ΔB_z and E_x are correlated well, when a Pc 5 pulsation is observed by DE-1 or at a ground station which is in geomagnetic conjunction with DE-2. This observation is explained by the model of small scale field-aligned currents each with latitudinal width of 0.5°–1.4°ILAT (60–168 km) as shown in Figure 2.4. Therefore we consider that Pc 5 pulsations have small scale resonance structures which are reported previously by observational studies [*Saka et al.*, 1992; *Walker et al.*, 1992] and a numerical study [*Wei et al.*, 1994]. This resonance structure can be formed due to the L-shell dependence of the eigenfrequency of the geomagnetic field lines. We assume an azimuthal Pc 5 pulsation for simplicity. This assumption is proper for the observed transverse Pc 5 pulsation because of its larger amplitude in the $\Delta B_{\perp 2}$ component. The eigenfrequencies of neighboring magnetic field lines are slightly different. Thus differences of the azimuthal magnetic field variations between the neighboring shells will arise, when the magnetic field lines begin to oscillate individually by field line resonance [*Southwood*, 1974; *Chen and Hasegawa*, 1974]. The difference of the azimuthal magnetic field variations makes the small scale structure radially (*i.e.*, latitudinally, if projected onto the ionosphere) in the resonant region. Although the width of the structure narrows as time goes on, it will saturate due to the damping effect of the Joule dissipation in the ionosphere [*Wei et al.*, 1994]. If resonance structure has a scale small enough to allow kinetic or electron inertia effects, Alfvén waves are converted to kinetic Alfvén waves [*Hasegawa*, 1976; *Hasegawa and Chen*, 1976] or inertial Alfvén waves [*Goertz and Boswell*, 1979; *Goertz*, 1984; *Lysak*, 1990] which have an electric field parallel to the geomagnetic field line ($E_{\parallel}$).

The dispersion relation of the Alfvén waves is

$$\omega^2 = k_{\parallel}^2 V_A^2,$$

where ω is the wave frequency, $k_{\parallel}$ is the wave number parallel to the ambient magnetic field, and V_A is the Alfvén velocity. Alfvén waves have no electric fields parallel to the ambient magnetic field line ($E_{\parallel} = 0$).

When a wavelength perpendicular to the magnetic field ($k_{\perp}$) becomes comparable to the electron inertia length, the dispersion relation is modified as

$$\omega^2 = \frac{k_{\parallel}^2 V_A^2}{1 + \left(k_{\perp} \frac{c}{\omega_{pe}}\right)^2}, \tag{2.1}$$

where c is the speed of light and ω_{pe} is the electron plasma frequency. Equation (2.1) is the dispersion

relation for the inertia Alfvén waves which have a finite value of $E_{\parallel}$ given by

$$|E_{\parallel}| = \frac{\left(k_{\perp}\frac{c}{\omega_{pe}}\right)^2}{1+\left(k_{\perp}\frac{c}{\omega_{pe}}\right)^2}\frac{|k_{\parallel}|}{|k_{\perp}|}|E_{\perp}|, \tag{2.2}$$

where $E_{\perp}$ is a perpendicular electric field.

The dispersion relation for the kinetic Alfvén waves having a wavelength comparable to the ion gyroradius in the perpendicular direction to the magnetic field line is given by

$$\omega = k_{\parallel}V_A\sqrt{1+k_{\perp}^2\rho_i^2\left(\frac{T_e}{T_i}+\frac{3}{4}\right)}, \tag{2.3}$$

where ρ_i is the ion gyroradius, T_e and T_i are the electron and ion temperature, respectively. The kinetic Alfvén waves also have a finite value of $E_{\parallel}$,

$$|E_{\parallel}| = (k_{\perp}\rho_i)^2\left(\frac{T_e}{T_i}+\frac{3}{4}\right)\frac{|k_{\parallel}|}{|k_{\perp}|}|E_{\perp}| \tag{2.4}$$

Figure 2.13 shows the altitude dependence of wave structure in radial direction, ion gyroradius, and electron inertia length along the geomagnetic field line of 70°ILAT. We calculated the altitude dependence of wave structure which has latitudinal width of 100 km at 400 km altitude, because the small scale resonance structure each with width of 0.5°–1.4°ILAT (60–168 km) at the DE-2 altitude was observed around 70°ILAT. The ion gyroradius is for a proton with energy of 10 keV; this energy is taken because the region around 70°ILAT in the dayside magnetosphere corresponds to the central plasma sheet [*Newell and Meng*, 1994], where ions have energies of tens of keV [*Newell et al.*, 1991; *Beaujardiere et al.*, 1993]. Using the model of the electron density on the morning side by *Takahashi and Anderson* [1992], the electron inertia length was calculated. From Figure 2.13 we see that the electron inertia length is much smaller than the radial scale size of wave structure, but ratio of the ion gyroradius to the wave structure is about 0.03–0.10 at altitudes higher than 20000 km. Therefore the ion gyroradius effect is thought to be relevant. If we put into the Equation (2.4) values of $k_{\perp}\rho_i \sim 0.3$, $\frac{T_e}{T_i}+\frac{3}{4} \sim 1$, $\frac{|k_{\parallel}|}{|k_{\perp}|} \sim 0.03$, and $E_{\perp} \sim 75$ mV/m, we obtain a result of $E_{\parallel} \sim 0.20$ mV/m, where the value of $E_{\perp}$ is estimated from 30 nT of the observed magnetic field by DE-1 and 2500 km/s of Alfvén velocity. This parallel electric field at altitudes higher than 20000 km makes a field-aligned potential of about 19 kV along the geomagnetic field line of 70°ILAT. Electrons will be accelerated by the $E_{\parallel}$ to about 19 keV, which is consistent with the energy range of electron flux enhancement observed by DE-2 (Figure 2.5).

The kinetic Alfvén waves have $E_{\parallel}$ which is proportional to $E_{\perp}$ (See Equation (2.4)) and the $E_{\perp}$ shows sinusoidal structure in the latitudinal direction as shown in Figure 2.4, then it is expected that the $E_{\parallel}$ also has a sinusoidal structure latitudinally. Figure 2.14 gives a plausible model of spatial structure for $E_{\parallel}$ and electron precipitation. We notice that DE-2 will pass alternatively the region where electrons accelerated by $E_{\parallel}$ are precipitating and the region where high energy electrons are not precipitating. This is consistent with the observation of Figure 2.5.

Figure 2.15 explains the phase difference between Pc 5 and CNA pulsations observed on the ground. A toroidal Pc 5 pulsation is thought to be a fundamental mode of standing Alfvén wave [*Sugiura*, 1961; *Nagata*, 1963; *Cummings et al.*, 1969], then the phase difference between the toroidal magnetic field variations and the radial electric field variations is 90° and the electric field leads the magnetic field in the southern hemisphere [*Singer et al.*, 1982; *Takahashi et al.*, 1988]. The toroidal magnetic field variations in the magnetosphere are observed in the H-component variations on the ground due to the ionospheric screening effect [*Hughes and Southwood*, 1976]. The radial electric field variations are related to the parallel electric field in the case of the kinetic Alfvén waves as discussed above, and the parallel electric field accelerates electrons which cause CNA pulsations. Thus Pc 5 pulsations in the H-component lags CNA pulsations by 90°, which is consistent with the results of Figures 2.7 and 2.9, and the statistical result of Figure 2.10.

It was observed at Syowa that the beginning time of CNA pulsations lags behind that of the Pc 5 pulsation. This fact will be explained by that it takes time for the wave structure in the radial direction to have the scale small enough to allow ion gyroradius effects.

2.4.2 MLT distribution of Pc 5 and CNA pulsation occurrence

We have found that Pc 5 pulsations in the H-component observed at Syowa Station appeared frequently on the dayside and have an occurrence peak in the MLT range of 07 to 10 hours (Figure 2.8a). This MLT distribution is consistent with the previous studies with satellite data [*Yumoto et al.*, 1983; *Takahashi and McPherron*, 1984; *Kokubun et al.*, 1985; *Kokubun et al.*, 1989; *Anderson et al.*, 1990; *Nosé et al.*, 1995; *Potemura and Blomberg*, 1996]. It was also found that Pc 5 pulsations at Syowa Station have much power on the morning side (04–10MLT) as shown in Figure 2.8b. *Potemura and Blomberg* [1996] found from Viking data a tendency for higher amplitude of Pc 5 pulsations to occur in the prenoon region (09–10MLT).

The top panel of Figure 2.10 shows that CNA pulsations accompanying Pc 5 pulsations appear mostly on the morning side (06–10MLT). This statistical result generally agrees with the previous studies by *Sato et al.* [1985], *Higuchi et al.* [1988], and *Paquette et al.* [1994]. The number of CNA pulsations becomes small on the afternoon side where Pc 5 pulsations appear frequently but their wave powers are small. The Pc 5 pulsations accompanied by CNA pulsations had wave power density of $10^{-1.42}$ nT^2/Hz on the average, which is much greater than the average power density of Pc 5 pulsation events in every MLT bin (Figure 2.8b). Therefore we can say that CNA pulsations are associated with intense Pc 5 pulsations. The electron acceleration mechanism by kinetic Alfvén waves is consistent with the idea, because intense Pc 5 pulsations are expected to have large $E_{\parallel}$ and supply electrons more energy. The small number of CNA pulsation events in the early morning (04–05MLT) may stem from the infrequent occurrence of Pc 5 pulsations.

2.4.3 Magnetic field variations observed on the ground

Pc 5 pulsations in the H-component on the ground are believed to be induced by the oscillating ionospheric Hall currents [*Hughes and Southwood*, 1976]. We investigated whether or not a small scale resonant structure with latitudinal width of 0.5°–1.4°ILAT (60–168 km), which is comparable to the height of the ionosphere, can produce relevant variations on the ground, because the magnetic effects could be cancelled out on the ground. We assumed a Hall current model of Figure 2.16a with a height of the ionosphere of 100 km, a height-integrated Hall conductivity of 8 S, an electric field of 15 mV/m, and a latitudinal width of structure of 130 km. This model has 4 current pairs which are uniform longitudinally. The magnetic field variations in the H-component induced by this current system are shown in Figure 2.16b. We can see that maximum amplitude of variations is about 90 nT and other peaks have values of 30–50 nT. The amplitude of variations calculated here is comparable to or a little bit smaller than the amplitudes of Pc 5 pulsations observed at Syowa Station. We conclude that a small scale structure of oscillating ionospheric currents is capable of producing Pc 5 pulsations with observed amplitudes.

From Figure 2.16b we notice that if the current system is shifted slightly in the latitudinal direction, amplitudes of Pc 5 pulsations observed at a ground station will change. The change of amplitude makes waveforms of Pc 5 pulsations like wave packets, which have been observed frequently on the ground.

2.5 Conclusions

We found electron precipitation phenomena accompanying Pc 5 pulsations from the observations of the DE-1 and -2 satellites and the ground station. The main results obtained in this study are as follows.

1. DE-2 observed sinusoidal disturbances in the magnetic and electric fields which are correlated well to each other above the ionosphere, when Pc 5 pulsation was observed by DE-1 or at the ground station which was in geomagnetic conjunction with DE-2.
2. The sinusoidal disturbances show that the Pc 5 pulsation has a small scale resonance structure each

with latitudinal width of 0.5°–1.4°ILAT (60–168 km), which is small enough to permit the ion gyroradius effects to become significant, giving rise to kinetic Alfvén waves.
3. The electron precipitation with energies of several tens of keV observed by DE-2 could be explained by acceleration due to the parallel electric fields of the kinetic Alfvén waves.
4. The phase difference of 90° between Pc 5 pulsations in the H-component and CNA pulsations on the ground would be caused by the electron precipitation due to the kinetic Alfvén waves.
5. The MLT dependence of the occurrence of CNA pulsations associated with Pc 5 pulsations stems from the MLT dependence of wave power of Pc 5 pulsations, that is, CNA pulsations were observed on the morning side where intense Pc 5 pulsations appear. This fact supports the electron acceleration by kinetic Alfvén waves.

We conclude that the electron acceleration by kinetic Alfvén waves is one of the ULF wave-particle interaction mechanisms. In a future study, the temporal development of the small scale resonance structure should be investigated observationally. It is also important to study statistically the phase relationship of CNA pulsations observed at Syowa Station and its conjugate station.

Chapter 3

ULF pulsations observed by the ETS-VI satellite: Substorm associated azimuthal Pc 4 pulsations on the nightside

3.1 Introduction

Pc 3–5 pulsations observed by satellites have been investigated by many researchers since the 1970s. A brief review of the previous studies employing satellite data which were published before 1989 is found in *Anderson et al.* [1990a].

Arthur and McPherron [1977] studied statistically 81 events of transverse Pc 3 pulsations observed by ATS-1, which were simultaneously observed on the ground. The transverse Pc 3 pulsations had the local time distribution with a strong midmorning peak and dominant frequencies between 40 mHz and 50 mHz. From analysis of the magnetic field data obtained by ATS-6, *Arthur and McPherron* [1981] found that radially polarized waves in the Pc 4 ranges occur predominantly at dusk.

Using the magnetic field data from the geosynchronous satellites, *Takahashi and McPherron* [1984] studied two different types of waves, that is, azimuthally polarized waves involving the fundamental and several harmonics, and radially polarized waves excited at the second harmonic. The former were observed through the dayside, and the occurrence of the fundamental wave was more biased toward the morning than that of harmonic waves. The latter were observed mainly on the afternoon side. They concluded that the azimuthal waves with fundamental and harmonics are driven externally, and the radial waves at second harmonic are likely to be excited internally through wave-particle interactions.

Kokubun et al. [1989] studied R-class (radial) Pc 4 waves and A-class (azimuthal) Pc 4–5 waves with the magnetic field data and particle flux data from ATS-6. Their results showed that R-class Pc 4 waves predominantly occur in the afternoon sector from 12 to 18LT, and A-class Pc 4–5 waves with the period range of 100–200 seconds predominantly appear in the morning sector. The oscillation of the azimuthal component for A-class Pc 4–5 waves was out of phase with proton flux (<120 keV), though the phase relationship for R-class Pc 4 waves was dependent on both energy and pitch angle of proton flux.

ULF pulsations (f=0–80 mHz) observed by the AMPTE/CCE satellite from L=5 to 9 in the equatorial magnetosphere were statistically investigated by *Anderson et al.* [1990a]. The occurrence distribution of fundamental toroidal waves in Pc 5 band had a dawn/dusk asymmetry, that is, the waves were observed frequently for L=8–9 at dawn but were less observed at dusk. They found that harmonic toroidal waves in Pc 3 band were dominant on the dayside, particularly in the prenoon hours. The toroidal Pc 3 waves occurred with frequencies which varied continuously with radial distance. Radially polarized pulsations in the Pc 4 frequency range were found to occur in width extending from 11 magnetic local time (MLT) through dusk to 04MLT. The radial Pc 4 pulsations were frequently observed for L<7 at noon and for L>7 on the nightside.

Takahashi and Anderson [1992] examined spatial distribution of ULF (f<80 mHz) energy in the inner magnetosphere (L=2.5–6.5), using the magnetic field data from the AMPTE/CCE satellite. They found that multiharmonic toroidal oscillations in the Pc 3 and Pc 4 frequency ranges appeared predominantly

on the dayside. Assuming that the toroidal oscillations are due to standing Alfvén waves, they determined the radial profile of the plasma mass density and Alfvén wave velocity.

Using the data from the AMPTE/CCE satellite and geosynchronous GOES-5 and -6 satellites, *Takahashi et al.* [1996] reported toroidal magnetic pulsations in the nightside magnetosphere in the form of transient oscillations typically lasting 10–20 minutes. These waves were called as transient toroidal waves (TTW). They showed two examples of TTW with frequency ranges of 11–17 mHz for L=5.5 to 7 and one example of TTW which consisted of a few discrete spectral components (5, 10, 16, and 28 mHz), and concluded that TTW are standing waves. It was also found that TTW on the nightside for $4<L<7$ were observed immediately following ~30% of substorm onsets.

Saka et al. [1996a] found that quasi-periodic oscillations (QPO) with frequency of 9 mHz were observed by GOES 5 and 6 in the night sector in association with the onset of ground Pi 2 pulsations. They also found that 16% of Pi 2 events (35 of 216 Pi 2 events) were accompanied by QPO. The QPO were polarized more or less in the azimuthal direction. The QPO in the postmidnight sector had more sinusoidal waveforms than those in the premidnight, and had an occurrence peak at 02MLT.

In this chapter we aim to investigate characteristics of pulsations in Pc 3–5 bands observed by Engineering Test Satellite -VI (ETS-VI). In respect of the azimuthal Pc 5 pulsations, the azimuthal Pc 3 pulsations, and the radial Pc 4 pulsations on the dayside, the results were consistent with those by the previous studies. We examined statistically the azimuthal Pc 4 pulsations on the nightside, which are considered as the same phenomena as TTW and QPO, and concluded that the azimuthal Pc 4 pulsations on the nightside are excited through coupling to the fast mode Alfvén waves which are radiated at substorm onsets. This excitation mechanism is different from that by the previous studies.

3.2 Experiment and Data Analysis

3.2.1 The satellite and magnetometer

The ETS-VI satellite, which was launched on August 28, 1994, had a perigee of $2.3R_E$, an apogee of $7.1R_E$, an inclination of 13.4°, and a 14.4-hour orbital period. The triaxial fluxgate magnetometer (MAM) on board ETS-VI has two observation modes, Range-L mode and Range-H mode. The dynamic range and resolution in Range-L mode are ±65536 nT and 32 nT, respectively. Range-H mode has the dynamic range of ±256 nT and the resolution of 0.125 nT. Range-H is used over approximately 11 hours at radial distances of 5.0–$7.1R_E$ and −15° to +25° magnetic latitudes (MLAT), and Range-L is used near perigee. The data were recorded with a sampling interval of 3 seconds. A more detailed description of the ETS-VI satellite and its observations are found in *Nagai et al.* [1996].

3.2.2 Data coverage

The data period used here is 496 days in total, from October 1994 through April 1996. We excluded the data period when the satellite was not three-axis stabilized. Only the data obtained near the apogee (where the altitude of the ETS-VI satellite is more than 28000 km) were used in this study, because the data obtained with Range-L mode are not useful for pulsation studies in respect of their low resolution. The ETS-VI satellite has changed the local time of the apogee from about 05MLT in November 1994, through midnight, to about 17MLT in June 1995, and again to about 05MLT in December 1995. The local time of the apogee in April 1996 was about 20MLT. Therefore the data set used here covers all MLT ranges, although the number of the data points on the nightside (20–05MLT) is larger than that on the dayside. Plates 3.1a and 3.1b give the distributions of data set in MLT-MLAT plane and MLT-invariant latitude (ILAT) plane, respectively. One mesh in Plate 3.1a corresponds to 1° of MLAT by 1 hour of MLT, and in Plate 3.1b, 0.5° of ILAT by 1 hour of MLT. The color images show hours of observation time. From Plate 3.1a we notice that generally the higher latitudes than 20°MLAT and −10°MLAT are less or not completely covered. The observation time in MLT-MLAT areas of 04–10MLT, −5° to −10°MLAT and 10–17MLT, 7°–12°MLAT are small. The coverage in ILAT is biased around 67°–68°ILAT (Plate 3.1b), because the ETS-VI satellite with the small inclination stayed for a long time

near the apogee of $7.1R_E$. Observation time in the ILAT ranges higher than 69°ILAT and lower than 64.5°ILAT are small at all MLT.

3.2.3 Preparation of pulsation list

We adopted the following procedures to make the lists of Pc-type geomagnetic pulsations. In the first step we have made the magnetic field variation data by subtracting the IGRF90 model fields from the observed magnetic fields. The magnetic field variation data were represented in the local magnetic (LMG) coordinate system, in which the $\Delta B_{\parallel}$ component is the tangential direction of model magnetic field, the $\Delta B_{\perp 1}$ component is perpendicular to the model magnetic field and directed radially outward, and the $\Delta B_{\perp 2}$ component is azimuthally eastward. The field components $\Delta B_{\parallel}$, $\Delta B_{\perp 1}$, and $\Delta B_{\perp 2}$ are referred to as the compressional, radial, and azimuthal components, respectively.

In the second step we calculated the power spectral density for each component by using Fast Fourier Transform (FFT) analysis. A unit time window for FFT analysis was 25 minutes (500 data points) and this window was shifted in 5-minute interval in each analysis. We could investigate pulsations in Pc 3–5 bands (10–600 seconds) because of the time window of 25 minutes and the time resolution of 3 seconds. Scanning the power spectral density of the $\Delta B_{\parallel}$ component, we located the peak of the power spectrum. If the power of the peak was more than ten times as large as that of the background levels, we decided that a compressional pulsation with the frequency at the spectral peak has appeared during the time interval of the window. To detect radial and azimuthal pulsations, the power spectrum densities of the $\Delta B_{\perp 1}$ and $\Delta B_{\perp 2}$ components were treated in the same way as the $\Delta B_{\parallel}$ component. If pulsations were detected in successive time windows, we regarded them as one pulsation event.

In the last step we visually scanned the plot of the magnetic field data and removed non-continuous events like Pi 2 pulsations from the pulsation lists. If a event had more than one component which satisfied the above criteria (*i.e.*, the power of the spectral peak is more than ten times as large as that of the background), that event was treated to overlap more than one category according to the components. For example, a pulsation, in which the azimuthal and radial components satisfy the criteria, is counted as one event in both of the azimuthal and radial categories. The number of pulsations selected by the above procedure was shown in Table 3.1.

3.3 Statistical Results

Based on the pulsation lists, we investigated occurrence distributions of pulsations classified by frequency ranges (Pc 3, Pc 4, and Pc 5) and components (compressional, radial, and azimuthal). Plate 3.2 is an example of the distributions of occurrence probability, which is for azimuthal Pc 5 pulsation. MLT-MLAT distribution of occurrence probability is shown in Plate 3.2a, in which one mesh represents a region of 1° of MLAT by 1 hour of MLT. Plate 3.2b gives MLT-ILAT distribution of occurrence probability with one mesh of 0.5° of ILAT by 1 hour of MLT. The occurrence probability is defined as the appearance time of the pulsation divided by the observation time (shown in Figure 3.1) in each mesh. A small open circle in mesh represents that in that mesh no observations were made or observation time was less than 1.5 hours in the MLT-MLAT plane and less than 4.5 hours in the MLAT-ILAT plane. The occurrence distributions for 9 kinds of pulsations shown in Table 3.1 were presented in the same format as Plate 3.2, and we have found prominent characteristics for the following pulsations: (1) azimuthal Pc 5 pulsation; (2) azimuthal Pc 3 pulsation; (3) radial Pc 4 pulsation on the dayside; (4) azimuthal Pc 4 pulsation on the nightside.

3.3.1 Azimuthal Pc 5 pulsation

Figure 3.1 gives an example of azimuthal Pc 5 pulsation observed by the ETS-VI satellite on 28 November 1995. The upper three panels are variations of the magnetic field in LMG coordinate system, and the bottom two panels show the location of the satellite in solar magnetic coordinate system. We notice a pulsation with period of about 3.2 minutes appeared from 0630UT to 0730UT in the $\Delta B_{\perp 2}$ component,

that is, in the azimuthal component. This azimuthal Pc 5 pulsation appeared between 06 and 07MLT. As shown in the bottom right panel, the ETS-VI satellite was off the geomagnetic equator.

The distributions of occurrence probability of azimuthal Pc 5 pulsations are shown in Plate 3.2. The MLT-ILAT distribution (Plate 3.2a) shows that azimuthal Pc 5 pulsations mostly appear in the off equatorial region (around 15°MLAT) except for an appearance near the geomagnetic equator at local noon. We could not conclude whether the azimuthal Pc 5 pulsations appear off the equator in the southern hemisphere, because ETS-VI did not pass the high latitude area of MLAT in the southern hemisphere. It is noticed that the Pc 5 pulsations occur frequently around 68°–69°ILAT of both 05–09MLT and 15–18MLT (Plate 3.2b), however the orbit of ETS-VI did not allow us to investigate whether the frequent occurrence regions of the azimuthal Pc 5 pulsations spread over higher latitude of ILAT. In the MLT-MLAT and MLT-ILAT regions where the azimuthal Pc 5 pulsations observed frequently, the occurrence probability of compressional and radial Pc 5 pulsations (not shown here) were much smaller than that of the azimuthal Pc 5 pulsations. This fact is consistent with the observation shown in Figure 3.1.

Figure 3.2 shows Kp dependence of Pc 5 occurrence probability which was defined as the ratio of the number of the azimuthal Pc 5 pulsations in the MLT range of 04–10MLT and 15–20MLT to the number of data sets in each class of Kp index. It can be seen that generally the larger the value of Kp index, the more frequent the Pc 5 occurrence.

3.3.2 Azimuthal Pc 3 pulsation

An example of azimuthal Pc 3 pulsation, which was observed on 18 July 1995, is shown in Figure 3.3. We can see fluctuations of the magnetic field with period of 20–30 seconds and with dominant component in $\Delta B_{\perp 2}$, that is, azimuthal Pc 3 pulsation. The azimuthal Pc 3 pulsation lasted for about 5 hours from 0600UT to 1100UT (magnetic field data after 0800UT are not shown here). ETS-VI was located near the geomagnetic equator at local noon.

The dynamic spectrum of the magnetic field data of Figure 3.3 is presented in Plate 3.3. Each panel corresponds to the $\Delta B_{\parallel}$, $\Delta B_{\perp 1}$, and $\Delta B_{\perp 2}$ components. In $\Delta B_{\perp 2}$ there are harmonic waves which have mainly 2 frequency bands, high and low frequency. The high frequency wave has a frequency of about 45 mHz around 0620UT, and changes its frequency gradually to about 37 mHz around 0740UT. The low frequency wave has also changed its frequency from 20 mHz to 17 mHz. The wave power of the high frequency wave is greater than that of the low frequency wave. We can notice other waves with a frequency of 65 mHz from 0620UT to 0645UT and with a frequency of 29 mHz from 0730UT to 0800UT. As it was also seen in Figure 3.3, wave power in the $\Delta B_{\perp 2}$ component are greater than those in the other two components.

The distributions of occurrence probability of the azimuthal Pc 3 pulsations are presented in Plate 3.4. It was found that the azimuthal Pc 3 pulsations were observed in the wide range of MLAT (Plate 3.4a). From Plate 3.4b we notice that Pc 3 appeared frequently in large MLT-ILAT region of 07–16MLT and 65°–68.5°ILAT, though the occurrence region of the azimuthal Pc 3 pulsations may spread over higher or lower latitude of ILAT. There is an occurrence peak around 09–13MLT and the occurrence probability becomes very small on the nightside (16–05MLT).

3.3.3 Radial Pc 4 pulsation on the dayside

Figure 3.4 shows an example of radial Pc 4 pulsation observed by ETS-VI on 26 July 1995. Waves having two packet structures and periods of about 100 seconds can be easily seen in the $\Delta B_{\perp 1}$ (radial) component. Periods of the waves were almost constant. Amplitudes of the radial component were 3 times as large as those of the azimuthal component. It is noticed that the pulsation appeared near the geomagnetic equator on the dayside (14–15MLT).

The distributions of occurrence probability of the radial Pc 4 pulsations are given in Plates 3.5a and 3.5b, which show the radial Pc 4 pulsations are frequently observed on the afternoon side (11–20MLT). Plate 3.5a shows that the radial Pc 4 pulsations appeared in the wide range of MLAT. It was found in Plate 3.5b that the occurrence peak lies in the MLT-ILAT area of 14–16MLT and 66°–67.5°ILAT. On the

night and morning side (20–09MLT), the occurrence probability was very small. Comparing Plate 3.5 with Plate 3.6 which shows the distributions of occurrence probability of the azimuthal Pc 4 pulsation, we notice that Pc 4 pulsations on the afternoon side (11–20MLT) appeared more frequently in the radial component than in the azimuthal component. This result is consistent with the larger amplitude of the Pc 4 pulsation in the radial component shown in Figure 3.4.

3.3.4 Azimuthal Pc 4 pulsation on the nightside

As described previously, Pc 4 pulsations on the dayside (11–20MLT) are polarized radially. However, on the nightside, we found from Plate 3.6 that the azimuthal Pc 4 pulsations have frequent occurrence in the MLT range of 23–04MLT, where the radial Pc 4 pulsations have a small occurrence probability. There is an occurrence peak of the azimuthal Pc 4 pulsations in the MLT-ILAT area of 01–02MLT and 66°–68.5°ILAT (Plate 3.6b). Plate 3.6a shows that occurrence probability on the nightside is larger in the high latitude of MLAT than in the low latitude of MLAT.

An example of azimuthal Pc 4 pulsation on the nightside, which was observed on 29 January 1996, is shown in Figure 3.5. Waves with periods of 80–100 seconds and larger amplitude in the azimuthal component started to oscillate from about 1302UT, 1312UT, and 1332UT, which are indicated by arrows. Each of these waves lasted for about 10 minutes. The observation was made around 02–03MLT in the off equatorial region, which supports the result of Plate 3.6a. In the first and second events, we found short-lived disturbances with small amplitudes in the compressional component, which are indicated by horizontal lines. However, there was no clear disturbances in the compressional component at 1332UT when the third event started.

Judging from the distribution of occurrence probability and waveform, we consider that the azimuthal Pc 4 pulsations on the nightside are the same phenomena as TTW reported by *Takahashi et al.* [1996] and QPO reported by *Saka et al.* [1996a].

3.4 Discussion

3.4.1 Azimuthal Pc 5 pulsation

Plate 3.2b indicates that the frequent occurrence regions of the azimuthal Pc 5 pulsations are around both 05–09MLT and 15–18MLT for 68°–69°ILAT. *Takahashi and McPherron* [1984], *Kokubun* [1985], and *Kokubun et al.* [1989] found that azimuthally polarized Pc 5 pulsations have a large peak of occurrence probability on the dawn side, using geosynchronous satellite (~67°ILAT) data. *Anderson et al.* [1990a] found that the occurrence distribution of fundamental toroidal waves in Pc 5 band observed by the AMPTE/CCE satellite has a strong bias towards the dawn flank for L=8–9. *Kokubun* [1985] and *Kokubun et al.* [1989] found that there is a secondary small peak of occurrence probability in the afternoon (around 15LT). Their results are generally consistent with the distribution of occurrence probability obtained by this study. *Nosé et al.* [1995] and *Potemra and Blomberg* [1996] examined the Pc 5 waves in the high-latitude region of ILAT, taking advantage of polar orbiting satellites. *Nosé et al.* [1995] analyzed the magnetic field data from the DE-1 satellite and found that the transverse Pc 5 pulsations occur most frequently around 72°ILAT between 08 and 10MLT. From morning to noon, Pc 5 pulsations observed by the Viking satellite are polarized primarily in the east-west direction [*Potemra and Blomberg*, 1996]. The Pc 5 pulsations occurred 2°–5° equatorward of the interface of the region 1/region 2 Birkeland currents (around 70°–73°MLAT) [see *Potemra and Blomberg*, 1996, Figure 8]. The average wave amplitudes were larger near 09–10MLT (about 40 nT) than those during the afternoon (about 25 nT). This indicates that Pc 5 pulsations are identified more readily in the prenoon region. The distribution of occurrence probability of the azimuthal Pc 5 pulsations obtained by the ETS-VI and geosynchronous satellites, which showed two occurrence peaks on the dawn and dusk sides, are consistent with the occurrence distribution by *Nosé et al.* [1995] and *Potemra and Blomberg* [1996] in the low latitude region. Thus we consider that the frequent occurrence regions in Plate 3.2b spread to the MLT-ILAT region higher than 70°ILAT around 08–10MLT.

Azimuthal Pc 5 pulsations have been considered as the fundamental mode of the standing Alfvén waves [e.g., *Hughes*, 1994]. This idea is supported by the statistical results shown in Plate 3.2a, which indicate the frequent occurrence of the azimuthal Pc 5 pulsations off the geomagnetic equator, because the fundamental mode of the standing Alfvén wave has a node in the geomagnetic equator. Assuming the wave equation [*Cummings et al.*, 1969] and the plasma mass density on the dayside [*Takahashi and Anderson*, 1992], we obtained the eigenperiod of 170–200 seconds for the fundamental mode at 68°–69°ILAT. The calculated period is almost the same as the period of observed wave (about 3.2 minutes) shown in Figure 3.1.

It was found that the azimuthal Pc 5 pulsations generally occur more frequently when the value of Kp index becomes larger (Figure 3.2). Kp index was thought to be correlated with the solar wind velocity [*Snyder et al.*, 1963; *Olbert*, 1968]. Thus the frequent occurrence of the azimuthal Pc 5 pulsations might be associated with the high-speed solar wind. This result is consistent with those of *Kokubun et al.* [1989] and *Nosé et al.* [1995]. *Anderson et al.* [1990b] found that toroidal fundamental pulsations are enhanced for high solar wind velocity. Thus we suggest the Kelvin-Helmholtz instability on the magnetopause for the energy source of Pc 5 pulsations.

3.4.2 Azimuthal Pc 3 pulsation

The azimuthal Pc 3 pulsations have frequent occurrence distribution from 07 to 16 MLT for 65°–68.5°ILAT, and a strong occurrence peak in the prenoon sector (09–13MLT) as shown in Plate 3.4b. *Arthur and McPherron* [1977] found a strong midmorning peak in the occurrence distribution of Pc 3 pulsations observed by the ATS-1 geosynchronous satellite. Analyzing data from the geosynchronous satellites, *Takahashi and McPherron* [1984] presented occurrence probability of the azimuthally polarized harmonic waves, which shows a high occurrence on the dayside and a peak before local noon. *Anderson et al.* [1990a] showed that harmonic toroidal waves in Pc 3 bands observed by AMPTE/CCE are dominant on the dayside and occur frequently in the morning. Our result is consistent with the occurrence distributions obtained by the previous studies. *Anderson et al.* [1990a] exhibited besides that intense Pc 3 pulsations have an uniform distribution in local time from 06 to 16MLT, suggesting that the morning side bias of occurrence distribution in the overall Pc 3 events may result from masking by other pulsations in the afternoon.

The continuous frequency change of the azimuthal Pc 3 pulsation seen on 18 July 1995 (Plate 3.3) is thought to be caused by the change of the satellite location, as reported by *Engebretson et al.* [1986]. We notice from Figure 3.3 that the ETS-VI satellite was moving away from the earth. The observed frequency of the harmonic waves is expected to decrease, because the length of the local geomagnetic field line becomes long. We calculated the frequencies of the harmonic waves for ILAT=66.8° and 67.7°, which correspond to the values of ILAT at 0620UT and 0740UT, respectively. The wave equation by *Cummings et al.* [1969] with the plasma mass density model by *Takahashi and Anderson* [1992] was solved numerically. The results are shown in Table 3.2. The high frequency wave, which changed its frequency from 45 mHz to 37 mHz, is concluded as the fifth harmonic wave. The low frequency wave with continuous frequency change from 20 mHz to 17 mHz might be the second harmonic waves. The other two waves, which appeared with a frequency of 65 mHz around 0630UT and with a frequency of 29 mHz around 0740UT, are thought to be the 7th and 4th harmonic waves, respectively. The two main frequency bands involved in the azimuthal Pc 3 pulsation, that is, the high (~40 mHz) and low (~20 mHz) frequency bands, are also found in the results by *Arthur and McPherron* [1977].

3.4.3 Radial Pc 4 pulsation on the dayside

The radially polarized Pc 4 pulsations have been investigated by many authors using satellites [*Arthur and McPherron*, 1981; *Takahashi and McPherron*, 1984; *Anderson et al.*, 1990a; *Takahashi and Anderson*, 1992]. The radial Pc 4 pulsations are found to be the phenomena from the afternoon to dusk sector, primarily in the early afternoon. The occurrence distribution exhibited a shift from $L<7$ on the dayside to $L>7$ at midnight [*Anderson et al.*, 1990a]. Our results, which showed the frequent occurrence from 11 to 20MLT, are in agreement with the results of the previous studies.

The radial Pc 4 pulsations on the afternoon side were thought to be generated by bounce resonance [*Arthur and McPherron*, 1981; *Takahashi and McPherron*, 1984; *Anderson et al.*, 1990a; *Takahashi and Anderson*, 1992]. *Takahashi and McPherron* [1984] and *Anderson et al.* [1990a] suggested that the spatial gradient in ion density is responsible for driving the waves through bounce resonance. We can not conclude the excitation mechanisms for the radial Pc 4 pulsations, because the particle data were not available in this study.

3.4.4 Azimuthal Pc 4 pulsation on the nightside

We have found the appearance of the azimuthally polarized Pc 4 pulsations on the nightside (23–04MLT). There were few works which dealt with this kind of pulsation, except for *Takahashi et al.* [1996] and *Saka et al.* [1996a, b]. We will discuss the following four subjects related to the azimuthal Pc 4 pulsations on the nightside (the nightside Pc 4 pulsations). (1) Are the nightside Pc 4 pulsations different phenomena from Pi 2 pulsations in the magnetosphere? (2) Are they standing Alfvén waves? (3) Is it possible for the nightside Pc 4 pulsations to continue oscillating for long time (~10 minutes)? (4) What is/are their energy source? In what mechanism(s) are they excited? Finally, the nightside Pc 4 pulsations will be discussed in relation to results of the previous studies.

Nightside Pc 4 pulsations and Pi 2 pulsations in the magnetosphere. In previous studies Pi 2 pulsations in the magnetosphere are considered to be dominant in the compressional and radial components [*Lin and Cahill*, 1975; *Sakurai and McPherron*, 1983; *Takahashi et al.*, 1995]. Pi 2 pulsations observed by Explorer 45 near L=5 had a strong compressional component [*Lin and Cahill*, 1975]. *Sakurai and McPherron* [1983] studied Pi 2 pulsations observed by the geosynchronous satellite and found that they had a significant compressional component in most cases. Within the magnetic latitude ±16° of the AMPTE/CCE satellite the Pi 2 pulsations are dominated by the radial and compressional components [*Takahashi et al.*, 1995]. On the other hand, The Pc 4 pulsations on the nightside have continuous waveforms and are dominant in the azimuthal component as can be seen in Figure 3.5. Thus we suggest that the nightside Pc 4 pulsations differ from the Pi 2 pulsations in the magnetosphere.

The local time dependence of Pi 2 occurrence in the magnetosphere was investigated by *Sakurai and McPherron* [1983] and *Singer et al.* [1983]. The most probable occurrence time of Pi 2 pulsations observed by the ATS-6 satellite is 21LT, with more events seen premidnight than postmidnight [*Sakurai and McPherron*, 1983]. The distributions of Pi 2 occurrence at GOES-2 and -3 orbits have peaks around 1–2 hours prior to local midnight [*Singer et al.*, 1983]. Both of their results showed that occurrence probability of Pi 2 pulsations decreases generally as the satellite moves to the dusk or the early morning side. We found 80 events of Pc 4 pulsations in the night sector (19 events for 19–23MLT, and 61 events for 23–04MLT), which have much power in the azimuthal component than in the radial and compressional components. The dependence of the nightside Pc 4 pulsation occurrence on MLT was investigated (Figure 3.6). We defined occurrence probability as the number of pulsations divided by the observation time in each bin of MLT. As shown in Figure 3.6, the nightside Pc 4 pulsations have frequent occurrence from 23 to 04MLT and an occurrence peak around 01–02MLT. Occurrence probability before midnight (19–23MLT) is generally smaller than that after midnight (23–04MLT). The nightside Pc 4 pulsations are seldom observed at the range of 22–23MLT, where Pi 2 pulsations have an occurrence peak. It is obvious that there are differences between the local time occurrence distribution of the nightside Pc 4 pulsations and that of the Pi 2 pulsations. The result of Figure 3.6 also confirms that the nightside Pc 4 pulsations are different phenomena from the Pi 2 pulsations in the magnetosphere.

Standing Alfvén wave. We investigated the ILAT dependence of the periods of the nightside Pc 4 pulsations for 23–04MLT (Figure 3.7). If we ignore a data point with a parenthesis, there seems to be a tendency that the higher the value of ILAT, the longer the periods of the nightside Pc 4 pulsations. The broken lines show the eigenperiods of the standing Alfvén waves for azimuthal waves calculated from the wave equation of *Cummings et al.* [1969]. The plasma density is assumed to be half the values of *Takahashi and Anderson* [1992] which gives the mass density model in the dayside magnetosphere (09–12MLT), because the observation of the Ogo-5 satellite shows that H^+ density in the prenoon sector is a few to ten times larger than that in the postmidnight sector [*Chappell et al.*, 1970]. The broken line which indicates the eigenperiod for the fundamental mode fits mostly the observation of the ETS-VI

satellite. We consider that the fundamental mode of the standing Alfvén waves is most plausible for the nightside Pc 4 pulsations.

Figure 3.8 shows the dependence of occurrence of the nightside Pc 4 pulsations on the absolute value of MLAT. Occurrence probability was defined as the number of nightside Pc 4 pulsation divided by the observation time in each bin of |MLAT|. In the low latitude of MLAT (|MLAT|<8°) the nightside Pc 4 pulsations were less observed. Occurrence probability in the high latitude of MLAT (|MLAT|>8°) is about 4 times as large as that in the low latitude of MLAT (|MLAT|<8°). This fact, which can be also seen in Plate 3.6a, supports that the nightside Pc 4 pulsations are the fundamental mode of the geomagnetic field line oscillation.

It should be noted that the nightside Pc 4 pulsations are expected to have periods longer than 150 seconds, which fall in the period range of Pc 5 pulsations, at larger radial distance than ETS-VI apogee, because they are considered to be the fundamental mode of standing Alfvén waves.

Oscillation lasting for long time (~ 10 minutes). The nightside Pc 4 pulsations were observed in continuous waveforms lasting for about 10 minutes (Figure 3.5). If the nightside Pc 4 pulsations are excited by impulsive energy source, which will be discussed later, duration of the pulsations depends on Joule dissipation in the ionosphere. Here we calculated the damping rate of the nightside Pc 4 pulsation which were derived by *Ellis and Southwood* [1983] with an emprical model of the ionospheric Pedersen conductivity [*Spiro et al.*, 1982].

Figure 3.9 shows ILAT dependence of the height-integrated Pedersen conductivity by *Spiro et al.* [1982] in the postmidnight sector (01–02MLT) for 300 nT<AE≤600 nT condition. The height-integrated Pedersen conductivity has large value (>8 mho) in the ILAT range of 63°–67°ILAT and a peak of 10.4 mho at 65°ILAT. *Ellis and Southwood* [1983] gives the damping rate of standing Alfvén waves γ by the form:

$$\gamma = \frac{V_A}{l} \ln \left\{ \left| \frac{\Sigma_A - \Sigma_P}{\Sigma_A + \Sigma_P} \right|^{-1} \right\},$$

where V_A is the Alfvén speed, l is the length of the geomagnetic field line, Σ_A is the Alfvén conductivity, and Σ_P is the height-integrated Pedersen conductivity. If we take V_A~3000 km/s, l~1.2×10^8 m, and Σ_A~0.5 S, the duration of the pulsation τ ($=\gamma^{-1}$) are calculated as a function of Σ_P (Table 3.3). Table 3.3 indicates that pulsations around 63°–67°ILAT on the nightside last for 6–7 minutes. Because the duration of the pulsation τ is defined as the time in which the wave amplitude decays to $\frac{1}{e}$ (*i.e.*, about 37%) of its initial amplitude, we can expect that pulsations appear with observable amplitude for a little longer than the estimated duration (6–7 minutes). This result is rather consistent with the observation.

Energy source and excitation mechanism. We expect magnetospheric substorms as a likely excitation source for the nightside Pc 4 pulsations, because substorms are distinctive phenomena occurring on the nightside. The above calculation that even pulsations which are excited by an impulsive source can be sustained for a little longer than 6–7 minutes also supports our expectation. To test the validity of our expectation, we utilized the magnetic field data from the Kakioka (KAK) ground observatory (26.9° geomagnetic latitude, LT=UT+9).

The first panel of Figure 3.10 gives the magnetic field variation in the azimuthal component observed by ETS-VI, which is the same event as that of Figure 3.5, and the second and third panels show the H- and D-components of the geomagnetic field at Kakioka. ETS-VI and Kakioka were around 02–03MLT and 22–23MLT, respectively. In the first panel three nightside Pc 4 pulsations in the magnetosphere appeared from 1302:00UT, 1312:30UT, and 1332:30UT which are indicated by arrows. These waves had continuous waveforms with periods of 80–100 seconds. The vertical broken lines show onset time of waves observed on the ground (1301:00UT, 1312:30UT, and 1332:30UT). We notice that these waves had periods of about 60 seconds and were damped within a few cycles, though the nightside Pc 4 pusations observed by the ETS-VI satellite lasted for about 10 minutes. Thus we consider these waves to be low-latitude Pi 2 pulsations, which are closely related to magnetospheric substorms [e.g., *Saito et al.*, 1976; *Sakurai and Saito*, 1976]. Comparing the arrows in the first panel with the vertical lines, we see that the onset of the nightside Pc 4 pulsation is simultaneous to or one minute later than that of the low-latitude Pi 2 pulsation. This fact shows that the nightside Pc 4 pulsations occur at almost the same time of magnetospheric substorms.

Figure 3.11 shows another event of nightside Pc 4 pulsation and low-latitude Pi 2 pulsation, which appeared on 27 December 1994, in the same format as Figure 3.10. A nightside Pc 4 pulsation started at 1054:00UT and continued to oscillate for about 15 minutes. At Kakioka a low-latitude Pi 2 pulsation whose onset time was 1053:00UT was observed around 20.3MLT. Duration of the Pi 2 pulsation is much shorter than that of the nightside Pc 4 pulsation. There is the time difference of one minute between the onset of the nightside Pc 4 pulsation and that of the Pi 2 pulsation. Figures 3.10 and 3.11 lead us to conclude that the nightside Pc 4 pulsations are associated with magnetospheric substorms.

We investigated difference of the onset time statistically, which is defined as the onset time of the nightside Pc 4 pulsation minus that of the low-latitude Pi 2 pulsation. Only the events in which Kakioka observed low-latitude Pi 2 pulsations in the MLT range of 19–01MLT were used. The difference of the onset time is plotted against MLT in which ETS-VI observed nightside Pc 4 pulsation (Figure 3.12). A bigger circle in Figure 3.12 represents two events. The time difference is zero or positive for almost all the events. The result indicates that the nightside Pc 4 pulsations appear at the same time of or a few minutes later than the low-latitude Pi 2 pulsations, which is consistent with Figures 3.10 and 3.11. We notice that the difference of the onset time tends to become larger for ETS-VI satellite locations further from the midnight. This shows that the sources for Pc 4 excitation are released at the same time of substorm onset and propagate from midnight to dawn. Drawing a regression line in Figure 3.12, we found that the sources propagated at the velocity of about 45 degrees per 1.2 minutes (1.1×10^{-2} rad/s).

Two possible scenarios are considered for excitation mechanisms of the nightside Pc 4 pulsations. (1) A fast mode wave radiated at substorm onset will excite azimuthally polarized waves at a local magnetic field line, whose eigenfrequency is covered by the the spectrum of the fast mode wave. This scenario is similar to the so-called field line resonance model to explain Pc 5 pulsations on the dayside [*Southwood*, 1974; *Chen and Hasegawa*, 1974]. (2) Energetic electrons injected at substorm onset drift eastward and might excite azimuthally polarized waves through an unspecified wave-particle interaction. We estimated the propagation velocity of sources for both scenarios and compared them with the observed delay times. We assume that the sources for Pc 4 excitation, that is, fast mode Alfvén waves or energetic electrons, are released at 22MLT, around where the occurrence probability of Pi 2 pulsation shows a peak (Figure 2 of *Singer et al.* [1983]). In the case of the first scenario, we calculated the propagation time from a region where the substorm occurred (L=20) to the location of the ETS-VI satellite (L=7) as shown in Figure 3.13, and derived the azimuthal propagation velocity to be 2.1×10^{-2}–2.8×10^{-2} rad/s. Even if we assume that the substorm occurred at a region closer to the earth (L=15, 10, and 8), the estimated azimuthal propagation velocity (2.3×10^{-2}–3.0×10^{-2} rad/s, 2.5×10^{-2}–4.0×10^{-2} rad/s, and 2.7×10^{-2}–4.8×10^{-2} rad/s, respectively) is not so different from that for L=20. In the second scenario, the energetic electrons were assumed to be injected to the region around L=7 and drift eastward. In the dipole magnetic field, the particle's bounce averaged drift velocity ω_d is given as follows [*Hamlin et al.*, 1961]:

$$\omega_d \sim \frac{3v^2}{\Omega_c(R_E L)^2}(0.35 + 0.15\sin\alpha),$$

where v is particle velocity, Ω_c is the gyrofrequency, R_E is the Earth's radius, and α is the equatorial pitch angle. If we take electrons with energy of 3–30 keV and pitch angle of 90° at L=7, we obtain ω_d~5.1×10^{-5}–5.1×10^{-4} rad/s. The estimation for Alfvén wave velocity are consistent with the observational result, but the estimated drift velocity of energetic electrons is much smaller than the observed. We therefore adopt the first scenario for excitation mechanism of the nightside Pc 4 pulsations.

Figure 3.12 shows that events in which the difference of the onset time is zero were found in the MLT range from 23.6MLT through midnight to 2.7MLT. This means that the propagation time of fast mode Alfvén wave from substorm occurrence region to the location of ETS-VI in the MLT range of 23.6–2.7MLT is the same as that from substorm occurrence region to the ground (Figure 3.13). From the calculation of the propagation time, we found that the fast mode Alfvén wave can propagate to the region of 1.4MLT at L=7 while fast mode Alfvén wave propagate from substorm occurrence region to the ground. The MLT value of 1.4MLT is contained in the observed MLT range of 23.6–2.7MLT. This result supports the first scenario that fast mode Alfvén waves excite the nightside Pc 4 pulsations. The spread of the observed MLT range of 23.6–2.7MLT is thought to be caused by change of the location where substorm occurred.

Comparison with the previous studies. Figure 3.6 indicates that the nightside Pc 4 pulsations occur more frequently in the postmidnight sector (23–04MLT) than in the premidnight sector (19–23MLT). The occurrence probability of the nightside Pc 4 pulsations has a minimum around 22–23MLT consistent with the result of *Saka et al.* [1996a]. Thus we can say that the occurrence of the nightside Pc 4 pulsations has an asymmetry to the substorm occurrence region. *Takahashi et al.* [1996] found a similar asymmetry in occurrence of TTW, and considered that masking effects due to nonsinusoidal magnetic fluctuations following substorms are more prominent in the premidnight sector. We suggest that the asymmetry in nightside Pc 4 occurrence might be explained by an asymmetry in the ionospheric Pedersen conductivity. Figure 3.14 shows MLT dependence of the average ionospheric Pedersen conductivity in the region of 64°–68°ILAT for 300 nT<AE$\leq$600 nT condition, which was derived from Table A2 of *Spiro et al.* [1982]. The Pedersen conductivity for 23–04MLT (8.5–9.5 mho) is higher than that for 19–23MLT (4.5–8.0 mho). As we can see in Table 3.3, the smaller the ionospheric Pedersen conductivity, the shorter the duration of pulsations. Therefore pulsations in the premidnight sector (19–23MLT) are damped more quickly and less readily observed than those in the postmidnight sector (23–04MLT). We consider that irregular magnetic disturbances accompanying substorm onsets are localized around the substorm occurrence region, and these disturbances cause the smallest occurrence probability of Pc 4 around 22–23MLT by masking or changing continuous waveforms of the nightside Pc 4 pulsations.

We concluded that the nightside Pc 4 pulsations are the fundamental mode of standing Alfvén waves. This is consistent with the results by *Takahashi et al.* [1996] that TTWs are standing Alfvén waves on individual magnetic field lines, which are suggested from the TTW frequencies at two satellites (AMPTE/CCE and GOES-5) and the phase relationship between oscillations in magnetic field and ion flux anisotropy.

Takahashi et al. [1996] solved the axisymmetric toroidal mode equation with the ionospheric conductivity model and concluded that a TTW lasts for about 5 cycles for $L\sim7$. If we assume the period of pulsations of 80–100 seconds, we found that a TTW lasts for 400–500 seconds. This duration is consistent with our calculation of 6–7 minutes.

Takahashi et al. [1996] proposed a change in magnetospheric convection during substorms for energy sources for TTW. The change of magnetospheric convection is transmitted to the ionosphere via Alfvén waves, and leads to damped transient standing Alfvén waves. They insisted that TTW is excited by even a small substorm or pseudo substorm which could change the convection pattern. *Saka et al.* [1996a, b] presented a model in which plasma pressure generated in the nightside magnetosphere in association with energetic particle injections acts as an in situ sources of QPO. They showed an azimuthal pressure gradient provided by energetic particle injections increases the field line curvature and leads to transient field line oscillations. Using the electron flux data for the energy ranges 30–300 keV from the geosynchronous satellites, *Saka et al.* [1996b] demonstrated that QPO observed by GOES-5 diminished when the pressure gradient was reduced. From a viewpoint of propagation velocity of sources, we consider that the nightside Pc 4 pulsations are excited through coupling to the fast mode Alfvén waves which are radiated at substorm onsets, rather than excited by energetic electrons injected at substorm onset. Even if we take high-energy electrons (30–300 keV), the estimated drift velocity of these electrons (5.1×10^{-4}–5.1×10^{-3} rad/s) is still smaller than the observation. The fast mode Alfvén waves are thought to be radiated at even a pseudo substorm onset, because Figure 6b of *Takahashi et al.* [1996] showed that a Pi 2 pulsation appeared in association with a pseudo substorm. Thus the excitation mechanism of the nightside Pc 4 pulsations proposed in this study is available in both cases of substorms and pseudo substorms.

The excitation mechanism proposed above is supported by the first and second events in Figure 3.5, in which short-lived disturbances in the compressional ($\Delta B_{\parallel}$) component appeared to be coincident with the nightside Pc 4 pulsations. These compressional disturbances are thought to be the fast mode Alfvén waves which were launched at substorm onsets and excited the nightside Pc 4 pulsations. It should be noted that the amplitudes of these compressional disturbances were very small (0.4 nT and 0.8 nT for the first and second events, respectively). In the third event in Figure 3.5, however, there was no clear disturbances in the compressional component at 1332UT when the nightside Pc 4 pulsation started. We can expect that the magnitude of substorm in the third event was smaller than that in the second event, because amplitude of the ground Pi 2 pulsation in the third event was smaller than that in the

second event (Figure 3.10). Thus one of the possible interpretations of this event is that the amplitude of compressional disturbances was so small that the magnetometer on board ETS-VI could not detect the disturbance (Note that the resolution in Range-H was 0.125 nT.). In the another interpretation, this event might be explained by the model proposed by *Takahashi et al.* [1996] because their model needs no consistent compressional disturbances at the onset of TTW. Although the propagation velocity of magnetospheric convection change is not clear, it might be as large as that of fast mode Alfvén waves. Further studies will be necessary to conclude which one of the three mechanisms is the most plausible.

A few previous studies have reported azimuthally polarized Pi 2 pulsations observed by satellites. Pi 2 pulsation which was dominant in the east-west component was observed by ATS-6 around 02MLT [*Kuwashima*, 1983]. *Sakurai and McPherron* [1983] found Pi 2 pulsation with an obvious sinusoidal oscillation only in the east-west component which were observed by ATS-6 around 02LT. Though these pulsations were called as Pi 2 pulsation, they should be classified into the nightside Pc 4 pulsations because they have continuous waveforms which are dominant in the azimuthal component and were observed around 02MLT where we found an occurrence peak of the nightside Pc 4 pulsations.

3.5 Conclusions

The magnetic field data from the ETS-VI satellite were analyzed statistically to investigate magnetic pulsations in Pc 3–5 bands. We found prominent features in the occurrence distributions of the four pulsations: (1) azimuthal Pc 5 pulsation; (2) azimuthal Pc 3 pulsation; (3) radial Pc 4 pulsation on the dayside; (4) azimuthal Pc 4 pulsation on the nightside. The main results for these pulsations are as follows.

1. The azimuthal Pc 5 pulsations occur frequently in the MLT ranges of both 05–09MLT and 15–18MLT, and are observed mostly in the off equatorial region. They are considered as the fundamental mode of the standing Alfvén waves. The energy of the azimuthal Pc 5 pulsations is thought to be supplied by the Kelvin-Helmholtz instability on the magnetopause.

2. The azimuthal Pc 3 pulsations appear frequently in the wide MLT range of 07–16MLT. The azimuthal Pc 3 pulsations are thought to be higher harmonics of the standing Alfvén waves, which can explain the observation that the frequencies of Pc 3 pulsations become lower as the satellite moves away from the earth.

3. The radial Pc 4 pulsations have high occurrence on the afternoon side (11–20MLT) and an occurrence peak in the MLT-ILAT area of 14–16MLT and 66°–67.5°ILAT. They might be excited by bounce resonance, as suggested by the previous studies [*Arthur and McPherron*, 1981; *Takahashi and McPherron*, 1984; *Anderson et al.*, 1990a, *Takahashi and Anderson*, 1992].

4. We have investigated in detail the azimuthal Pc 4 pulsations on the nightside (nightside Pc 4 pulsations), which were called as TTW by *Takahashi et al.* [1996] and as QPO by *Saka et al.* [1996], and obtained the following results.

(a) The nightside Pc 4 pulsations have high occurrence in the MLT range of 23–04MLT and an occurrence peak at 01–02MLT.

(b) They are considered as the fundamental mode of the standing Alfvén waves. This is supported by correspondence between the eigenperiod calculated from standing wave model and the observed period, and the observation that the nightside Pc 4 pulsations are less observed near the geomagnetic equator.

(c) The nightside Pc 4 pulsations continue to oscillate for about 10 minutes, which are expected from calculation of damping rate of standing waves on the nightside.

(d) The nightside Pc 4 pulsations start at almost the same time of magnetospheric substorm onsets, but they are different from Pi 2 pulsations in the magnetosphere. They are thought to be excited through coupling to the fast mode Alfvén waves launched at substorm onsets.

The excitation mechanism(s) for the radial Pc 4 pulsations on the dayside was left for future study. In respect of the nightside Pc 4 pulsations, we have proposed an excitation mechanism which is different from the mechanism proposed by *Takahashi et al.* [1996] and that by *Saka et al.* [1996a, b]. It will be necessary to examine by further studies which one of the three excitation mechanisms is the most plausible. A simultaneous observation by satellites and ground stations which are on the same geomagnetic field line will be important to investigate the nightside Pc 4 pulsations.

Chapter 4

Dayside Pi 2 pulsations observed at low-latitude ground station

4.1 Introduction

Dayside Pi 2 pulsations have been investigated mostly from a viewpoint of simultaneous occurrence with nightside Pi 2 pulsations. *Yanagihara and Shimizu* [1966] investigated simultaneous occurrence of dayside Pi 2 pulsations at the dip equator, using the rapid-run magnetograms at Fredericksburg (49.6° geomagnetic latitude (GMLAT)), Koror (−3.2°GMLAT), and Guam (3.9°GMLAT). They found that among 112 Pi 2 pulsations observed at Fredericksburg in the night hours, 74 events correspond clearly in occurrence time and phase to those observed on the dayside at Koror and Guam. *Stuart and Barsczus* [1980] reported that 59 of the 83 Pi 2 pulsations observed at Eskdalemuir (58.5°GMLAT) are coincident with daytime Pi 2's identified at Pamatami (15.3°GMLAT). About 40% of nightside Pi 2 events identified at Fredericksburg correspond with dayside Pi 2 pulsations identified at low-latitude Onagawa station [*Yumoto et al.*, 1980]. *Sutcliffe and Yumoto* [1989, 1991] investigated the occurrence of dayside Pi 2 pulsations, utilizing the Correlated data Adaptive Noise Canceling (CANC) method. *Sutcliffe and Yumoto* [1989] reported that dayside Pi 2 pulsations which correspond to nightside Pi 2 pulsations at low-latitude (Onagawa) are identified commonly (83%) at low latitude (Hermanus) and occasionally (18%) at mid-latitude (Marion). *Sutcliffe and Yumoto* [1991] found that 29 nighttime Pi 2 pulsations were identified at Hermanus, of which 24 events (79%) were accompanied by daytime Pi 2 pulsations at Onagawa. Using geomagnetic field measurements at Green Hill (52°GMLAT) and L'Aquila (42.5°GMLAT), *Villante et al.* [1992] showed clear dayside Pi 2-like pulsations can occasionally be detected at mid-latitude.

Some previous authors reported equatorial enhancement of dayside Pi 2 pulsations in the equatorial region. *Yanagihara and Shimizu* [1966] found that an amplitude of dayside Pi 2 at equatorial region is about 4 times as large as that at Kakioka (26.0°GMLAT). Daytime Pi 2's existed in a narrow band belt around the equator [*Stuart and Barsczus*, 1980]. *Sastry et al.* [1983] examined the ratio of Pi 2 amplitude in the H-component observed at Etaiyapuram (−0.6°GMLAT) to that at Choutuppal (7.5°GMLAT) and found the average value of the ratio reaching maximum of 2.6 between 11 and 12LT. They suggested that the enhancement of daytime Pi 2 pulsations is ascribed to the enhanced ionospheric conductivity in the equatorial electrojet region. Recently, *Shinohara et al.* [1997] showed that the amplitude of daytime Pi 2 pulsations at dip equator is 3–4 times those at low-latitude, using multipoint measurements from the 210° magnetic meridian magnetometer chain. The phase of daytime Pi 2 pulsation at dip equator is found to lag ∼34° behind those at low-latitude. They suggested that the dayside Pi 2 pulsations at the equator are caused by the electric field which penetrates from the nightside polar ionosphere to the dayside equatorial ionosphere.

An excitation mechanism for dayside Pi 2 pulsations at low-latitudes was proposed by some authors. *Sutcliffe and Yumoto* [1991] found that spectra of the dayside and nightside Pi 2 pulsations are almost identical, and concluded that these characteristics are a consequence of the cavity mode nature of low-latitude Pi 2 pulsations. The periods of Pi 2 pulsations detected at high- and low-latitude stations on

the nightside and those at low-latitude station on the dayside are found to be identical by *Yumoto et al.* [1990]. They also suggested that Pi 2 events are a forced field line oscillation of global scale, coupled with the magnetospheric cavity resonance wave in the inner magnetosphere. *Yumoto* [1990] reviewed the wave characteristics of global Pi 2 pulsations and proposed magnetospheric cavity model for excitation mechanism.

In this chapter we investigated dayside Pi 2 pulsations observed at Mineyama observatory (25.5°GMLAT). Dayside Pi 2 pulsations are shown to be rather common phenomena. We found new characteristics of dayside Pi 2 pulsations which support the magnetospheric cavity model.

4.2 Analysis

We investigated statistical characteristics of Pi 2 pulsations observed at Mineyama from November 1994 through June 1996, using an algorithm to detect Pi 2 pulsation automatically, which is based on the wavelet analysis (Appendix A). Dayside Pi 2 pulsations are mainly concerned, because only a few papers treat their characteristics statistically.

4.2.1 Preparation of Pi 2 list

Pi 2 pulsations were selected from the Mineyama data by utilizing the algorithm to detect Pi 2 pulsations and other selection procedures, as illustrated in Figure 4.1. In the first step, we analyzed the H- and D-components of the 1-second-resolution geomagnetic field data from Mineyama by the algorithm to detect Pi 2 pulsations (Appendix A), and made a list of events.

In the second step, we checked if the detected events are associated with clear substorm signatures, in order to ensure Pi 2 selection. A longitudinally asymmetric (ASY) disturbance index [*Iyemori et al.*, 1992] are used to identify substorm, because ASY-H and ASY-D indices show variations which correspond to mid-latitude positive bay at substorm onset [*Iyemori and Rao*, 1996]. An event which satisfies the following two criteria is identified as a substorm-associated event. (1) ASY-H or ASY-D index shows only small fluctuations for the time interval of 10 minutes before the occurrence of the event (variance for the time period of less than 2.0 nT^2). (2) ASY-H or ASY-D index exhibits a rise more than 10 nT over the time interval of 10 minutes after the occurrence of the event, and besides a rise more than 10 nT over the next time interval of 10 minutes.

In the last step, we also used the geomagnetic field data obtained at 7 high-latitude stations (65.1°–69.7°GMLAT) and the electron flux data from the LANL geosynchronous satellites, in order to identify substorm. The names (geomagnetic latitudes) of the high-latitude stations used here are College (65.1°), Kiruna (65.1°), Pos. de la Baleine (66.2°), Fort Churchill (68.5°), Barrow (69.1°), Yellowknife (69.1°), and Leirvogur (69.7°). We checked if (1) the event shows decaying oscillation; (2) the H-components of the magnetic field data at high-latitude decrease after midnight or increase before midnight around the occurrence time of the event; (3) the LANL geosynchronous satellites observed electron flux enhancement around the occurrence time of the event. Using the criteria above, we identified 251 Pi 2 pulsations associated with clear substorm signatures.

Examples of Pi 2 pulsations detected by this selection procedure are shown in Figure 4.2. Figure 4.2a gives an example of Pi 2 pulsation on the nightside (21.3MLT) observed on 19 April 1996. Pi 2 pulsation with a peak-to-peak amplitude of about 2 nT and a period of about 45 seconds appeared clearly at 1232UT. Figure 4.2b shows an example of Pi 2 pulsation on the dayside (14.4MLT) observed on 20 September 1995. We can see that a distinctive Pi 2 pulsation, which has a peak-to-peak amplitude of about 2 nT and a period of about 80 seconds, appeared even on the dayside. The onset time of this Pi 2 pulsation was 0538UT.

4.2.2 Observational results

MLT dependence of Pi 2 occurrence

Figure 4.3 gives MLT dependence of the occurrence of Pi 2 pulsations observed at Mineyama. Pi 2 pulsations occur frequently in the MLT range of 21–01MLT and have an occurrence peak at 23–00MLT. Although there are dips of number of event at 01–03MLT and 22–23MLT, we consider these dips are due to the statistics based on small number of data set. The number of events decreases generally as the local time shifts from midnight to dawn and dusk sides. This occurrence distribution of the nightside Pi 2 pulsations are consistent with the previous results [*e.g.*, *Saito and Matsushita*, 1968; *Smith*, 1973; *Sakurai and McPherron*, 1983; *Singer et al.*, 1983].

Pi 2 pulsations appear in the wide range of MLT on the dayside (06–18MLT) and have a small occurrence peak at 12–13MLT. Out of 251 events, 60 events of Pi 2 pulsations were observed on the dayside. Thus the ratio of the number of dayside Pi 2 pulsations to that of nightside Pi 2 pulsations was calculated to be about 31% (60/191).

Polarization of Pi 2 pulsation

Figure 4.4 shows examples of Pi 2 pulsation on the dayside. Figure 4.4a gives Pi 2 pulsation which were observed before local noon (7.7MLT). The Pi 2 pulsation started with a negative variation in the H-component at 2242UT. The vertical solid and broken lines in Figure 4.4 indicate the times of peaks and troughs in the H-component of the magnetic field, respectively. Comparing the H- and D-components of the magnetic field, we found that the oscillation in the H-component leads that in the D-component. The relative phase difference between the H- and D-component was derived to be 60° Therefore the Pi 2 pulsation before local noon is right-handed polarized, where the polarization is defined in the H-D plane from a view looking down onto the earth. Pi 2 pulsation observed after local noon (14.6MLT) is shown in Figure 4.4b, which is the same event as that in Figure 4.2b. The H-component of this Pi 2 pulsation also started with a negative variation at 0538UT. The oscillation in the H-component lags behind that in the D-component by the relative phase difference of 134°, indicating that the Pi 2 pulsation after local noon is left-handed polarized.

The polarization of Pi 2 pulsations were examined statistically. Figure 4.5 shows MLT dependence of phase difference ($\Delta\phi_{HD}$) between the H- and D-components, which is defined as the phase of the D-component minus that of the H-component. A left-handed polarized wave is represented by the positive phase difference, and vice versa. A small dot in Figure 4.5 corresponds to one Pi 2 event which has the coherency between the H- and D- components more than 0.70. We can see three clusters of dots in Figure 4.5, that is, first cluster after local midnight with $\Delta\phi_{HD}$~90°–180°, second cluster before midnight with $\Delta\phi_{HD}$~0°–90°, and third cluster on the dayside with $\Delta\phi_{HD}$ which depends on MLT. The first and second clusters of dots indicate that (1) Pi 2 pulsations on the nightside are predominantly left-handed polarized; (2) the major axis of the wave ellipse is located in the first (third) quadrant of the H-D plane before midnight, and in the second (fourth) quadrant after midnight. These characteristics of the nightside Pi 2 pulsations are consistent with those at mid-latitude stations reported by the previous studies [*e.g.*, *Lester et al.*, 1983, 1984; *Lanzerotti and Medford*, 1984]. The third cluster of dots shows that the polarization is right-handed before local noon and left-handed after local noon. The examples of polarization found in Figure 4.4 are consistent with this statistical result. We also found that the phase difference of dayside Pi 2 pulsations is roughly proportional to MLT, that is, the phase difference increases from about −180° around dawn side through about 0° at local noon to about 180° around dusk side. The characteristics of Pi 2 polarization on the dayside are quite different from those on the nightside.

Wave power of Pi 2 pulsation

Figure 4.6 shows MLT dependence of power spectral density of Pi 2 pulsations in the H-component. The power spectral density which is subtracted background level are indicated by small open squares. We used only Pi 2 events which are associated with ASY index whose rise to the peak is less than 40 nT, because wave power of Pi 2 pulsations could depend on magnitude of substorms. The large diamonds in

the Figure 4.6 indicate running averages of power spectral density for the interval of 3 hours of MLT, and are plotted in the center of the interval. For the interval in which the number of events (small open squares) is small, large diamonds are not shown. We found a peak of wave power around local noon and dips on both dawn and dusk sides. The average wave power around local noon is about $10^{0.5}$ times as large as that at dawn/dusk side.

4.3 Discussion

We found from Figure 4.3 that the number of dayside Pi 2 pulsations is about 31% of that of nightside Pi 2 pulsations. This result can be interpreted that about 31% of nightside Pi 2 pulsations have simultaneous occurrence of dayside Pi 2 pulsations. Some previous studies reported that 71–83% of the nightside Pi 2 pulsations correspond to dayside Pi 2 pulsations at low-latitude [*Stuart and Barsczus*, 1980; *Sutcliffe and Yumoto*, 1989, 1991]. The difference of the rate of dayside Pi 2 observation between this study and the previous studies is thought to be due to the difference of the detection procedure, that is, in previous studies dayside Pi 2 pulsations were identified using the onset times of nightside Pi 2 pulsations as reference or the CANC method, but in this study dayside Pi 2 pulsations were detected by the same procedure as that for nightside Pi 2 pulsations. The rate of dayside Pi 2 observation will have much larger value than 31% if we adopt a detection procedure similar to that in the previous studies. Thus we conclude that Pi 2 pulsations are observed commonly even on the dayside, which suggests that Pi 2 pulsations are global phenomena.

Figure 4.7a shows the H-component of dayside Pi 2 pulsation observed on 19 March 1996 at Mineyama. The magnetic field data in the period from 120 seconds before the onset time (0358UT) to 392 seconds after the onset time are shown. This dayside Pi 2 pulsation had a period of about 60 seconds and a duration of about 5 minutes. We calculated a power spectral density for the period of 512 seconds using a Fast Fourier Transform method. The power spectral density, which is subtracted background level, is shown in Figure 4.7b. We notice that three harmonics are clearly observed at 17.6 mHz, 29.3 mHz, and 39.1 mHz, which correspond to periods of 56.8 seconds, 34.1 seconds, and 25.6 seconds, respectively. It should be noted that the fundamental harmonic wave has the strongest power. The period of the fundamental harmonic wave is consistent with the observation in Figure 4.7a. The ratio from the fundamental to the third harmonic is 1:1.66:2.22, which accords with the previous observation of 1:(1.5±0.3):(2±0.4) by *Lin et al.* [1991]. To explain this frequency ratio, *Lin et al.* [1991] solved the MHD equations in the rectangular box in x-z plane which corresponds to the meridian plane of the magnetosphere, and showed that frequency ratio of the waves excited by a magnetosphere cavity model is about 1:1.5:2.0.

The results that dayside Pi 2 pulsations are observed commonly and have frequency ratio of 1:1.5:2.0 strongly suggest that they are due to magnetospheric cavity mode waves. Figure 4.8a shows a fundamental mode oscillation of magnetospheric cavity mode waves at $t=(n+\frac{1}{4})T$, where T is a wave period, n is an integer, and $t=0$ corresponds to the onset time of dayside Pi 2 pulsations. The left panel of Figure 4.8a illustrates displacement of geomagnetic field lines in the equatorial plane on the dayside. An arc of the largest semicircle represents the magnetopause. The right panel of Figure 4.8a shows the configuration of the geomagnetic field lines in the meridian plane of 12MLT. For simplicity, the magnetosphere is represented by a box with straight field lines. We suppose that the oscillation was caused by a compressional wave which was launched at substorm onset. The compressional wave is thought to be trapped effectively in the local time region where the wave normal is perpendicular to the inner and outer boundaries [*Takahashi et al.*, 1995]. Thus the wave trapped most effectively will be found in the meridian plane which includes substorm occurrence region, that is, around midnight. The compressional wave propagating to the dayside hemisphere could also establish cavity model oscillation effectively around local noon. This idea led us to depict Figure 4.8a with the outward initial displacement of the magnetic field lines which has the largest amplitude around local noon. We assume perturbations in the radial component in the magnetosphere map to the ground in the H-component without phase changes, because the cavity mode wave is due to fast mode waves which are not rotated by transmitting the ionosphere. [*Hughes and Southwood*, 1976; *Nishida*, 1978; *Kivelson and Southwood*, 1988]. This assumption was also adopted by *Takahashi et al.* [1995] and *Allan et al.* [1996], which treated the cavity mode waves on the

nightside. Therefore it is expected that the ground stations at both northern and southern hemispheres observe decreases of the H-component at the onset of dayside Pi 2 pulsations as shown in the right panel of Figure 4.8a, which is consistent with the observations of Figure 4.4. We can expect that the amplitude of dayside Pi 2 pulsations in the H-component has a peak around local noon and minimum values at both dawn and dusk sides. This expectation is in accordance with the observational result shown in Figure 4.6 and the previous observation by *Lin et al.* [1991] in which large-amplitude Pi 2 pulsations are more frequently observed during local noon (11–13LT) and midnight (23–01LT).

The left panel of Figure 4.8a shows that the oscillation in the H-component has the identical phase in all range of MLT on the dayside. The observations show that the phase difference between H- and D-components, which is defined as the phase of the D-component minus that of the H-component, changes from about $-180°$ around dawn side through about $0°$ at local noon to about $180°$ around dusk side (Figure 4.5). Therefore the phase of dayside Pi 2 oscillation in the D-component is thought to depend on MLT, as shown in Figure 4.8b. This MLT dependence of the phase suggests that wave which causes the oscillation in the D-component propagates westward, that is, from dusk side through local noon to dawn side. The azimuthal wave number m of the westward propagating wave was estimated to be about 2 from Figure 4.8b. *Li* [1994] showed that the azimuthal wave numbers of nightside Pi 2 pulsations at $L\sim-1.6$ are small (typically $|m|<3$) with predominantly westward propagation and the absolute values of m number derived from the D-component are larger than those from the H-component. If the waves described by *Li* [1994] can propagate to the dayside through dusk side, it is consistent with our estimation.

In this chapter, we showed some new characteristics of dayside Pi 2 pulsations such as MLT dependence of wave power or phase difference between H- and D-components, and proposed an excitation model of dayside Pi 2 pulsations in which the H- and D-components are due to the cavity mode waves and the westward propagating waves with $|m|\sim2$, respectively. This model was rather consistent with statistical results derived from Mineyama observation. However, there still remain some problems. (1) Is the coincidence of frequency between the cavity mode waves and the westward propagating waves plausible? (2) Why the waves which cause the D-component oscillation propagate westward? To solve these problems further studies will be needed. Observations of ground stations which distribute longitudinally at low-latitude will give some clues to investigate azimuthal propagation of Pi 2 pulsations. Simultaneous observations of ground stations and satellites on the dayside will be also useful.

4.4 Conclusions

Pi 2 pulsations observed at Mineyama observatory were studied statistically. We focused on dayside Pi 2 pulsations. The followings are the main results.

1. Pi 2 pulsations occurred frequently near local midnight, but they were observed even on the dayside (06–18MLT). The ratio of the number of Pi 2 pulsations on the dayside to that on the nightside was about 31%.
2. Pi 2 pulsations on the nightside have predominance of left-handed polarization, and the major axis of the wave ellipse which is located in the first (third) quadrant of the H-D plane before midnight and in the second (fourth) quadrant after midnight. The polarization of the dayside Pi 2 pulsations changed from right-handed before local noon to left-handed after local noon. Dayside Pi 2 pulsations have the phase difference between H- and D-components which is generally proportional to MLT.
3. Wave power of dayside Pi 2 pulsations in the H-component has a peak around local noon and dips on both dawn and dusk sides.

An excitation model of dayside Pi 2 pulsations based on the cavity model was suggested to interpret these observations.

Appendix A

Automated detection of Pi 2 pulsations using wavelet analysis for substorm monitoring

A.1 Introduction

It is generally accepted that Pi 2 pulsations are almost always observed on the ground at substorm onsets and appear clearly in mid- or low-latitude on the nightside [*Saito et al.*, 1976a; *Saito et al.*, 1976b; *Sakurai and Saito*, 1976]. Substorm onsets are also identified by other phenomena, for example, auroral breakups, sudden increases of the *AE* index, and mid-latitude positive bays. However, Pi 2 pulsations are more useful than these phenomena for substorm detection, because Pi 2 pulsations in mid- or low-latitudes are more sensitive to substorm onset [*Saito et al.*, 1976b]. *Saito et al.* [1976a] proposed "Pi 2 index" to infer the characteristics of the substorm, which can be determined from the induction magnetograms obtained at three low-latitude stations with a mutual longitudinal separation of about 120°

In this paper we describe a real-time detection system for Pi 2 pulsations. In section A.2 its application for nowcasting of substorm onsets will be introduced. In section A.3 we describe the wavelet analysis mathematically, which is utilized to detect Pi 2 pulsations. We show the validity of wavelet analysis for Pi 2 detection in section A.4. In section A.5 the automated Pi 2 detection system at Mineyama observatory is explained and detection results are presented.

A.2 Application for Nowcasting of Substorm Onsets

The project aims at the nowcasting of substorm onsets by detecting Pi 2 pulsations in real-time using wavelet analysis. We use real-time geomagnetic field data, with a sampling rate of 1 second, obtained at mid- and low-latitude stations (Mineyama in Japan, the York SAMNET station in the U.K., and Boulder in the U.S.) shown in Figure A.1. The locations of the three stations are listed in Table A.1. These stations are each separated by about 120° in longitude, so at least one station is on the nightside at all times. The real-time data are analyzed, using essentially the same algorithm for detecting Pi 2 pulsations at each station, and the detection results will be exchanged among these stations via the Internet. Therefore we can obtain information about substorm onsets in real-time, even if we are on the dayside. The results of Pi 2 detection are also useful for statistical studies of Pi 2 pulsations, because Pi 2 pulsations are detected objectively by wavelet analysis.

A.3 Orthonormal Wavelet Analysis

A.3.1 Basics

Wavelet analysis, which has been developed recently, is a suitable method for investigating the wave power of phenomena which are limited in both time and frequency, such as Pi 2 pulsations. Wavelet

analysis is similar to Fourier analysis in respect that the data are expanded by orthonormal functions.

In Fourier analysis, harmonic functions are adopted for the orthonormal functions. Relations between a function $h(t)$ in the time domain and its Fourier transform $H(f)$ in the frequency domain are as follows,

$$h(t) = \int_{-\infty}^{\infty} H(f) e^{i2\pi ft} df, \tag{A.1}$$

$$H(f) = \int_{-\infty}^{\infty} h(t)(e^{i2\pi ft})^* dt, \tag{A.2}$$

where the asterisk denotes the complex conjugate. The Fourier transform is utilized widely to analyze time series data, but it has a problem which comes from the characteristics of the harmonic functions. As the harmonic functions have finite values for $t \rightarrow \pm\infty$, Fourier analysis is sometimes not appropriate to analyze phenomena localized in time.

The basis function of the wavelet transform is localized in time and limited in a specified frequency range, so the time series data are mapped to the time-frequency domain. Thus the wavelet transform has two parameters which correspond to time and frequency. There are two types of wavelet transform, namely, the continuous transform and the discrete transform. The continuous wavelet transform is not orthonormal, but the discrete wavelet can construct an orthonormal set. For time series data $x(t)$, the discrete wavelet transform is expanded as

$$x(t) = \sum_j \sum_k \alpha_{j,k} \psi_{j,k}(t), \tag{A.3}$$

$$\alpha_{j,k} = \int_{-\infty}^{\infty} x(t) \psi^*_{j,k}(t) dt, \tag{A.4}$$

where $\alpha_{j,k}$ is wavelet coefficient and $\psi_{j,k}(t)$ is discrete wavelet set. $\psi_{j,k}$ is constructed from an analyzing wavelet $\psi(t)$, which generates the orthonormal discrete wavelet set, by

$$\psi_{j,k}(t) = 2^{\frac{j}{2}} \psi(2^j t - k), \tag{A.5}$$

where j and k are integers. From Equation (A.5) we can see that j is related to the dilation of $\psi(t)$ and k is related to the shift of $\psi(t)$. Thus j and k correspond to frequency and time, respectively.

Assuming a time series $x(t)$ which has a sampling rate Δt and a number of data points N (N=2^n, n is integer), we will obtain wavelet coefficients $\alpha_{j,k}$ confined in $0 \leq j \leq n-1$ and $0 \leq k \leq 2^j - 1$. The frequency band for each j is $2^j/3T \leq f \leq 2^{j+2}/3T$, where T is the data length (T=$N\Delta t$). Note that the width of time and frequency ranges covered by $\alpha_{j,k}$ are $T/2^j$ and $2^j/T$, respectively. This shows that the wavelet coefficient with a large value of j has high resolution in time and low resolution in frequency, and vice versa. The Nyquist frequency is included in the frequency range supported by the maximum value of j.

A.3.2 Meyer wavelet

A number of analyzing wavelets to generate an orthonormal discrete wavelet set have been found. For example, the Haar wavelet, the Daubechies wavelet, and the Meyer wavelet. It is reasonable to use the Meyer wavelet for analyzing time series data because the Meyer wavelet is band-limited in frequency. The Meyer wavelet is expressed as follows [*Yamada and Ohkitani*, 1991; *Sasaki et al.*, 1992; *Yamanaka et al.*, 1994]:

$$\psi(t) = \frac{1}{2\pi} \int_{-\infty}^{\infty} \Psi(\omega) e^{i\omega t} d\omega, \tag{A.6}$$

where

$$\Psi(\omega) = \begin{cases} 0 & |\omega| \le \frac{8}{3}\pi \\ e^{-i\frac{\omega}{2}}\left[1+\exp\left\{\frac{32}{3}\pi\frac{|\omega|-2\pi}{(|\omega|-\frac{8}{3}\pi)^2(|\omega|-\frac{4}{3}\pi)^2}\right\}\right]^{-\frac{1}{2}} & \frac{4}{3}\pi < |\omega| < \frac{8}{3}\pi \\ e^{-i\frac{\omega}{2}} & |\omega| = \frac{4}{3}\pi \\ e^{-i\frac{\omega}{2}}\left[1+\exp\left\{-\frac{4}{3}\pi\frac{|\omega|-\pi}{(|\omega|-\frac{4}{3}\pi)^2(|\omega|-\frac{2}{3}\pi)^2}\right\}\right]^{-\frac{1}{2}} & \frac{2}{3}\pi < |\omega| < \frac{4}{3}\pi \\ 0 & 0 \le |\omega| \le \frac{2}{3}\pi \end{cases} \quad \text{(A.7)}$$

Figure A.2 shows time plots of the wavelet functions $\psi_{j,k}(t)$ which were generated from the Meyer wavelet with a number of data points N=1024=2^{10} Note that the Meyer wavelet has a symmetrical waveform. From Figures A.2a–A.2c which give examples of wavelet functions with different j's, we see that the smaller the value of j, the more the wavelet functions are dilated. Figures A.2d–A.2f which give examples of wavelet functions with different k's show that the smaller the value of k, the earlier in time the wavelet functions appear. Therefore we can discuss phenomena from the view point of both frequency (j) and time (k). Even if more than one wave packet which have the same frequency appear at different times, these phenomena are characterized by wavelet coefficients with different k's. This is one of the advantages of wavelet analysis.

A.4 Detection of Pi 2 Pulsations by Wavelet Analysis

A.4.1 Example of wavelet analysis

We have analyzed geomagnetic field data from Kakioka (26.9° geomagnetic latitude, 208.3° geomagnetic longitude) for 512 seconds, using the Meyer wavelet. The frequency range and time resolution of the wavelet functions for j=3–9 used in this study are shown in Table A.2. We note that Pi 2 pulsations which have a frequency range from 6.67 to 25.0 mHz are mainly represented by wavelets with j=4 and 5. Examples of the wavelet analysis for the geomagnetic field data from Kakioka are shown in Figure A.3. The left four panels of Figures A.3a–A.3d show the H-component and each panel shows data for the 512 second interval before the time indicated on the top of each panel. Thus it should be noticed that 3 minutes have passed from Figure A.3a (1517UT) to Figure A.3d (1520UT). The right panels show wavelet coefficients for j=4–6 corresponding to the geomagnetic field data in the left panels. Scanning the right panels, we find large wavelet coefficients for j=5 in Figures A.3c and A.3d, which are indicated by shading. It was found in the left panels of Figures A.3c and A.3d that Pi 2 pulsations with a period of about 50 seconds (f~20 mHz) appeared at the same time that the large wavelet coefficients appeared. Therefore we can find Pi 2 pulsations by detecting large wavelet coefficients for j=4 or 5.

In the left panels of Figures A.3a–A.3d, we see that artificial noise with an amplitude of about 1 nT appeared approximately 4 minutes before the onset time of the Pi 2 pulsation. However, this artificial noise like spikes has no effect on the wavelet coefficients for j=4 and 5, because it is too limited in time to be represented by wavelet functions for j=4 and 5. Figure A.4 shows the H-component of the geomagnetic field data, which is the same as that of Figure A.3c, and corresponding wavelet coefficients for j=4–9. The artificial noise in the left panel was represented by the large wavelet coefficient for j=9 which is indicated by an arrow. The Pi 2 pulsation which appeared around 1517UT is represented by a large wavelet coefficient for j=5 and did not affect wavelet coefficients for j=9. Thus we can distinguish spiky noise by checking the wavelet coefficients for large values of j. In the case of Fourier analysis, it is difficult to distinguish artificial noise from other phenomena, because artificial noise like spikes affects the spectral powers in all frequency ranges. The wavelet analysis has the advantage that spiky noise can be distinguished easily from Pi 2 pulsations.

A.4.2 Algorithm for Pi 2 detection

We have developed an algorithm to detect Pi 2 pulsations automatically. The algorithm consists of procedures to analyze the H- and D-components of the geomagnetic field data every one minute using

the Meyer wavelet and to detect large wavelet coefficients for j=4 and 5. We tested whether the algorithm can detect Pi 2 pulsations properly, using Kakioka data on the nightside (from 18LT through midnight to 06LT) in the period of January 1993. The results of the algorithm detection were compared with those of visual detection.

Comparison between the algorithm detection and the visual detection (Amplitude)

Table A.3 shows the number of events detected by these two methods. Events detected as Pi 2 pulsations by the algorithm were classified into 4 categories (*i.e.*, Quality-AA, -A, -B, and -C), according to peak-to-peak amplitudes of events which were calculated from the value of the wavelet coefficients. Quality-AA represents events whose peak-to-peak amplitudes are more than 3.0 nT. Quality-A, -B, and -C are for events which have peak-to-peak amplitudes from 1.8 nT up to 3.0 nT, from 1.2 nT up to 1.8 nT, and from 0.6 nT up to 1.2 nT, respectively. The detection algorithm neglects events whose peak-to-peak amplitudes given by the wavelet coefficients are less than 0.6 nT. We scanned visually time plots of the raw and bandpass filtered magnetic field data from Kakioka to detect Pi 2 pulsations. The period range of the bandpass filter is from 40 to 150 seconds. Pi 2 pulsations detected visually were also classified into the similar 4 categories as those for the algorithm detection, according to peak-to-peak amplitudes which were determined from the bandpass filtered magnetic field data. The class denoted by X in Table A.3 indicates events which were detected by one detection method but were not detected by the another method. If the difference between the onset time determined by the algorithm and that by the visual detection is less than 3 minutes, we considered that both detection methods found the same event.

We note that 3 Quality-AA events found by wavelet analysis were also detected by the visual inspection as Pi 2 pulsations in Quality-AA. Out of 19 Quality-A events from the algorithm detection, 14 events were also detected visually as Pi 2 pulsations in Quality-A, and 5 events were found by the visual inspection as the Pi 2 pulsations in other categories (Quality-AA and -B). Twenty-three events are recognized as Quality-B by both the algorithm and the visual inspection. Fourteen events are found as Quality-B events by the algorithm and as Quality-A or -C pulsations by the visual inspection. There were 4 events which were detected as Quality-B events by the algorithm but were not found by the visual inspection. We notice that out of 239 Quality-C events from the algorithm detection, 159 events were detected visually in the same category (Quality-C) and 22 events were detected visually in the different category (Quality-B), but 58 events were not found by the visual inspection. From Table A.3 we conclude that out of 302 events detected by the wavelet analysis, 240 events (79.5%) were detected as Pi 2 pulsations by the visual inspection, and 199 events (65.9%) were detected visually as Pi 2 pulsations in the same categories as those by the wavelet analysis.

An examination of the 62 events which were not detected by the visual inspection showed that 10 of the events were actual Pi 2 pulsations and 30 of the events were different phenomena from Pi 2 pulsations. It is thought that the visual inspection method failed to detect these 10 events of Pi 2 pulsations. With respect to the rest of the events (22 events), although the onset time of a Pi 2 pulsation was detected properly, the detection algorithm reported occurrence of another event while that Pi 2 pulsations was decaying. Thus the rate of proper detection by this algorithm, which is defined as the ratio of the number of Pi 2 pulsations detected properly to the number of the events detected by the wavelet analysis, is calculated to be 82.8% ((240+10)/302).

It should be noticed that there were 72 Pi 2 pulsations in Quality-C which were not detected by the detection algorithm. These pulsations are thought to have peak-to-peak amplitudes close to 0.6 nT which is the minimum detection threshold of Pi 2 detection for the algorithm.

Comparison between the algorithm detection and the visual detection (Onset time)

From Kakioka data on the nightside (18–06LT) during January 1993, 240 Pi 2 pulsations were detected by both the algorithm and the visual inpection, as indicated in Table A.3. We investigated the difference between the onset time determined by the algorithm detection and that by the visual detection for these 240 events. The onset time of Pi 2 pulsation by the visual detection was determined as the time when a sudden change of the geomagnetic field followed by damped oscillations appeared. The result is presented in Figure A.5a. The onset time difference was defined as the onset time determined by the algorithm

detection minus that by the visual detection. A positive value of the onset time difference means that the onset time by the algorithm detection lags behind that by the visual detection. Figure A.5a shows that the onset time by the algorithm detection is the same as or 1 minute later than that by the visual detection in most of the events. Figures A.5b and A.5c give typical examples of these events. Figure A.5a also shows that there are much more events in the bins of positive time difference than those of negative time difference. Thus we can say that the onset time determined by the algorithm detection tends to lag behind that by the visual detection. We suppose these results are due to the way of Pi 2 detection by the algorithm, that is, detecting a large wavelet coefficient as mentioned above. A large wavelet coefficient corresponds to a peak in oscillation of the geomagnetic field. Thus the onset time determined by the algorithm detection is close to the time of the first peak of a Pi 2 pulsation which lags behind the beginning of a Pi 2 pulsation.

There are some events in the bins of time difference larger than 2 minutes. These events are thought to start oscillating with a small amplitude and then develop amplitudes larger than 0.6 nT a few minutes later. Figure A.5d shows an example of the onset time difference of 2 minutes. Notice that the peak-to-peak amplitude of the Pi 2 pulsation in Figure A.5d was about 0.5 nT at first and increased to about 0.7 nT later.

We found that in 90.8% of the events the onset time determined by the algorithm detection coincides with that by the visual detection with an accuracy of ± 1 minute. The average of the onset time difference is calculated to be +0.56 minutes (+34 seconds).

A.5 Operation at Mineyama Observatory

A.5.1 Pi 2 detection system

We have constructed a system for observation of the geomagnetic field data at Mineyama, which is about 100 km northwest of Kyoto. The data are obtained by a fluxgate magnetometer with a sampling rate of 1 second. We have also constructed both hardware and software systems to detect Pi 2 pulsations automatically for monitoring substorm onsets (Figure A.6). The data obtained by the fluxgate magnetometer are sent to a UNIX work station at Mineyama observatory every minute through a PC, in which a time adjustment is carried out. The geomagnetic field data are analyzed immediately by the software installed in the work station, which contains the algorithm to detect Pi 2 pulsations. If a Pi 2 pulsation is detected, information about the Pi 2 pulsation is transmitted to a work station at Kyoto University through telephone line by UUCP We can obtain the information about Pi 2 pulsations within 3 minutes of the onset time for almost all the events. The detection system has been operating since February 1996.

A.5.2 Detection results

Using the results of detection at Mineyama for the period from February through August 1996, we examined the validity of the detection results. The detection system sometimes fails to distinguish between Pi 2 pulsations and phenomena with same frequency range such as Pc 3–4 pulsations. Thus the events detected by this system were checked visually and classified into 3 categories (*i.e.*, Pi 2 pulsations, Pc 3–4 pulsations, and other phenomena) according to the waveforms. The events classified into Pi 2 pulsations are thought to be those detected properly by this system. Figure A.7 gives the magnetic local time (MLT) dependence of the number of events for each category. On the nightside (18–06MLT), 1736 events were detected by this system. Out of 1736 events, 1447 events were Pi 2 pulsations and the rate of proper detection is calculated to be 83.4%, which is almost the same as that derived from Kakioka data shown in the previous section. If the detection results near local midnight (20–02MLT) are considered, the rate of proper detection has a higher value of 93.2%. Thus we confirm that this detection system works well on the nightside. We found, however, 956 events out of 2043 events on the dayside (06–18MLT) were not Pi 2 pulsations but Pc 3–4 pulsations. Pc 3–4 pulsations were detected frequently in MLT range of 06–09MLT. Besides these Pc 3–4 pulsations, 26.7% (545/2043) of the events on the dayside were phenomena different from both Pi 2 and Pc 3–4, or artificial noises that mainly come from

DC electrified train. We found 542 events of Pi 2 pulsations on the dayside, hence the rate of proper detection on the dayside is 26.5%. It should be noted that the detection results on the dayside contain a large number of phenomena different from Pi 2 pulsations, especially in the MLT range of 06–09MLT. The low rate of proper detection on the dayside will be improved by installing similar systems at both York and Boulder and comparing the results of detection among these three sites. As Pc 3–4 pulsations and other phenomena on the dayside are thought to be observed locally, we can distinguish dayside Pi 2 pulsations from them using detection results at York and Boulder.

The top panel of Figure A.7 shows that Pi 2 pulsations are observed frequently in the MLT range of 19–02MLT and have an occurrence peak around 00–01MLT. The ratio of the number of Pi 2 pulsations with large amplitudes (Quality-AA, -A, and -B) to the number of all Pi 2 pulsations in each MLT bin is high in the MLT range of 19–02MLT. This result means that Pi 2 pulsations with large amplitudes are likely to occur around local midnight. We also found that the ratio of the number of dayside Pi 2 pulsations (18–06MLT) to that of nightside Pi 2 pulsations (06–18MLT) was 37.5% (542/1447).

A.6 Conclusions

In this paper we introduced our project which aims at the nowcasting of substorm onsets by detecting Pi 2 pulsations in real-time using wavelet analysis. We can summarize as follows.

1. For detecting Pi 2 pulsations in real-time we applied wavelet analysis which is a suitable method to investigate waves which are limited in both time and frequency. The Meyer wavelet was adopted as the analyzing wavelet.
2. An algorithm to detect Pi 2 pulsations automatically by wavelet analysis was developed. We tested this algorithm using Kakioka data on the nightside and found that (a) The rate of proper detection of Pi 2 pulsations was 82.8%; (b) In 90.8% of the events the onset time reported by the algorithm was consistent with that determined visually with an accuracy of ± 1 minute.
3. At Mineyama observatory, we have constructed both hardware and software systems to detect Pi 2 pulsations. The detection system has operated since February 1996. From the detection results of the first six months, the rate of proper detection of Pi 2 pulsations was calculated to be 83.4% for the nightside (18–06MLT) and 26.5% for the dayside (06–18MLT). If we use the detection results near local midnight (20–02MLT), the rate of proper detection increases to 93.2%.

We started to operate the Pi 2 detection system at York site in May 1997. In the near future we plan to install a similar system at the Boulder site. As Mineyama and these two stations are each separated by about 120° in longitude, this will make it possible to obtain information about substorm onsets at any time as there will be always at least one station on the nightside.

Acknowledgments

I wish to thank my supervisor, Dr. T. Iyemori for his guidance and concern throughout the study. I also thank Professors M. Sugiura and T. Araki, and Dr. M. Takeda for valuable discussions. The data from the DE-1 and -2 satellites are provided by the courtesy of Drs. J. A. Slavin, N. C. Maynard, and J. D. Winningham. The data from Syowa Station are provided by Dr. N. Sato. ETS-VI data are provided by National Space Development Agency of Japan through Messrs. H. Matsumoto, T. Goka, and Dr. T. Nagai. The electron flux data from the LANL geosynchronous satellites were provided by the courtesy of Dr. G. D. Reeves. I am indebted to Drs. D. K. Milling, D. Orr, H. J. Singer, B. Worthington, and N. Sumitomo for their cooperation in Pi 2 detection project. Thanks are due to Drs. K. Yumoto, K. Takahashi, O. Saka, M. Itonaga, and S. Ohtani for their helpful comments. Drs. S. Machida, T. Kamei, Ms. S. Nakabe, and other colleagues in Kyoto University are acknowledged for daily discussions and helpful comments in seminars. I wish to express my gratitude to my family for their care and encouragement during the study. Part of the analysis was made by using the facilities at the Data Analysis Center for Geomagnetism and Space Magnetism of Kyoto University. This work was supported in part by grants from JSPS Research Fellowships for Young Scientists.

References

Allan, W., F. W. Menk, B. J. Fraser, Y. Li, and S. P. White, Are low-latitude Pi 2 pulsations cavity/waveguide modes?, *Geophys. Res. Lett.*, *23*, 765, 1996.

Anderson, B. J., An overview of spacecraft observations of 10 s to 600 s period magnetic pulsations in the earth's magnetosphere, in *Solar wind sources of magnetospheric Ultra-Low-Frequency waves*, *Geophys. Monogr. Ser.*, vol. 81, edited by M. J. Engebretson, K. Takahashi, and M. Scholer, pp. 1, AGU, Washington, D. C., 1994.

Anderson, B. J., M. J. Engebretson, S. P. Rounds, L. J. Zanetti, and T. A. Potemra, A statistical study of Pc 3-5 pulsations observed by the AMPTE/CCE magnetic fields experiment, 1. Occurrence distributions, *J. Geophys. Res.*, *95*, 10495, 1990a.

Anderson, B. J., T. A. Potemra, L. J. Zanetti, and M. J. Engebretson, Statistical correlations between Pc 3-5 pulsations and solar wind/IMF parameters and geomagnetic indicies, *Physics of Space Plasmas*, *SPI Conference Proceedings and Reprint Series*, Number 10, Scientific Publishers, Inc., Cambridge, MA, 419, 1990b.

Arthur, C. W., and R. L. McPherron, Micropulsations in the morning sector, 3. Simultaneous ground-satellite observations of 10- to 45-s period waves near L=6.6, *J. Geophys. Res.*, *82*, 2859, 1977.

Arthur, C. W., and R. L. McPherron, The statistical character of Pc 4 magnetic pulsations at synchronous orbit, *J. Geophys. Res.*, *86*, 1325, 1981.

de la Beaujardiere, O., J. Watermann, P. Newell, and F. Rich, Relationship between Birkeland current regions, particle precipitation, and electric fields, *J. Geophys. Res.*, *98*, 7711, 1993.

Bilitza, D., International reference ionosphere 1990, National Space Science Data Center, NSSDC/WDC-A-R&S 90-20, Greenbelt, Maryland, 1990.

Chapell, C. R., K. K. Harris, and G. W. Sharp, A study of the influence of magnetic activity on the location of the plasmapause as measured by OGO 5, *J. Geophys. Res.*, *75*, 50, 1970.

Chen, L., and A. Hasegawa, A theory of long-period magnetic pulsations, 1. Steady state excitation of field line resonance, *J. Geophys. Res.*, *79*, 1024, 1974.

Cladis, J. B., and O. W Lennartsson, On the loss of O^+ ions (< 17 keV/e) in the ring current during the recovery phase of a storm, in *Ion Acceleration in the Magnetosphere and Ionosphere*, *Geophys. Monogr. Ser.*, vol. 38, edited by T. Chang, pp. 153, AGU, Washington, D. C., 1986.

Cornwall, J. M., Micropulsations and the outer radiation zone, *J. Geophys. Res.*, *71*, 2185, 1966.

Coroniti, F. V., and C. F. Kennel, Electron precipitation pulsations, *J. Geophys. Res.*, *75*, 1279, 1970.

Cummings, W. D., R. J. O'Sullivan, and P. J. Coleman, Jr., Standing Alfvén waves in the magnetosphere, *J. Geophys. Res.*, *74*, 778, 1969.

Ellis, P., and D. J. Southwood, Reflection of Alfvén waves by non-uniform ionospheres, *Planet. Space Sci.*, *31*, 107, 1983.

Engebretson, M. J., L. J. Zanetti, T. A. Potemra, and M. H. Acuna, Harmonically structured ULF pulsations observed by the AMPTE CCE magnetic field experiment, *Geophys. Res. Lett.*, *13*, 905, 1986.

Farthing, W. H., M. Sugiura, B. G. Ledley, and L. J. Cahill, Jr., Magnetic field observations on DE-A and -B, *Space Sci. Instrum.*, *5*, 551, 1981.

Fujii, R., N. Sato, and H. Fukunishi, H., Upper atmosphere physics data, Syowa Station, 1982, *JARE Data Rep.*, 105, 1985.

Goertz, C. K., Kinetic Alfvén waves on auroral field lines, *Planet. Space Sci.*, *32*, 1387, 1984.

Goertz, C. K., and R. W. Boswell, Magnetosphere-ionosphere coupling, *J. Geophys. Res.*, *84*, 7239, 1979.

Gurnett, D. A., R. L. Huff, J. D. Menietti, J. L. Burch, J. D. Winningham, and S. D. Shawhan, Correlated low-frequency electric and magnetic noise along the auroral field lines, *J. Geophys. Res.*, *89*, 8971, 1984.

Hamlin, D. A., R. Karplus, R. C. Vik, and K. M. Watson, Mirror and azimuthal drift frequencies for geomagnetically trapped particles, *J. Geophys. Res.*, *66*, 1, 1961.

Hasegawa, A., Particle acceleration by MHD surface wave and formation of aurora, *J. Geophys. Res.*, *81*, 5083, 1976.

Hasegawa, A., and L. Chen, Kinetic processes in plasma heating by resonant mode conversion of Alfvén wave, *Phys. Fluids*, *19*, 1924, 1976.

Higuchi, Y., S. Shibuya, and N. Sato, CNA pulsations accompanying hydromagnetic waves at conjugate stations, *Planet. Space Sci.*, *36*, 1255, 1988.

Hoffman, R. A., and E. R. Schmerling, Dynamic Explorer program: An overview, *Space Sci. Instrum.*, *5*, 345, 1981.

Hughes, W. J., Magnetospheric ULF waves: A tutorial with a historical perspective, in *Solar wind sources of magnetospheric Ultra-Low-Frequency waves*, *Geophys. Monogr. Ser.*, vol. 81, edited by M. J. Engebretson, K. Takahashi, and M. Scholer, pp. 1, AGU, Washington, D. C., 1994.

Hughes, W J., and D. J. Southwood, The screening of micropulsation signals by the atmosphere and ionosphere, *J. Geophys. Res.*, *81*, 3234, 1976.

Iyemori, T., T. Araki, T. Kamei, and M. Takeda, *Mid-latitude geomagnetic indices ASY and SYM (provisional) No. 1 1989*, Data Analysis Center for Geomag. and Space Magnetism, Kyoto Univ., Kyoto, 1992.

Iyemori, T., and D. R. K. Rao, Decay of the Dst field of geomagnetic disturbance after substorm onset and its implication to storm-substorm relation, *Ann. Geophysicae*, *14*, 608, 1996.

Jacobs, J. A., Geomagnetic pulsations, in *Physics and Chemistry in Space*, vol. 1, edited by J. G. Roederer, and J. Zähringer, Springer-Verlag, New York, 1970.

Jacobs, J. A., Y. Kato, S. Matsushita, and V A. Troitskaya, Classification of geomagnetic micropulsations, *J. Geophys. Res.*, *69*, 180, 1964.

Kivelson, M. G., and D. J. Southwood, Hydromagnetic waves and the ionosphere, *Geophys. Res. Lett.*, *15*, 1271, 1988.

Kokubun, S., Statistical characteristics of Pc 5 waves at geostationary orbit, *J. Geomag. Geoelectr.*, *37*, 759, 1985.

Kokubun, S., M. G. Kivelson, R. L. McPherron, C. T. Russell, and H. I. West, Jr., Ogo 5 observations of Pc 5 waves: Particle flux modulations, *G. Geophys. Res.*, *82*, 2774, 1977.

Kokubun, S., K. N. Erickson, T. A. Fritz, and R. L. McPherron, Local time asymmetry of Pc 4-5 pulsations and associated particle modulations at synchronous orbit, *J. Geomag. Geoelectr.*, *94*, 6607, 1989.

Kuratani, Y, and K. Igarashi, Riometer records of 30 MHz cosmic noise at Syowa Station, Antarctica in 1982, *JARE Data Rep.*, *87*, 1984.

Kuwashima, M., Wave characteristics of magnetic Pi 2 pulsations in the magnetosphere and on the ground, *Mem. Kakioka Magn. Obs.*, *20*, 1, 1983.

Lanzerotti, L. J., and L. V. Medford, Local night, impulsive (Pi 2-type) hydromagnetic wave polarization at low latitudes, *Planet. Space Sci.*, *32*, 135, 1984.

Lester, M., W J. Hughes, and H. J. Singer, Polarization patterns of Pi 2 magnetic pulsations and the substorm current wedge, *J. Geophys. Res.*, *88*, 1983.

Lester, M., W J. Hughes, and H. J. Singer, Longitudinal structure in Pi 2 pulsations and the substorm current wedge, *J. Geophys. Res.*, *89*, 1984.

Li, X., M. Hudson, A. Chan, and I. Roth, Loss of ring current O^+ ions due to interaction with Pc 5 waves, *J. Geophys. Res.*, *98*, 215, 1993.

Li, Y., Characteristics of low latitude Pi 2 geomagnetic pulsations, Ph. D. Thesis, University of Newcastle, New South Wales, Australia, March, 1994.

Lin, C. A., L. C. Lee, and Y. J. Sun, Observations of Pi 2 pulsations at a very low latitude (L=1.06) station and magnetospheric cavity resonances, *J. Geophys. Res.*, *96*, 21105, 1991.

Lin, C. C., and L. J. Cahill, Jr., Pi 2 pulsations in the magnetosphere, *Planet. Space. Sci.*, *23*, 693, 1975.

Lysak, R. L., Electrodynamic coupling of the magnetosphere and ionosphere, *Space Sci. Reviews*, *52*, 33, 1990.

Maynard, N. C., E. A. Bielecki, and H. F. Burdick, Instrumentation for vector electric field measurements from DE-B, *Space Sci. Instrum.*, *5*, 523, 1981.

Nagai, T., T. Ondoh, H. Matsumoto, T. Goka, T. Fukuda, M. Nosé, T. Iyemori, K. Takahashi, and S. Kokubun, ETS-VI magnetic field observations of the near-earth magnetotail during substorms, *J. Geomag. Geoelectr.*, *48*, 741, 1996.

Nagata, T., S. Kokubun, and T. Iijima, Geomagnetically conjugate relationships of giant pulsations at Syowa base, Antarctica, and Reykjavik, Iceland, *J. Geophys. Res.*, *68*, 4621, 1963.

Newell, P. T., and C.-I., Meng, Ionospheric projections of magnetospheric regions under low and high solar wind pressure conditions, *J. Geophys. Res.*, *99*, 273, 1994.

Newell, P. T., S. Wing, C.-I. Meng, and V. Sigillito, The auroral oval position, structure, and intensity of precipitation from 1984 onward: An automated on-line data base, *J. Geophys. Res.*, *96*, 5877, 1991.

Nishida, A., *Geomagnetic Diagnosis of the Magnetosphere*, Springer-Verlag, New York, 1978.

Nosé, M., T. Iyemori, M. Sugiura, and J. A. Slavin, A strong dawn/dusk asymmetry in Pc 5 pulsation occurrence observed by the DE-1 satellite, *Geophys. Res. Lett.*, *22*, 2053, 1995.

Olbert, S., Summary of experimental results from M.I.T. detector on IMP-1, in *Physics of the magnetosphere*, edited by R. L. Carovillano, J. F. McClay, and H. R. Radoski, pp. 641, Reidel Doredrecht, 1968.

Orr, D., Magnetic pulsations within the magnetosphere: A review, *J. Atmos. Terr. Phys.*, *35*, 1, 1973.

Paquette, J. A., D. L. Matthews, T. L. Rosenberg, L. J. Lanzerotti, and U. S. Inan, Source regions of long-period pulsation events in electron precipitation and magnetic fields at South Pole Station, *J. Geophys. Res.*, *99*, 3869, 1994.

Potemra, T. A., and L. G. Blomberg, A survey of Pc 5 pulsations in the dayside high-latitude regions observed by Viking, *J. Geophys. Res.*, *101*, 24801, 1996.

Saito, T., Long-period irregular magnetic pulsation, Pi 3, *Space Sci. Rev.*, *21*, 427, 1978.

Saito, T., and S. Matsushita, Solar cycle effects on geomagnetic Pi 2 pulsations, *J. Geophys. Res.*, *73*, 267, 1968.

Saito, T., T. Sakurai, and Y. Koyama, Mechanism of association between Pi 2 pulsation and magnetospheric substorm, *J. Atmos. Terr. Phys.*, *38*, 1265, 1976a.

Saito, T., K. Yumoto, and Y. Koyama, Magnetic pulsation Pi 2 as a sensitive indicator of magnetospheric substorm, *Planet. Space Sci.*, *24*, 1025, 1976b.

Saka, O., T. Iijima, H. Yamagishi, N. Sato, and D. N. Baker, Excitation of Pc 5 pulsations in the morning sector by a local injection of particles in the magnetosphere, *J. Geophys. Res.*, *97*, 10693, 1992.

Saka, O., H. Akaki, O. Watanabe, and D. N. Baker, Ground-satellite correlation of low-latitude Pi 2 pulsations: A quasi-periodic field line oscillation in the magnetosphere, *J. Geophys. Res.*, *101*, 15433, 1996a.

Saka, O., O. Watanabe, and D. N. Baker, A possible driving source for transient field line oscillations in the postmidnight sector at geosynchronous altitudes, *J. Geophys. Res.*, *101*, 24719, 1996b.

Sakurai, T., and T. Saito, Magnetic pulsation Pi 2 and substorm onset, *Planet. Space Sci.*, *24*, 573, 1976.

Sakurai, T., and R. L. McPherron, Satellite observations of Pi 2 activity at synchronous orbit, *J. Geophys. Res.*, *88*, 7015, 1983.

Sasaki, F., T. Maeda, and M. Yamada, Study of time history data using wavelet transform, *J. Struc. Eng. Architec. Inst. Japan*, *38B*, 9, 1992 (in Japanese with English abstract).

Sato, N., and S. Kokubun, Interaction between ELF-VLF emissions and magnetic pulsations: Quasi-periodic ELF-VLF emissions associated with Pc 3–4 magnetic pulsations and their geomagnetic conjugacy, *J. Geophys. Res.*, *85*, 101, 1980.

Sato, N., S. Shibuya, K. Maezawa, Y. Higuchi, and Y. Tonegawa, CNA pulsations associated with quasi-periodic VLF emissions, *J. Geophys. Res.*, *90*, 10968, 1985.

Shinohara, M., K. Yumoto, A. Yoshikawa, O. Saka, S. I. Solovyev, E. F. Vershinin, N. B. Trivedi, J. M. Da Costa, and The 210° MM Magnetic Observation Group, Wave characteristics of daytime and nighttime Pi 2 pulsations at the equatorial and low latitudes, *Geophys. Res. Lett.*, *24*, 2279, 1997.

Singer, H. J., W. J. Hughes, and C. T. Russell, Standing hydromagnetic waves observed by ISEE 1 and

2: Radial extent and harmonic, *J. Geophys. Res.*, *87*, 3519, 1982.

Singer, H. J., W J. Hughes, P. F Fougere, and D. J. Knecht, The localization of Pi 2 pulsations: Ground-satellite observations, *J. Geophys. Res.*, *88*, 7029, 1983.

Smith, B. P., On the occurrence of Pi 2 micropulsations, *Planet. Space Sci.*, *21*, 1973.

Snyder, C. W., M. Neugebauer, and U. R. Rao, The solar wind velocity and its correlation with cosmic-ray variations and with solar and geomagnetic activity, *J. Geophys. Res.*, *68*, 6361, 1963.

Southwood, D. J., Some features of field line resonances in the magnetosphere, *Planet. Space Sci.*, *22*, 483, 1974.

Southwood, D. J., J. W. Dungey, and R. J. Etherington, Bounce resonant interaction between pulsations and trapped particles, *Planet. Space Sci.*, *17*, 349, 1969.

Southwood, D. J., and M. G. Kivelson, Charged particle behavior in low-frequency geomagnetic pulsations, 2. Graphical approach, *J. Geophys. Res.*, *87*, 1982.

Spiro, R. W., P H. Reiff, and L. J. Maher, Jr., Precipitating electron energy flux and auroral zone conductances An empirical model, *J. Geophys. Res.*, *87*, 8215, 1982.

Stuart, W. F., and H. G. Barsczus, Pi's observed in the daylight hemisphere at low latitudes, *J. Atmos. Terr. Phys.*, *42*, 487, 1980.

Sugiura, M., Evidence of low-frequency hydromagnetic waves in the exosphere, *J. Geophys. Res.*, *66*, 4087, 1961.

Sugiura, M., A fundamental magnetosphere-ionosphere coupling mode involving field-aligned currents as deduced from DE-2 observations, *Geophys. Res. Lett.*, *9*, 877, 1984.

Sutcliffe, P. R., and K. Yumoto, Dayside Pi 2 pulsations at low latitude, *Geophys. Res. Lett.*, *16*, 887, 1989.

Sutcliffe, P. R., and K. Yumoto, On cavity mode nature of low-latitude Pi 2 pulsations, *J. Geophys. Res.*, *96*, 1543, 1991.

Takahashi, K., ULF waves in the magnetosphere, *Rev. Geophys.*, 1066, 1991.

Takahashi, K., Studies of magnetospheric ULF waves using Active Magnetospheric Particle Tracer Explorers Charge Composition Explorer, *J. Geomag. Geoelectr.*, *46*, 953, 1994.

Takahashi, K., New observations, new theoretical results and controversies regarding Pc 3-5 waves, *Adv. Space Res.*, *17*, (10)63, 1996.

Takahashi, K., and R. L. McPherron, Standing hydromagnetic oscillations in the magnetosphere, *Planet. Space Sci.*, *32*, 1343, 1984.

Takahashi, K., and B. J. Anderson, Distribution of ULF energy (f<80 mHz) in the inner magnetosphere: A statistical analysis of AMPTE CCE magnetic field data, *J. Geophys. Res.*, *97*, 10751, 1992.

Takahashi, K., S. Kokubun, T. Sakurai, R. W McEntire, T. A. Potemura, and R. E. Lopez, AMPTE/CCE observations of substorm-associated standing Alfvén waves in the midnight sector, *Geophys. Res. Lett.*, *15*, 1287, 1988.

Takahashi, K., S. Ohtani, and B. J. Anderson, Statistical analysis of Pi 2 pulsations observed by the AMPTE CCE spacecraft in the inner magnetosphere, *J. Geophys. Res.*, *100*, 21929, 1995.

Takahashi, K., B. J. Anderson, and S. Ohtani, Multisatellite study of nightside transient toroidal waves, *J. Geophys. Res.*, *101*, 24815, 1996.

Villante, U., M. Vellante, M. De Biase, L. J. Lanzerotti, and L. V Medford, Pi 2 pulsations at separated sites ($\Delta\Phi \cong 90°$): a comparison between mid- and low-latitude observations, *Ann. Geophysicae*, *10*, 472, 1992.

Walker, A. D. M., J. M. Ruohoniemi, K. B. Baker, and R. A. Greenwald, Spatial and temporal behavior of ULF pulsations observed by the Goose Bay HF radar, *J. Geophys. Res.*, *97*, 12187, 1992.

Wei, C. Q., J. C. Samson, R. Rankin, and P. Frycz, Electron inertia effects on geomagnetic field line resonances, *J. Geophys. Res.*, *99*, 11265, 1994.

Winningham, J. D., J. L. Burch, N. Eaker, V A. Blevins, and R. A. Hoffman, The low altitude plasma instrument (LAPI), *Space Sci. Instrum.*, *5*, 465, 1981.

Yamada, M. and K. Ohkitani, Orthonormal wavelet analysis of turbulence, *Fluid Dyn. Res.*, *8*, 101, 1991.

Yamanaka, M. D., T. Shimomai, and S. Fukao, A model of quasi-monochromatic field of middle-atmospheric internal gravity waves, *Proc. of the 1992 STEP Symposium/5th COSPAR Colloquium*,

511, 1992.

Yanagihara, K., and N. Shimizu, Equatorial enhancement of micropulsation pi-2, *Mem. Kakioka Mag. Obs.*, *12*, 57, 1966.

Yeoman, T. K., and D. Orr, Phase and spectral power of mid-latitude Pi 2 pulsations: Evidence for a plasmaspheric cavity resonance, *Planet. Space Sci.*, *37*, 1367, 1989.

Yumoto, K., Generation and propagation mechanisms of low-latitude magnetic pulsations – A review, *J. Geophys.*, *60*, 79, 1986.

Yumoto, K., Evidence of magnetospheric cavity Pi 2 waves, *J. Geomag. Geoelectr.*, *42*, 1281, 1990.

Yumoto, K., T. Saito, A. Eitoku, and Y. Kamide, A statistical study of low-latitude Pi 2's associated with magnetospheric substorms, *Proc. Symp. on Magnetosphere and Ionosphere*, held at IASA, Tokyo Univ., on 27–28 Nov., 1980, pp. 139, 1980.

Yumoto, K., T. Saito, and T. Sakurai, Local time asymmetry in the characteristics of Pc 5 magnetic pulsations, *Planet. Space Sci.*, *31*, 459, 1983.

Yumoto, K., K. Takahashi, T. Sakurai, P. R. Sutcliffe, S. Kokubun, H. Lühr, T. Saito, M. Kuwashima, and N. Sato, Multiple ground-based and satellite observations of global Pi 2 magnetic pulsations, *J. Geophys. Res.*, *95*, 15175, 1990.

Figure and Plate captions

Figure 2.1. Transverse Pc 5 pulsation observed by DE-1 on 20 October 1982 (DAY82293). The upper panel ($\Delta B_{\parallel}$) shows variation in the magnetic field tangential to the model magnetic field. The lower two panels ($\Delta B_{\perp 1}, \Delta B_{\perp 2}$) give variations in the plane perpendicular to the model magnetic field, $B_{\perp 1}$ being directed radially outward and $B_{\perp 2}$ eastward. Pc 5 pulsation appeared in the ILAT range between two broken lines.

Figure 2.2. The magnetic and electric field data from DE-2 at the footprint of the high altitude region in which DE-1 observed transverse Pc 5 pulsation as shown in Figure 2.1. The top three panels show the B_x, B_y, and B_z components of the magnetic field perturbation in spacecraft coordinate system, where the x-axis is in the direction of the satellite velocity and the y-axis is upward, with the z-axis completing a right-handed coordinate system. The lower two panels show the E_x and E_y components of the electric field. The sinusoidal disturbances in ΔB_z and E_x appear in the ILAT range between two broken lines where the transverse Pc 5 pulsation was observed by DE-1. The disturbances in ΔB_z and E_x have a good correlation.

Figure 2.3. The paths of DE-1 and -2 in the MLT-ILAT plane for the DAY82293 event.

Figure 2.4. A small scale field-aligned current model to explain the sinusoidal disturbances in ΔB_z and E_x observed by DE-2. The current system have small scale structures latitudinally and uniformity longitudinally.

Figure 2.5. (a) The x-component of the electric field same as the fourth panel of Figure 2.2. (b)–(d) The energy spectra of electron flux for two different pitch angles. (e)–(g) The pitch angle distributions of electron flux for four energies. Each pair of (b, e), (c, f) and (d, g) gives the observation at one of the three epochs indicated by the arrows in Figure 2.5a.

Figure 2.6. The upper and lower panels show the H-component magnetic field data and the riometer data at Fort Yukon, which is located in the same ILAT range as that of the DE-1 and -2 observations for the DAY82293 event. Pc 5 and CNA pulsations were observed 6 hours before DE-1 observed transverse Pc 5 pulsation.

Figure 2.7. The first and second panels give the H-component magnetic field data and the 30MHz riometer data at Syowa Station. The lower two panels present the ELF-VLF wave intensities at the frequency bands of 750 Hz and 1.2 kHz. Syowa Station observed Pc 5 and CNA pulsations 6 hours after the observation of DE-1.

Figure 2.8. (a) MLT dependence of the occurrence time of Pc 5 pulsations at Syowa Station, which were observed in the H-component during the period from August 1981 to February 1983. (b) MLT dependence of average wave power of Pc 5 pulsations in each bin of two hours of MLT. The average wave power of the Pc 5 pulsations accompanied by clear CNA pulsations is indicated by broken line.

Figure 2.9. An example of Pc 5 pulsation accompanied by clear CNA pulsation observed at Syowa Station on 1 June 1982 (DAY82152).

Figure 2.10. The bottom left panel shows MLT dependence of phase difference between Pc 5 and CNA pulsations observed at Syowa Station. The phase difference greater than 0° means that Pc 5 pulsation leads CNA pulsation, and vice versa. The top and bottom right panels show the occurrence number of events against MLT and the phase difference, respectively.

Figure 2.11. (a) The orbit of DE-2 and the location of Syowa Station in the MLT-ILAT plane for the geomagnetic conjunction event on 30 May 1982 (DAY82150). (b) Same as Figure 2.7 for the DAY82150 event. (c) The top and bottom panels show the ΔB_z and E_x data from DE-2, respectively. The data high-pass filtered with a cut-off period of 25 seconds are presented. The sinusoidal disturbances in ΔB_z and E_x which have a good correlation appeared.

Figure 2.12. (a)–(c) Same as Figures 2.11a–c, respectively, except for the event on 19 December 1982 (DAY82353), and a cut-off period of 30 seconds.

Figure 2.13. The altitude dependence of Pc 5 wave structure in radial direction, ion gyroradius, and electron inertia length along the geomagnetic field line of 70°ILAT. The wave structure of Pc 5 pulsation has latitudinal width of 100 km at 400 km altitude.

Figure 2.14. A plausible model of electron precipitation associated with Pc 5 pulsation which has the electric field parallel to the ambient magnetic field due to the ion gyroradius effects.

Figure 2.15. A schematic figure to explain the phase difference between Pc 5 and CNA pulsations observed on the ground in the southern hemisphere.

Figure 2.16. (a) An ionospheric Hall current model to investigate whether or not a small scale resonant structure can produce relevant variations on the ground. (b) The magnetic field variations in the H-component induced on the ground by the current model of Figure 2.16a.

Figure 3.1. An example of azimuthal Pc 5 pulsation observed by ETS-VI on 28 November 1995. The upper three panels are magnetic variations in LMG coordinate system, where the $\Delta B_{\parallel}$ component is the tangential direction of model magnetic field, the $\Delta B_{\perp 1}$ component is perpendicular to the model magnetic field and directed radially outward, and the $\Delta B_{\perp 2}$ component is azimuthally eastward. The bottom two panels show the location of the satellite in solar magnetic coordinate system.

Figure 3.2. Kp dependence of Pc 5 occurrence which was defined as the ratio of the number of the azimuthal Pc 5 pulsations in the MLT range of 04–10MLT and 15–20MLT to the number of data set in each class of Kp index.

Figure 3.3. An example of azimuthal Pc 3 pulsation observed on 18 July 1995. Format is the same as for Figure 3.1.

Figure 3.4. An example of radial Pc 4 pulsation on the dayside observed on 26 July 1995. Format is the same as for Figure 3.1.

Figure 3.5. An example of azimuthal Pc 4 pulsation on the nightside observed on 29 January 1996. Azimuthal Pc 4 pulsations started to oscillate from about 1302UT, 1312UT, and 1332UT, which are

indicated by arrows. Format is the same as for Figure 3.1.

Figure 3.6. Dependence of the nightside Pc 4 pulsation occurrence on MLT. Occurrence probability was defined as the number of pulsation divided by the observation time in each bin of MLT.

Figure 3.7. ILAT dependence of the periods of the nightside Pc 4 pulsations for 23–04MLT. The broken lines show the eigenperiods of the standing Alfvén waves for azimuthal waves calculated from the wave equation of *Cummings et al.* [1969] with plasma density model which has half the values of *Takahashi and Anderson* [1992].

Figure 3.8. Dependence of occurrence of the nightside Pc 4 pulsations on |MLAT|. Occurrence probability was defined as the number of nightside Pc 4 pulsation divided by the observation time in each bin of |MLAT|.

Figure 3.9. ILAT dependence of the height-integrated Pedersen conductivity by *Spiro et al.* [1982] in the postmidnight sector (01–02MLT) for 300 nT<AE$\leq$600 nT condition.

Figure 3.10. The first panel gives the magnetic field variation in the azimuthal component from ETS-VI, which is the same event as that of Figure 3.5. The second and third panels show the H- and D-components of the geomagnetic field at Kakioka. Three nightside Pc 4 pulsations in the magnetosphere appeared from 1302:00UT, 1312:30UT, and 1332:30UT, which are indicated by arrows. The vertical broken lines show onset times of Pi 2 pulsation observed on the ground (1301:00UT, 1312:30UT, and 1332:30UT). The onset of the nightside Pc 4 pulsation is simultaneous to or one minute later than that of Pi 2 pulsation.

Figure 3.11. A nightside Pc 4 pulsation observed by ETS-VI and a Pi 2 pulsation observed at Kakioka which appeared on 27 December 1994. The nightside Pc 4 pulsation started at 1054:00UT (an arrow), and the Pi 2 pulsation started at 1053:00UT (a vertical broken line). The difference of onset time between Pc 4 and Pi 2 is one minute. Format is same as for Figure 3.10.

Figure 3.12. MLT dependence of the onset time difference which is defined as the onset time of the nightside Pc 4 pulsation minus that of the low-latitude Pi 2 pulsation. A bigger circle represents two events. A solid line represents a regression line.

Figure 3.13. A schematic figure to estimate the azimuthal propagation velocity of fast mode Alfvén wave. It was assumed that substorm occurred in the region of 22MLT at L=20.

Figure 3.14. MLT dependence of the average ionospheric Pedersen conductivity in the region of 64°–68°ILAT for 300 nT<AE$\leq$600 nT condition, which was derived from Table A2 of *Spiro et al.* [1982].

Plate 3.1. Distribution of data set in (a) MLT-MLAT plane and (b) MLT-ILAT plane. One mesh corresponds to (a) 1° of MLAT by 1 hour of MLT, and (b) 0.5° of ILAT by 1 hour of MLT. The color images show hours of observation time.

Plate 3.2. Distributions of occurrence probability of azimuthal Pc 5 pulsations in (a) MLT-MLAT plane with one mesh of 1° of MLAT by 1 hour of MLT, and (b) MLT-ILAT plane with one mesh of 0.5° of ILAT by 1 hour of MLT. The color images show occurrence probability of azimuthal Pc 5 pulsations which is defined as the appearance time of azimuthal Pc 5 divided by the observation time in each mesh. A small open circle in mesh represents that in that mesh no observation were made or observation time

was small (less than 1.5 hours for (a), and less than 4.5 hours for (b)).

Plate 3.3. Dynamic spectrum of the magnetic field data obtained by ETS-VI from 06 to 08UT on 18 July 1995.

Plate 3.4. Same as in Plate 2 except for azimuthal Pc 3 pulsations.

Plate 3.5. Same as in Plate 2 except for radial Pc 4 pulsations on the dayside.

Plate 3.6. Same as in Plate 2 except for azimuthal Pc 4 pulsations on the nightside.

Figure 4.1. Procedure for selecting Pi 2 pulsations from the Mineyama data.

Figure 4.2. Examples of Pi 2 pulsation detected by the selection procedure shown in Figure 4.1. (a) An example of nightside Pi 2 pulsation observed on 19 April 1996. (b) An example of dayside Pi 2 pulsation observed on 20 September 1995.

Figure 4.3. MLT dependence of the occurrence of Pi 2 pulsations observed at Mineyama.

Figure 4.4. (a) An example of dayside Pi 2 pulsation observed before local noon (7.7MLT). The vertical solid and broken lines indicate the times of peaks and troughs in the H-component, respectively. (b) Same as Figure 4.4a except for dayside Pi 2 pulsation observed after local noon (14.6MLT).

Figure 4.5. MLT dependence of phase difference between H- and D-components, which is defined as the phase of the D-component minus that of the H-component. A left-handed polarized wave is represented by the positive phase difference, and vice versa, where the polarization is defined in the H-D plane from a view looking down onto the earth. A small dot shows one Pi 2 pulsation event which has the coherency between the H- and D-components more than 0.70.

Figure 4.6. MLT dependence of power spectral density of Pi 2 pulsations in the H-component. A small open square shows power spectral density of one Pi 2 event which is subtracted background level. Large diamonds indicate running average of power spectral density for the interval of 3 hours of MLT, and are plotted in the center of the interval. Only Pi 2 events which are associated with ASY index whose rise to the peak is less than 40 nT are shown.

Figure 4.7. (a) The H-component of dayside Pi 2 pulsation observed on 19 March 1996. The onset time is 0358UT which corresponds to 0 minute in the horizontal axis. (b) The power spectral density of the dayside Pi 2 pulsation shown in Figure 4.7a, which is subtracted background level.

Figure 4.8. (a) A fundamental mode oscillation of magnetospheric cavity mode waves. The left panel illustrates displacement of geomagnetic field lines in the equatorial plane on the dayside. The right panel shows the configuration of the geomagnetic field lines in the meridian plane of 12MLT. (b) Time plots of the magnetic field variations in the H- and D-components which are deduced from the model of Figure 4.8a and the observation of Figure 4.5.

Figure A.1. Map showing the locations of the three stations (Mineyama in Japan, the York SAMNET station in the U.K., and Boulder in the U.S.) in geographic coordinates. The three stations are each separated by about 120° in longitude.

Figure A.2. Time plots of wavelet functions, which were generated from the Meyer wavelet, with (j, k) of (a) (4, 8), (b) (5, 16), (c) (6, 32), (d) (5, 8), (e) (5, 16), and (f) (5, 24).

Figure A.3. Examples of wavelet analysis for the geomagnetic field data. (a) The left panel shows the H-component of the geomagnetic field data from Kakioka for the interval 512 seconds before 1517UT. The right panel shows wavelet coefficients for j=4–6 corresponding to the geomagnetic field data in the left panel. (b)–(d) Same as Figure A.3a except for the end of time of 1518UT, 1519UT, and 1520UT, respectively.

Figure A.4. The H-component of the geomagnetic field data, which is the same as that of Figure A.3c, and corresponding wavelet coefficients for j=4–9.

Figure A.5. (a) Distribution of the onset time difference, which is defined as the onset time determined by the algorithm detection minus that by the visual detection. (b)–(d) Examples of Pi 2 pulsations with onset time differences of 0, 1, and 2 minute(s), respectively.

Figure A.6. Schematic diagram of the automated Pi 2 detection system at Mineyama site.

Figure A.7. MLT dependence of the number of events for each category ((top) Pi 2 pulsations, (middle) Pc 3–4 pulsations, and (bottom) other phenomena). The events were detected by the automated Pi 2 detection system at Mineyama in the interval February through August 1996 and classified into 3 categories according to the visual inspection of the waveforms.

Notation		Period range (sec.)
Pc	Pc 1	0.2–5
	Pc 2	5–10
	Pc 3	10–45
	Pc 4	45–150
	Pc 5	150–600
Pi	Pi 1	1–40
	Pi 2	40–150

Table 1.1. Classification and notation of geomagnetic pulsations proposed by IAGA.

Station (ABB code)	Geographic lat.	Geographic lon.	Geomagnetic lat.	Geomagnetic lon.	ILAT
Fort Yukon (FYU)	66.6	214.7	67.2	260.8	67.0
Tixie Bay (TIX)	71.6	129.0	61.3	193.3	65.3
Cape Chelyuskin (CCS)	77.7	104.3	67.0	177.7	71.4
Dixon (DIK)	73.6	80.6	63.6	162.6	68.0
Tromso (TRO)	69.7	19.0	67.1	116.9	66.5
Syowa Station (SYW)	−69.0	39.4	−70.0	79.4	66.2 (deg.)

Table 2.1. The locations of ground stations used here. There stations have the values of ILAT which are contained in or close to the ILAT range of the DE observations.

	Events		
	Pc 3	Pc 4	Pc 5
$\Delta B_{\parallel}$ (compressinal)	59	148	18
$\Delta B_{\perp 1}$ (radial)	119	221	37
$\Delta B_{\perp 2}$ (azimuthal)	196	290	72

Table 3.1. The number of pulsations found in the data set. These pulsations were identified by the Fast Fourier Transform method and checked by visual scanning if they have continuous waveforms.

	Eigenfrequency (mHz)	
harmonic	66.8°ILAT	67 7°ILAT
1	7.65	6.39
2	17.4	14.5
3	27.2	22.7
4	36.8	30.9
5	46.3	39.1
6	55.6	47.2
7	65.8	55.6

Table 3.2. The frequencies of the harmonic waves for 66.8°ILAT and 67.7°ILAT. The wave equation by *Cummings et al.* [1969] was solved numerically with the plasma mass density model by *Takahashi and Anderson* [1992].

Σ_P (mho)	4	6	8	9	10	11	12
$\tau(=\gamma^{-1})$ (seconds)	159	239	320	360	400	440	480

Table 3.3. Dependence of the duration of the pulsation τ on the ionospheric Pedersen conductivity Σ_P.

Station	Geographic		Geomagnetic	
	Lat.(°N)	Lon.(°E)	Lat.(°N)	Lon.(°E)
Mineyama	35.6	135.1	25.5	203.2
York	54.0	359.0	51.0	78.6
Boulder	40.1	254.8	48.7	319.8

Table A.1. Coordinates of the three stations (Mineyama in Japan, the York SAMNET station in the U.K., and Boulder in the U.S.).

j	Frequency Range (mHz)	Time Resolution (sec.)
9	167–677	2
8	83.3–333	4
7	41.7–167	8
6	20.8–83.3	16
5	10.4–41.7	32
4	5.21–20.8	64
3	2.60–10.4	128

Table A.2. Frequency range and time resolution of the wavelet functions for j=3–9 used in this study.

(events)

Visual detection		Algorithm detection (Wavelet Analysis) Quality AA	A	B	C	X	Total	Grand Total
Quality	AA	3	2	0	0	0	5	312
	A	0	14	4	0	0	18	
	B	0	3	23	22	0	48	
	C	0	0	10	159	72	241	
X		0	0	4	58			
Total		3	19	41	239			
Grand Total		302						

Table A.3. The number of events detected by the wavelet analysis and the visual inspection from Kakioka data on the nightside (18–06LT) during January 1993.

Figure 2.1

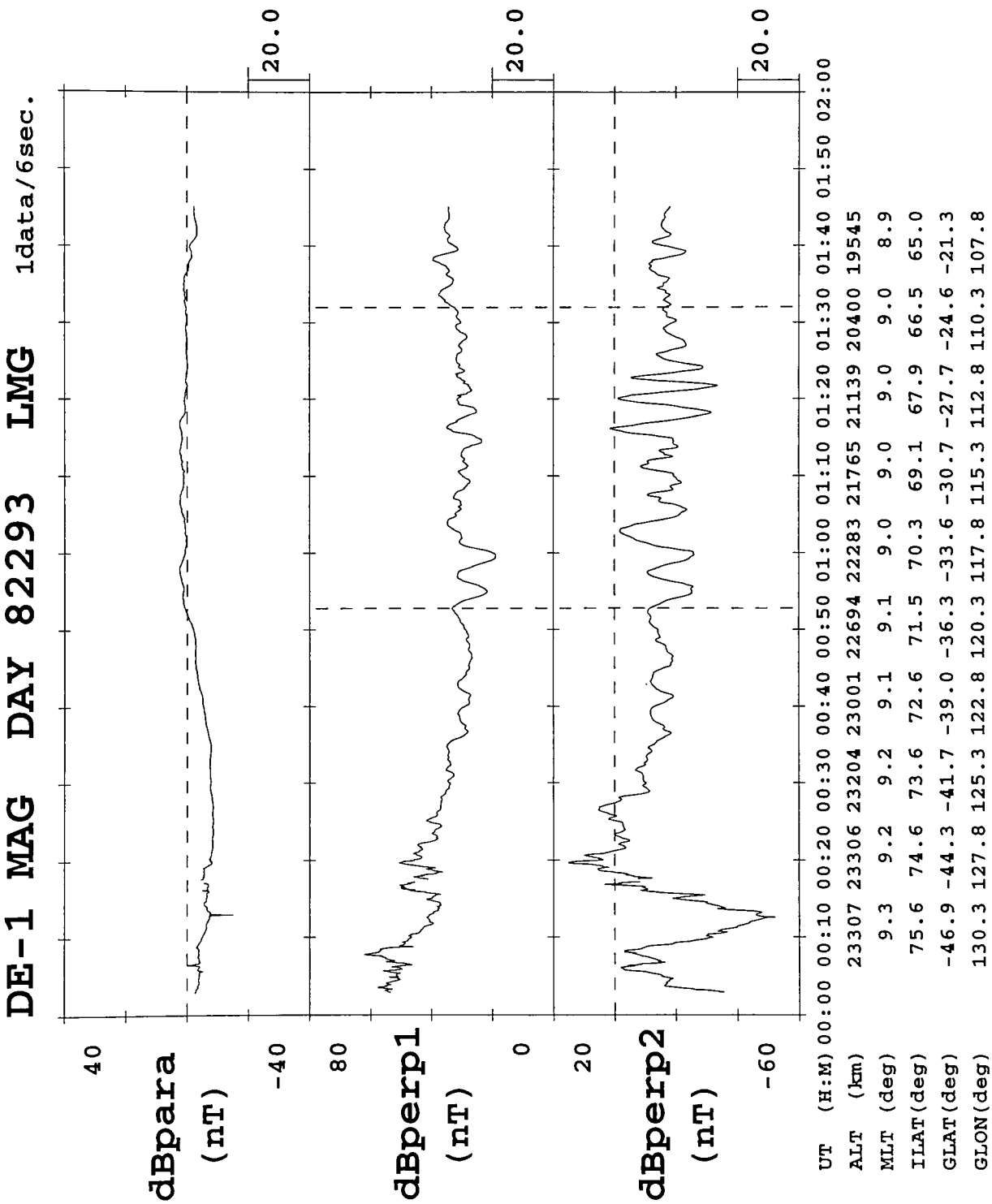
DE-1 MAG DAY 82293 LMG 1data/6sec.
20.0
20.0
20.0
dBpara (nT)
dBperp1 (nT)
dBperp2 (nT)
40
-40
80
0
20
-60
UT (H:M) 00:00 00:10 00:20 00:30 00:40 00:50 01:00 01:10 01:20 01:30 01:40 01:50 02:00
ALT (km) 23307 23306 23204 23001 22694 22283 21765 21139 20400 19545
MLT (deg) 9.3 9.2 9.2 9.1 9.1 9.0 9.0 9.0 9.0 8.9
ILAT(deg) 75.6 74.6 73.6 72.6 71.5 70.3 69.1 67.9 66.5 65.0
GLAT(deg) -46.9 -44.3 -41.7 -39.0 -36.3 -33.6 -30.7 -27.7 -24.6 -21.3
GLON(deg) 130.3 127.8 125.3 122.8 120.3 117.8 115.3 112.8 110.3 107.8

Figure 2.2

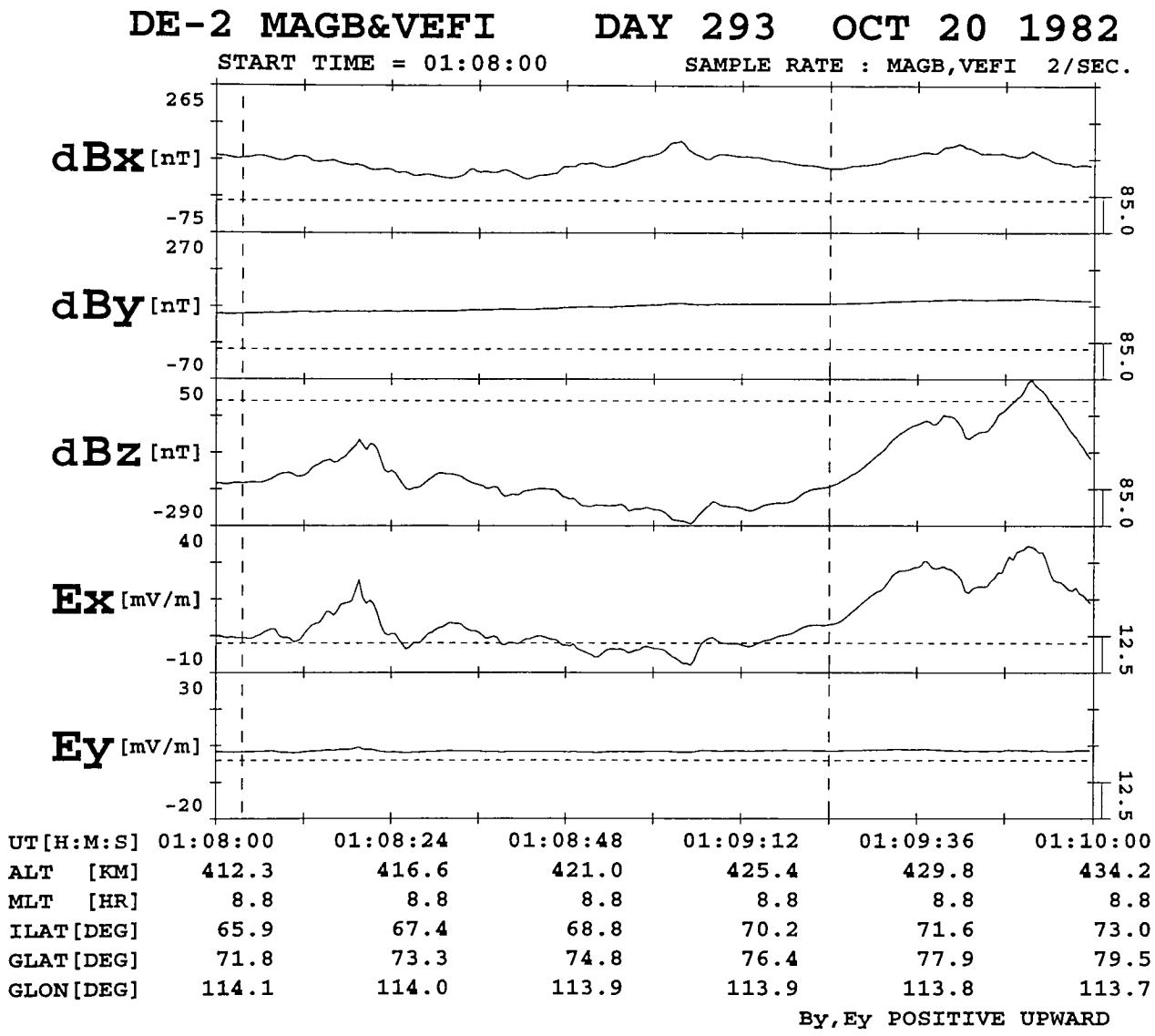
DE-2 MAGB&VEFI DAY 293 OCT 20 1982
START TIME = 01:08:00
SAMPLE RATE : MAGB,VEFI 2/SEC.
265
dBx [nT]
-75
85.0
270
dBy [nT]
-70
85.0
50
dBz [nT]
-290
85.0
40
Ex [mV/m]
-10
12.5
30
Ey [mV/m]
-20
12.5
UT[H:M:S] 01:08:00 01:08:24 01:08:48 01:09:12 01:09:36 01:10:00
ALT [KM] 412.3 416.6 421.0 425.4 429.8 434.2
MLT [HR] 8.8 8.8 8.8 8.8 8.8 8.8
ILAT[DEG] 65.9 67.4 68.8 70.2 71.6 73.0
GLAT[DEG] 71.8 73.3 74.8 76.4 77.9 79.5
GLON[DEG] 114.1 114.0 113.9 113.9 113.8 113.7
By,Ey POSITIVE UPWARD

Figure 2.3

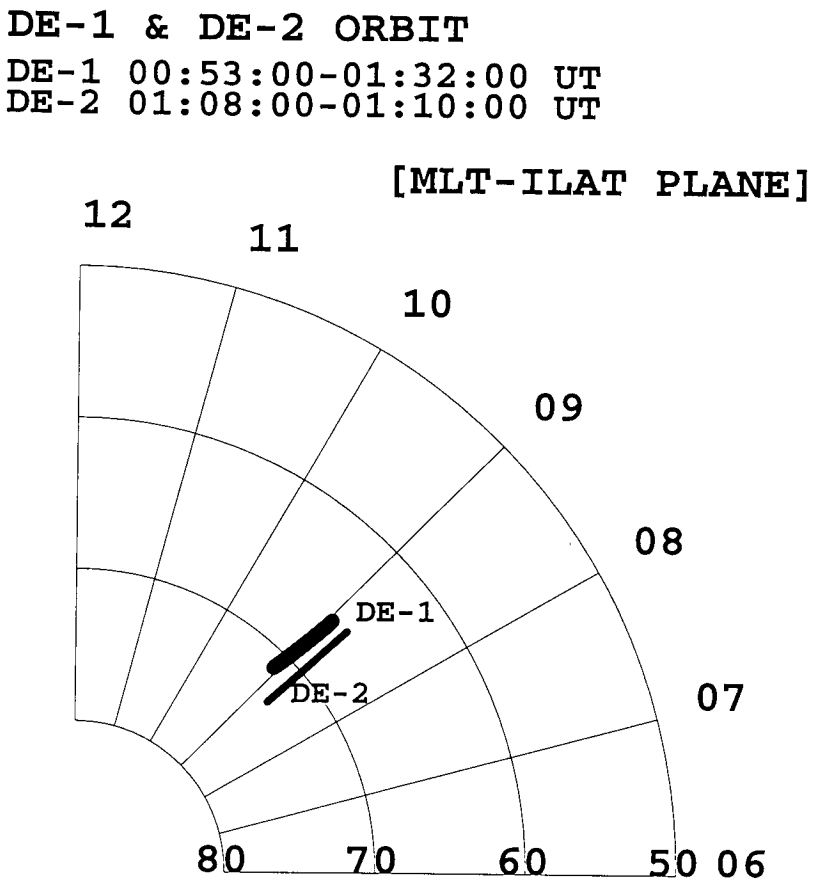
DE-1 & DE-2 ORBIT
DE-1 00:53:00-01:32:00 UT
DE-2 01:08:00-01:10:00 UT
[MLT-ILAT PLANE]
12
11
10
09
08
07
06
DE-1
DE-2
80
70
60
50

Figure 2.4

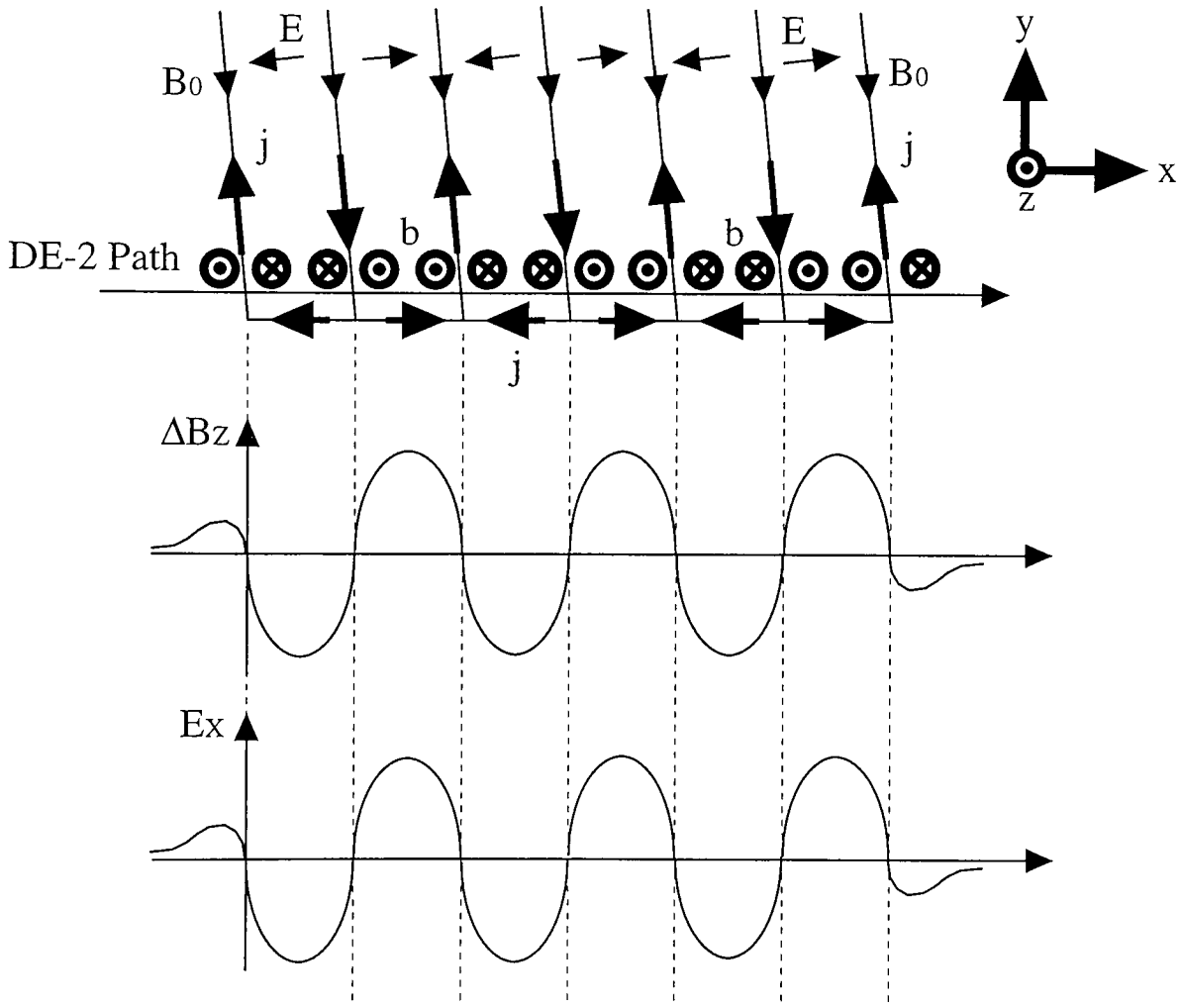

Figure 2.5

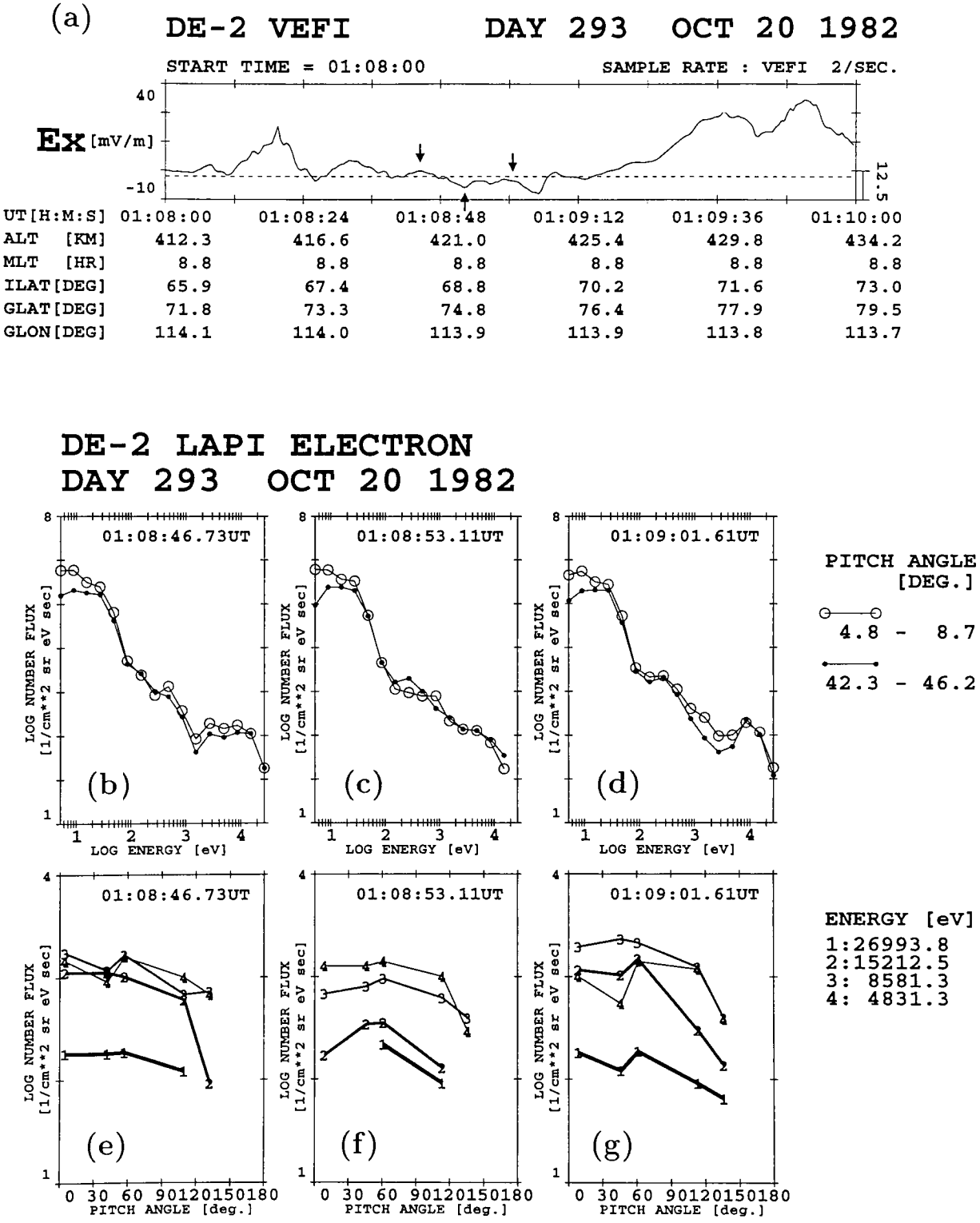
(a)
DE-2 VEFI DAY 293 OCT 20 1982
START TIME = 01:08:00
SAMPLE RATE : VEFI 2/SEC.
Ex [mV/m]
40
-10
12.5
UT[H:M:S] 01:08:00 01:08:24 01:08:48 01:09:12 01:09:36 01:10:00
ALT [KM] 412.3 416.6 421.0 425.4 429.8 434.2
MLT [HR] 8.8 8.8 8.8 8.8 8.8 8.8
ILAT[DEG] 65.9 67.4 68.8 70.2 71.6 73.0
GLAT[DEG] 71.8 73.3 74.8 76.4 77.9 79.5
GLON[DEG] 114.1 114.0 113.9 113.9 113.8 113.7
DE-2 LAPI ELECTRON
DAY 293 OCT 20 1982
01:08:46.73UT
01:08:53.11UT
01:09:01.61UT
LOG NUMBER FLUX [1/cm**2 sr eV sec]
LOG ENERGY [eV]
(b)
(c)
(d)
PITCH ANGLE [DEG.]
4.8 - 8.7
42.3 - 46.2
(e)
(f)
(g)
PITCH ANGLE [deg.]
0 30 60 90120150180
ENERGY [eV]
1:26993.8
2:15212.5
3: 8581.3
4: 4831.3

Figure 2.6

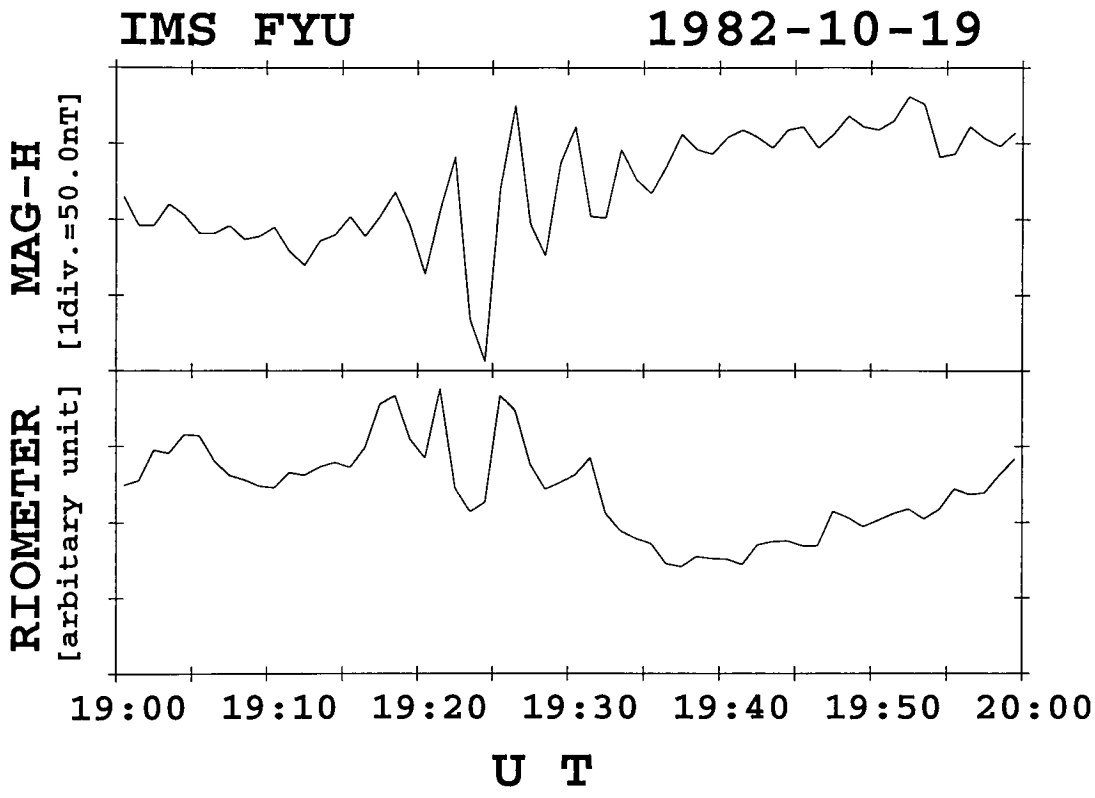
IMS FYU
1982-10-19
MAG-H
[1div.=50.0nT]
RIOMETER
[arbitary unit]
19:00
19:10
19:20
19:30
19:40
19:50
20:00
U T

Figure 2.7

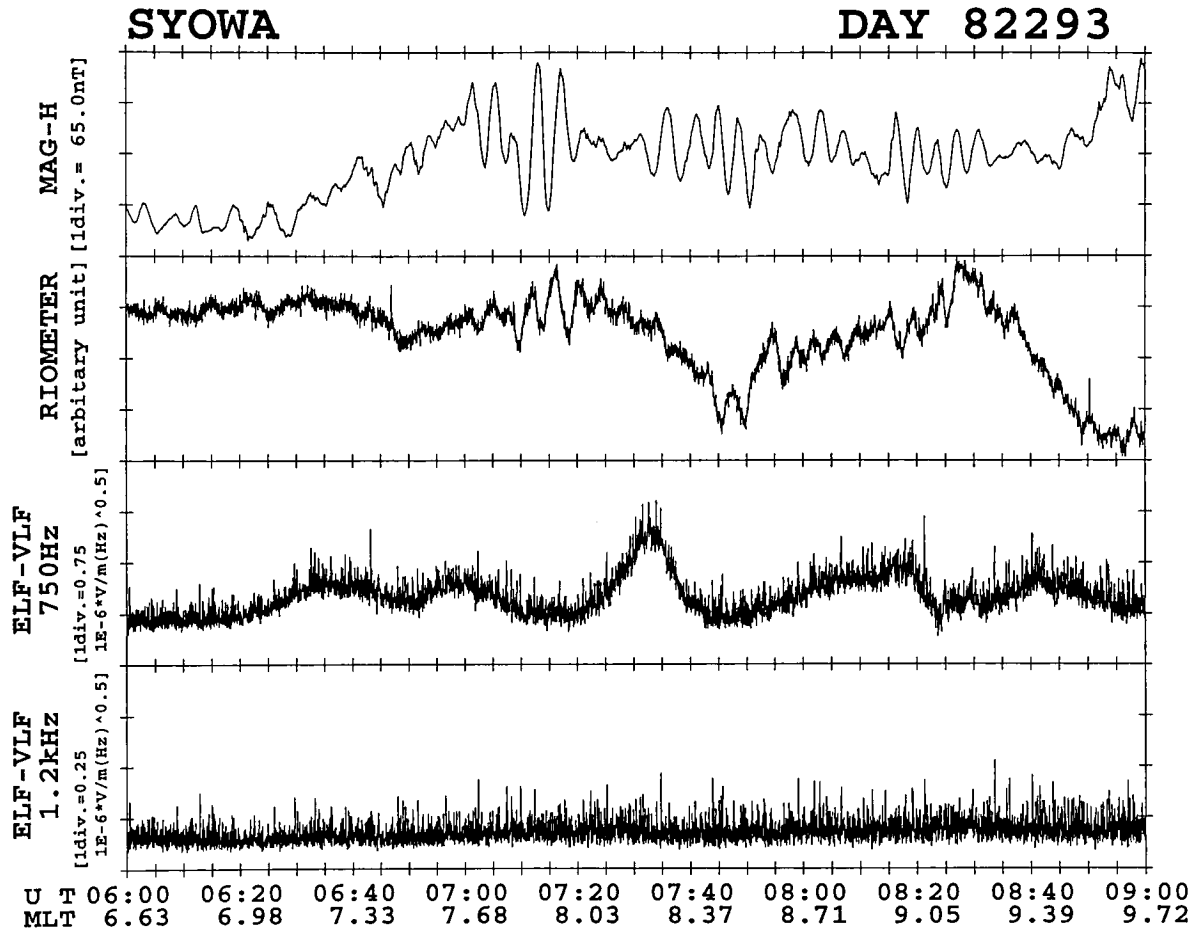
SYOWA
DAY 82293
MAG-H
[1div.= 65.0nT]
RIOMETER
[arbitary unit]
ELF-VLF
750Hz
[1div.=0.75
1E-6*V/m(Hz)^0.5]
ELF-VLF
1.2kHz
[1div.=0.25
1E-6*V/m(Hz)^0.5]
UT
MLT
06:00 06:20 06:40 07:00 07:20 07:40 08:00 08:20 08:40 09:00
6.63 6.98 7.33 7.68 8.03 8.37 8.71 9.05 9.39 9.72

Figure 2.8

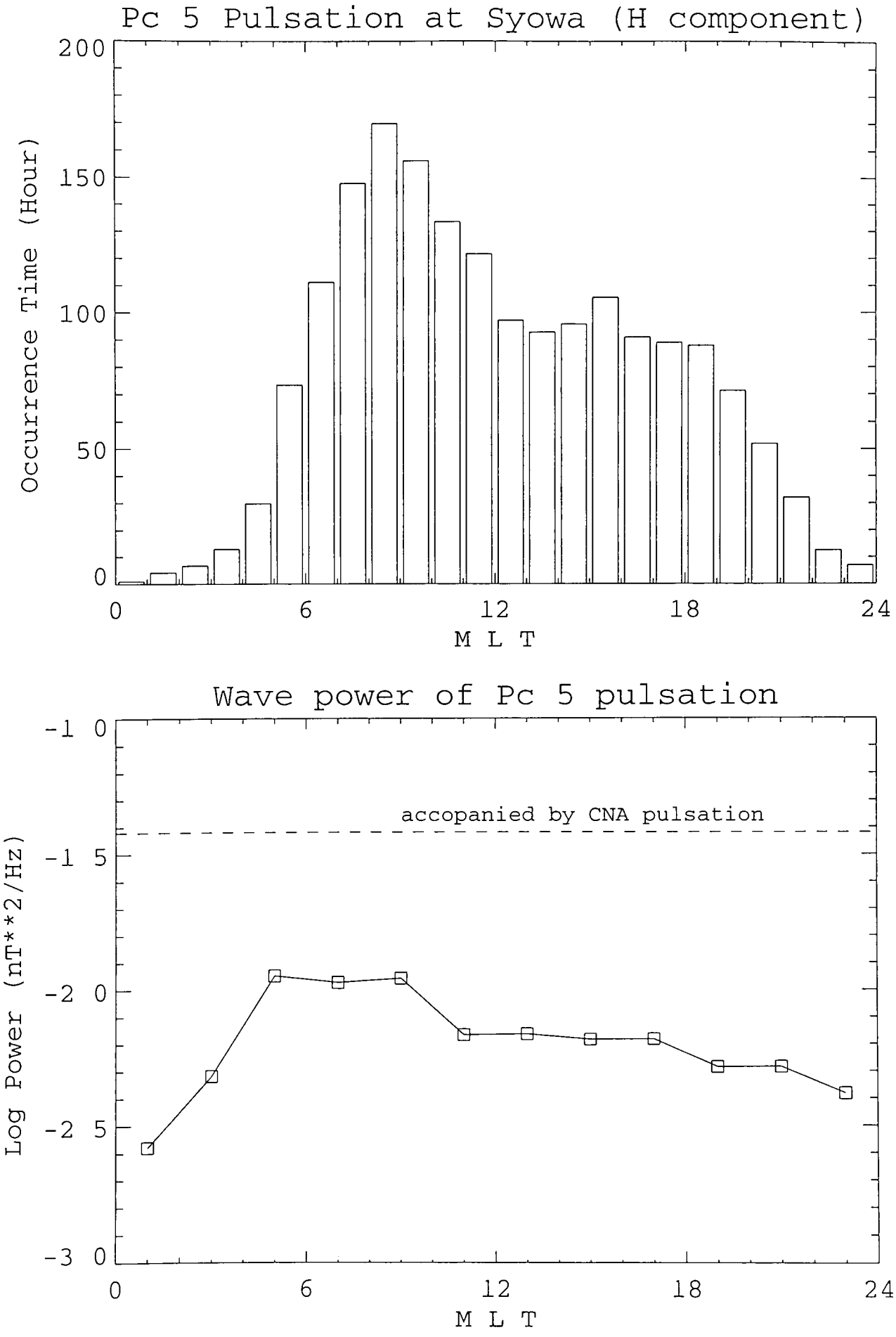
Pc 5 Pulsation at Syowa (H component)
Occurrence Time (Hour)
200
150
100
50
0
0
6
12
18
24
M L T
Wave power of Pc 5 pulsation
accopanied by CNA pulsation
Log Power (nT**2/Hz)
-1 0
-1 5
-2 0
-2 5
-3 0
0
6
12
18
24
M L T

Figure 2.9

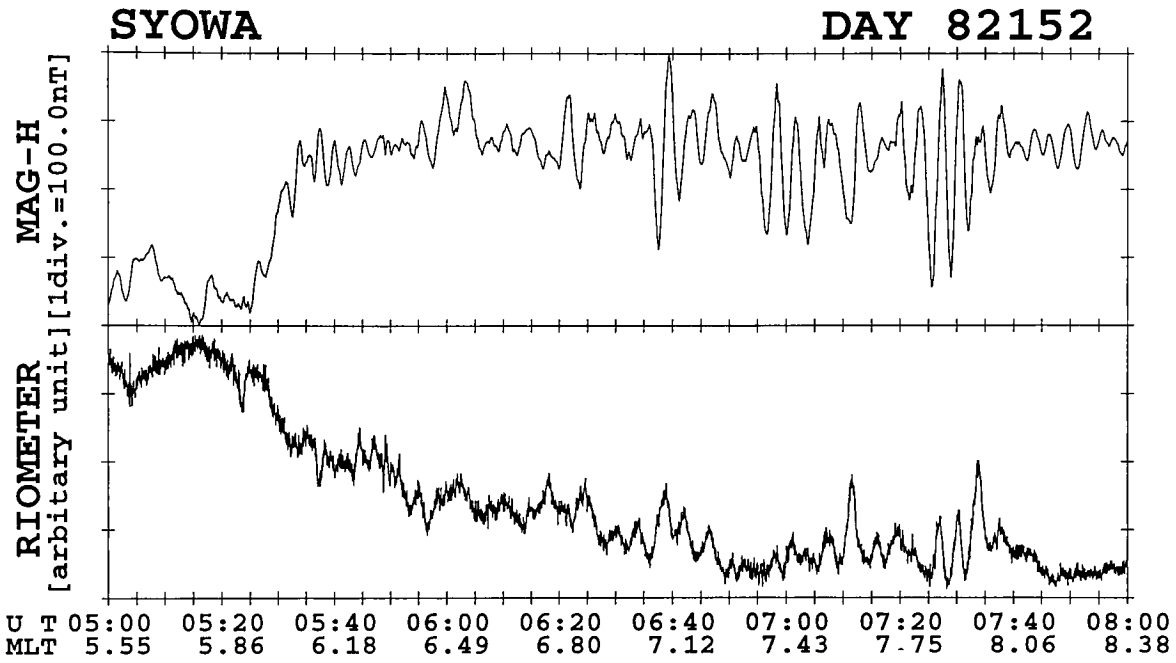
SYOWA
DAY 82152
MAG-H
[1div.=100.0nT]
RIOMETER
[arbitary unit]
UT 05:00 05:20 05:40 06:00 06:20 06:40 07:00 07:20 07:40 08:00
MLT 5.55 5.86 6.18 6.49 6.80 7.12 7.43 7.75 8.06 8.38

Figure 2.10

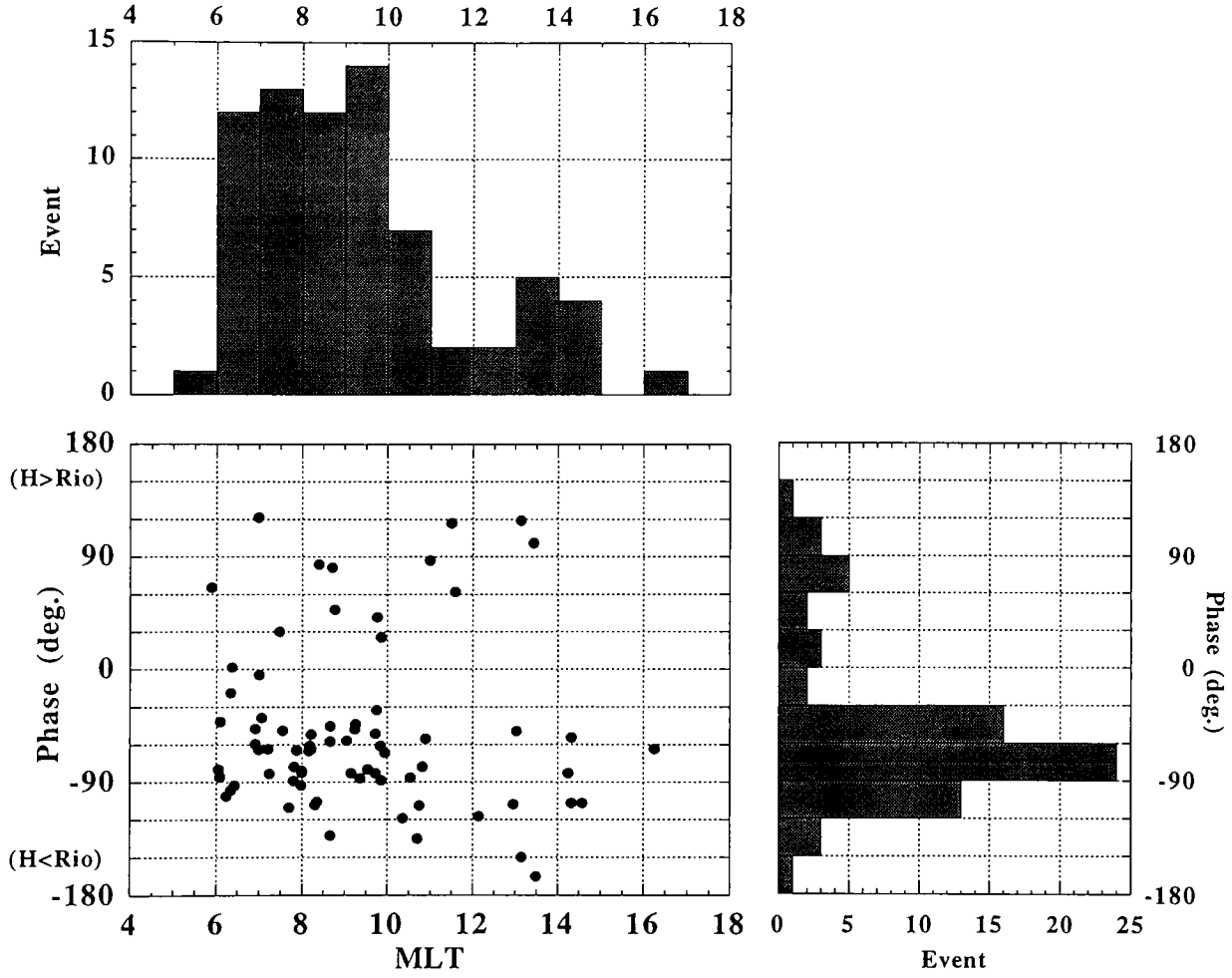
4
6
8
10
12
14
16
18
15
10
5
0
Event
180
(H>Rio)
90
0
-90
(H<Rio)
-180
Phase (deg.)
MLT
0
5
10
15
20
25
Event
Phase (deg.)

Figure 2.11

(a)

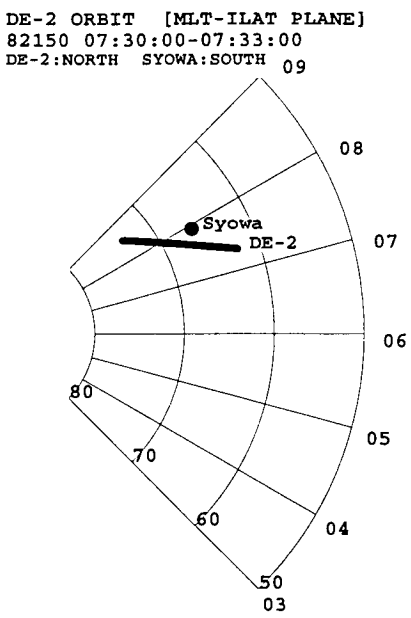

(b)

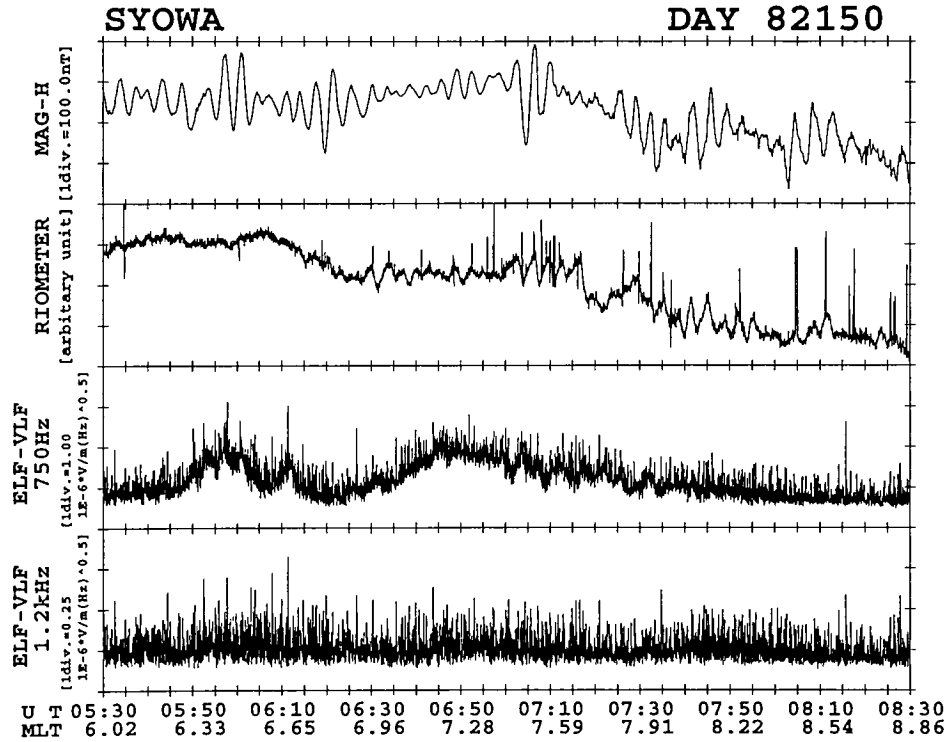

(c)

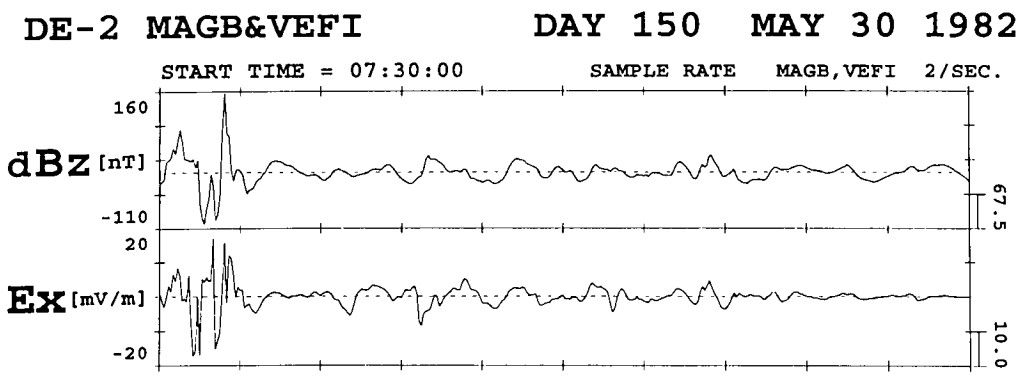

UT[H:M:S]	07:30:00	07:30:36	07:31:12	07:31:48	07:32:24	07:33:00
ALT [KM]	452.2	443.5	434.7	426.0	417.4	408.9
MLT [HR]	8.5	8.2	7.9	7.7	7.5	7.3
ILAT[DEG]	73.5	71.3	69.2	66.9	64.7	62.4
GLAT[DEG]	71.6	69.3	67.0	64.6	62.3	59.9
GLON[DEG]	-20.2	-20.3	-20.5	-20.6	-20.8	-20.9

HIGH-PASS FILTER 25.0SEC.

Figure 2.12

(a)

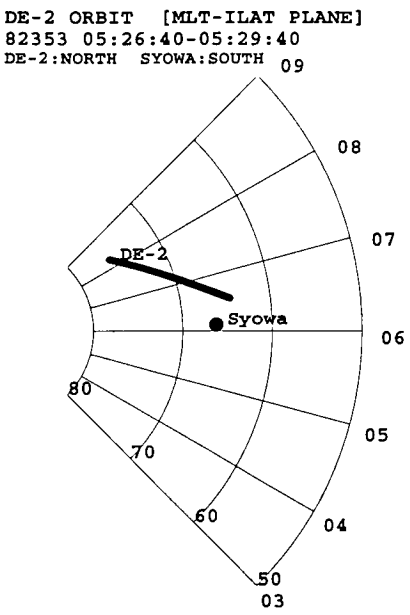

(b)

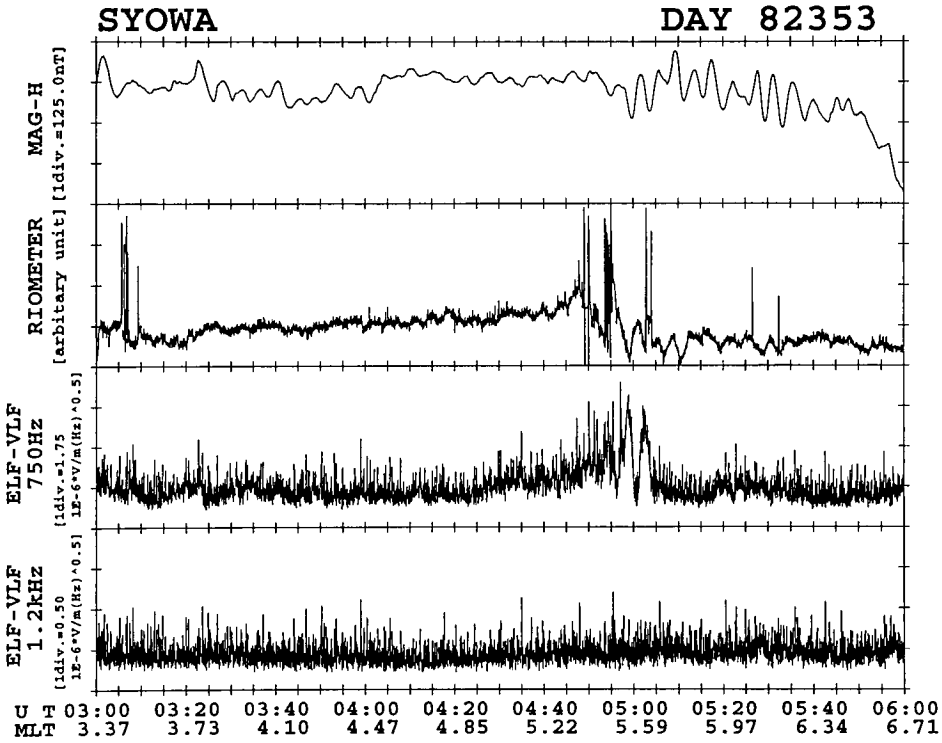

(c)

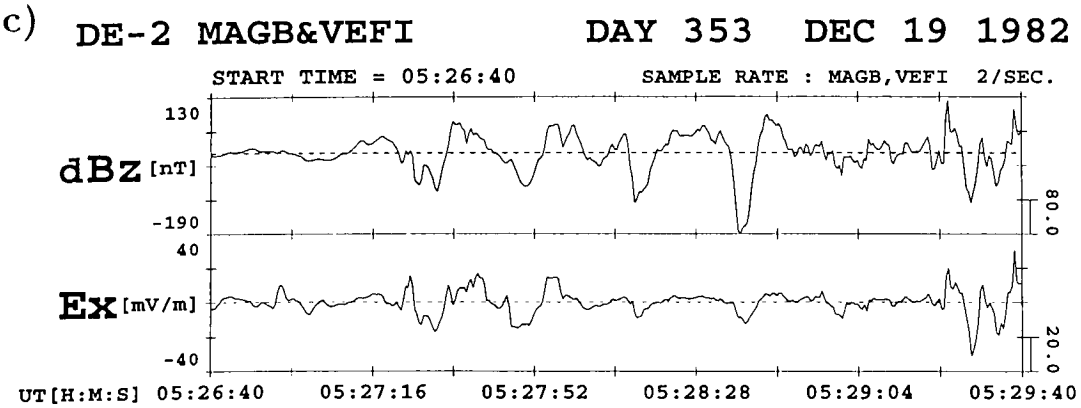

UT[H:M:S]	05:26:40	05:27:16	05:27:52	05:28:28	05:29:04	05:29:40
ALT [KM]	289.7	287.2	284.9	282.6	280.4	278.4
MLT [HR]	6.6	6.8	7.0	7.3	7.8	8.3
ILAT[DEG]	64.5	66.8	69.1	71.4	73.7	75.9
GLAT[DEG]	63.9	66.3	68.7	71.1	73.5	75.9
GLON[DEG]	-10.4	-10.5	-10.7	-10.8	-10.9	-11.0

HIGH-PASS FILTER 30.0SEC.

Figure 2.13

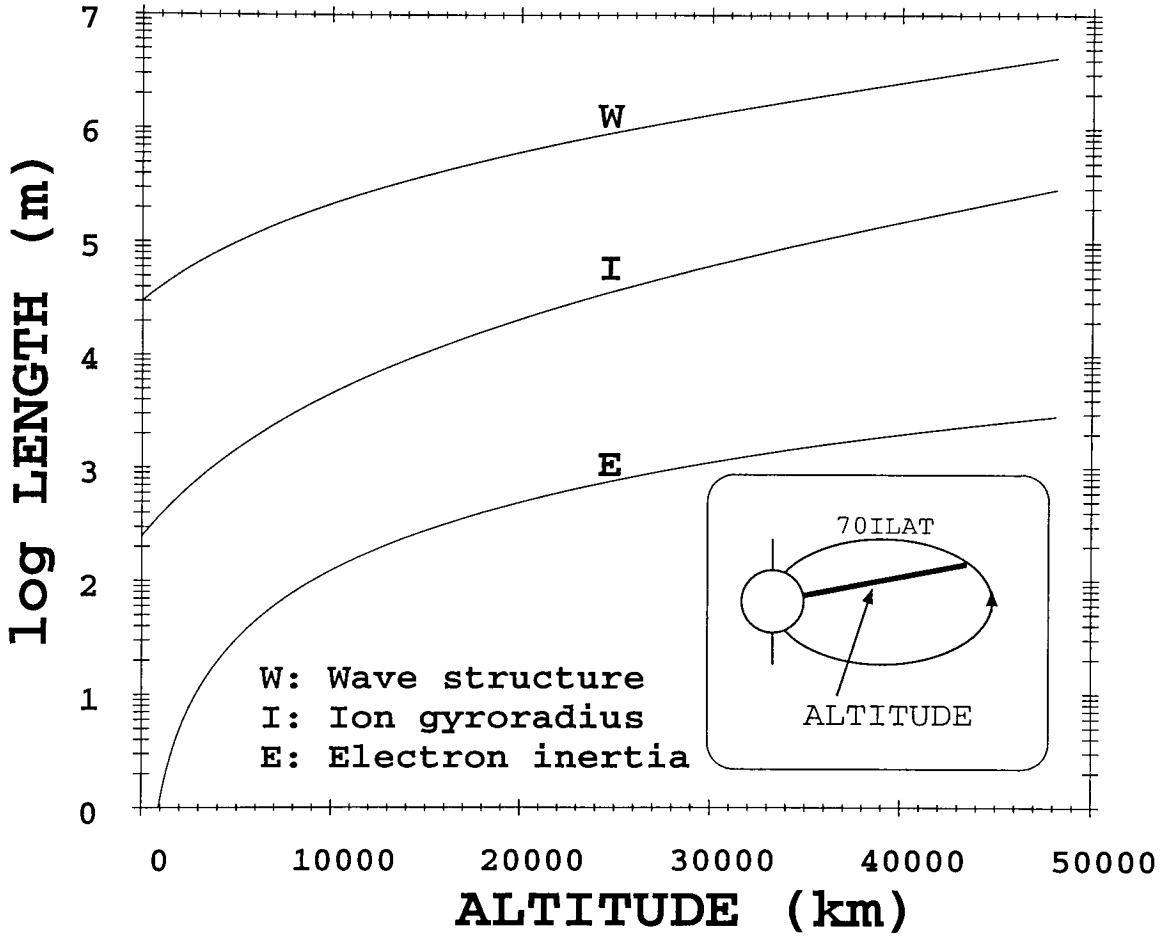
log LENGTH (m)
7
6
5
4
3
2
1
0
W
I
E
W: Wave structure
I: Ion gyroradius
E: Electron inertia
70ILAT
ALTITUDE
0
10000
20000
30000
40000
50000
ALTITUDE (km)

Figure 2.14

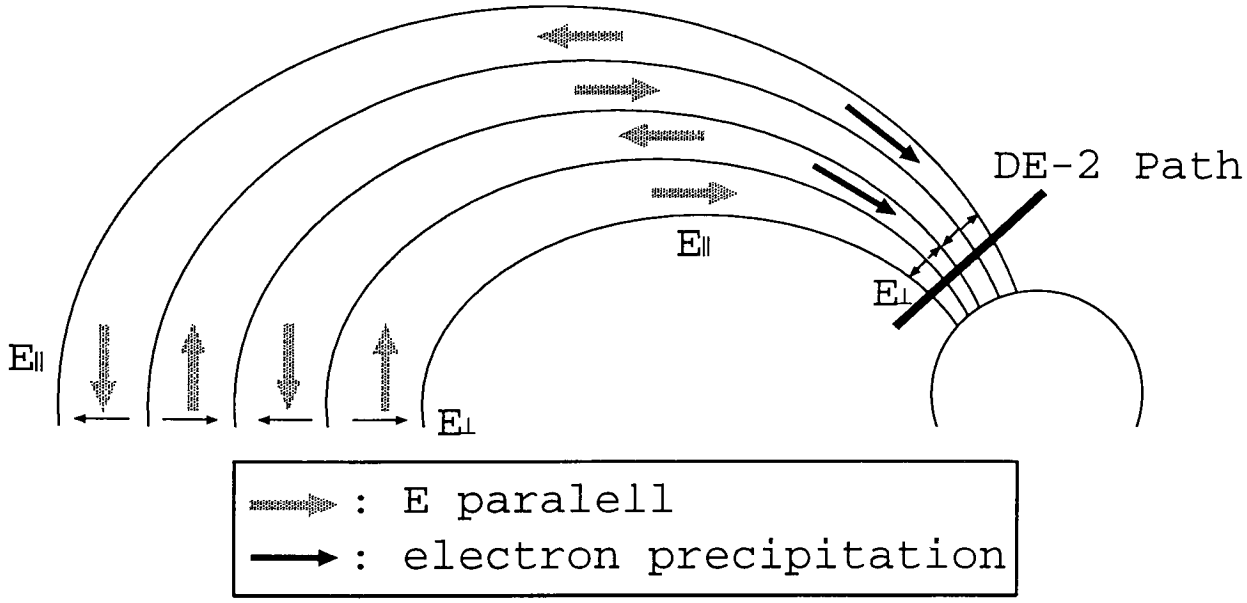

Figure 2.15

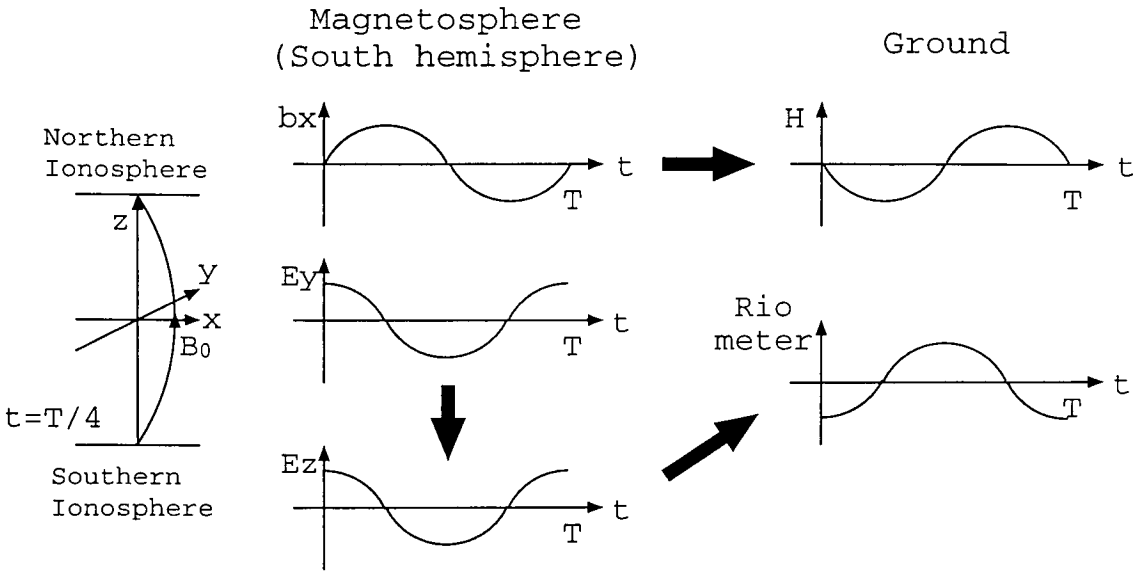
Magnetosphere
(South hemisphere)
Ground
Northern
Ionosphere
z
y
x
B0
t=T/4
Southern
Ionosphere
bx
t
T
Ey
t
T
Ez
t
T
H
t
T
Rio
meter
t
T

Figure 2.16

(a)

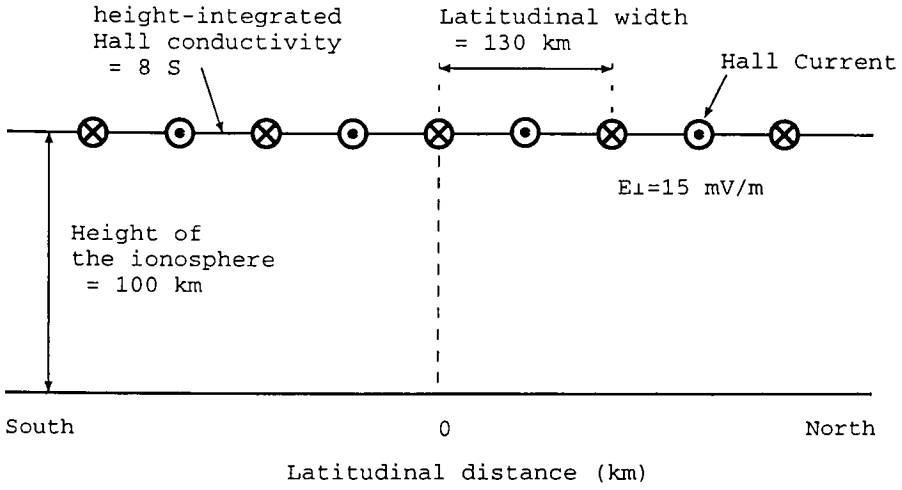

(b)

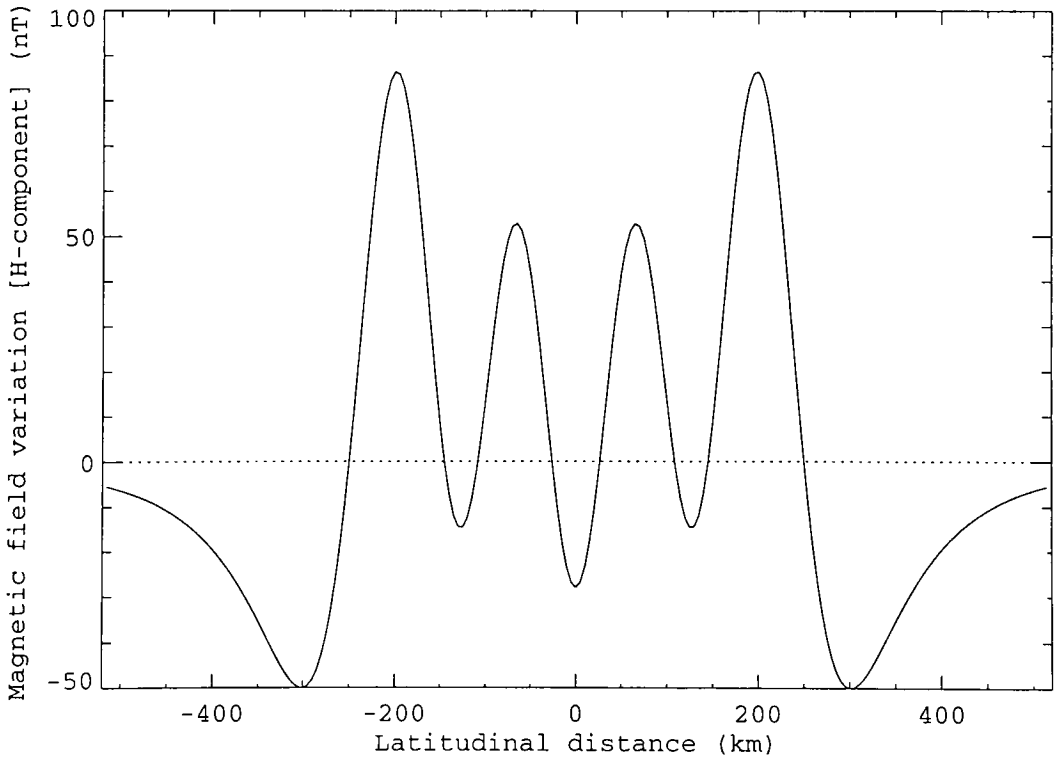

Figure 3.1

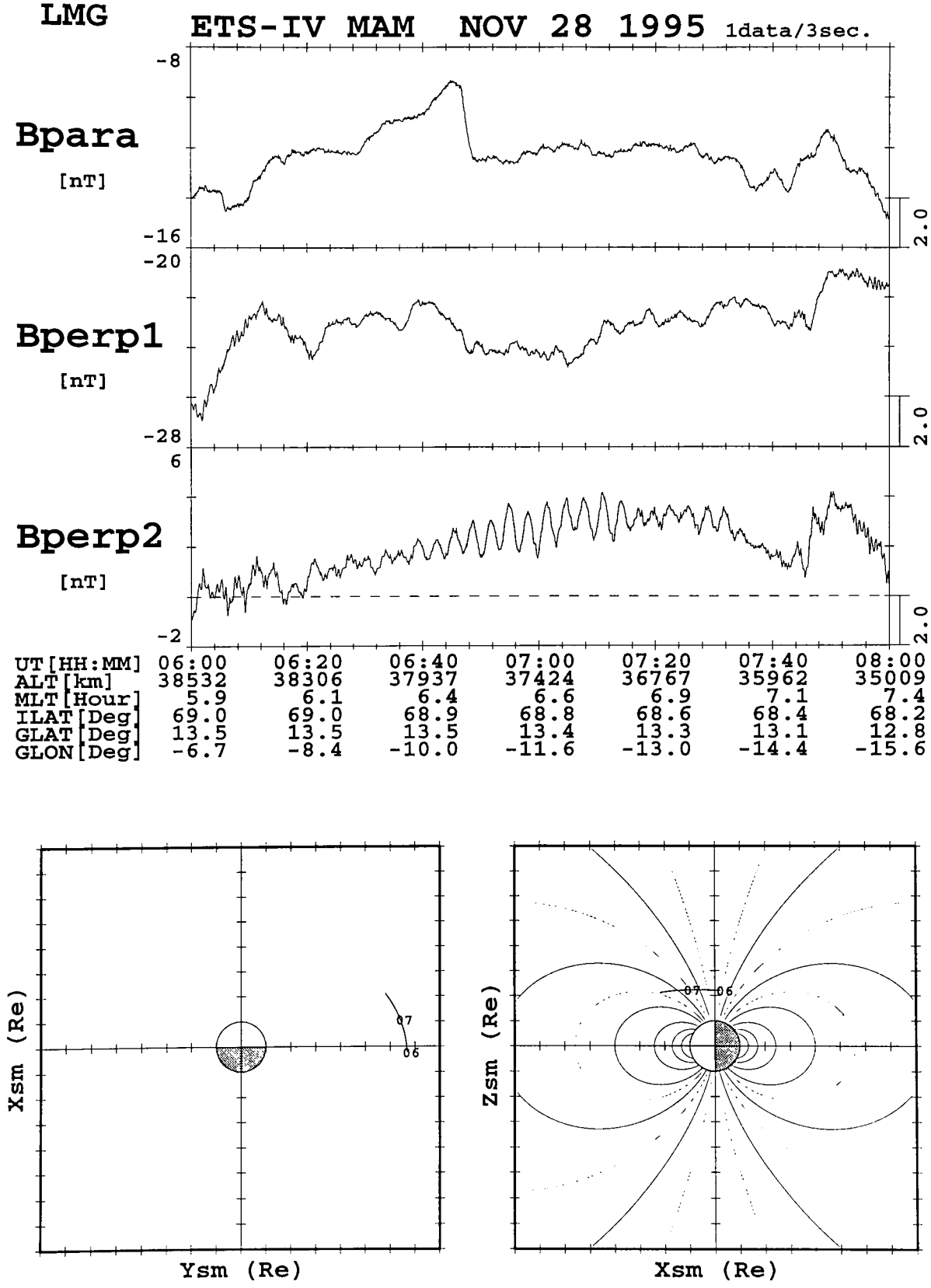
LMG
ETS-IV MAM NOV 28 1995 1data/3sec.
Bpara
[nT]
-8
-16
2.0
Bperp1
[nT]
-20
-28
2.0
Bperp2
[nT]
6
-2
2.0
UT[HH:MM] 06:00 06:20 06:40 07:00 07:20 07:40 08:00
ALT[km] 38532 38306 37937 37424 36767 35962 35009
MLT[Hour] 5.9 6.1 6.4 6.6 6.9 7.1 7.4
ILAT[Deg] 69.0 69.0 68.9 68.8 68.6 68.4 68.2
GLAT[Deg] 13.5 13.5 13.5 13.4 13.3 13.1 12.8
GLON[Deg] -6.7 -8.4 -10.0 -11.6 -13.0 -14.4 -15.6
Xsm (Re)
Ysm (Re)
07
06
Zsm (Re)
Xsm (Re)
07
06

Figure 3.2

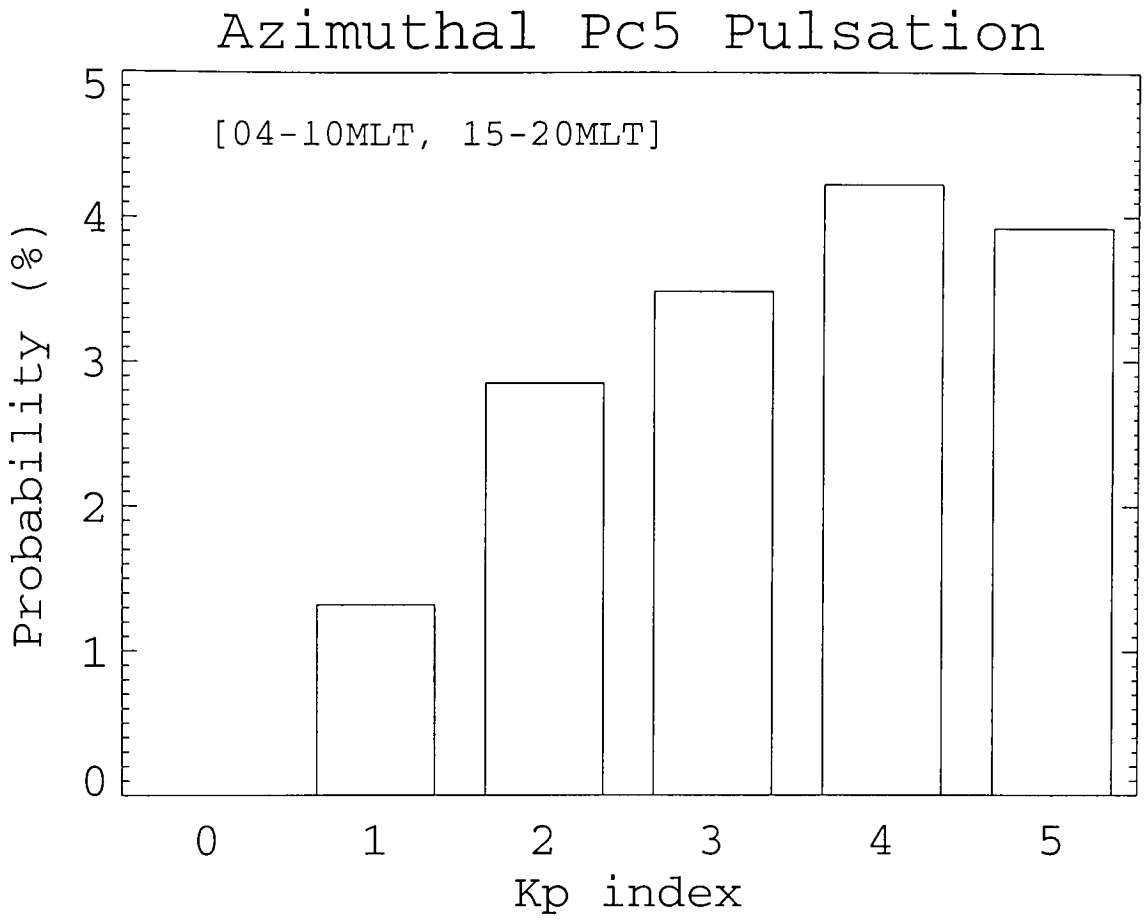
Azimuthal Pc5 Pulsation
[04-10MLT, 15-20MLT]
Probability (%)
0
1
2
3
4
5
0
1
2
3
4
5
Kp index

Figure 3.3

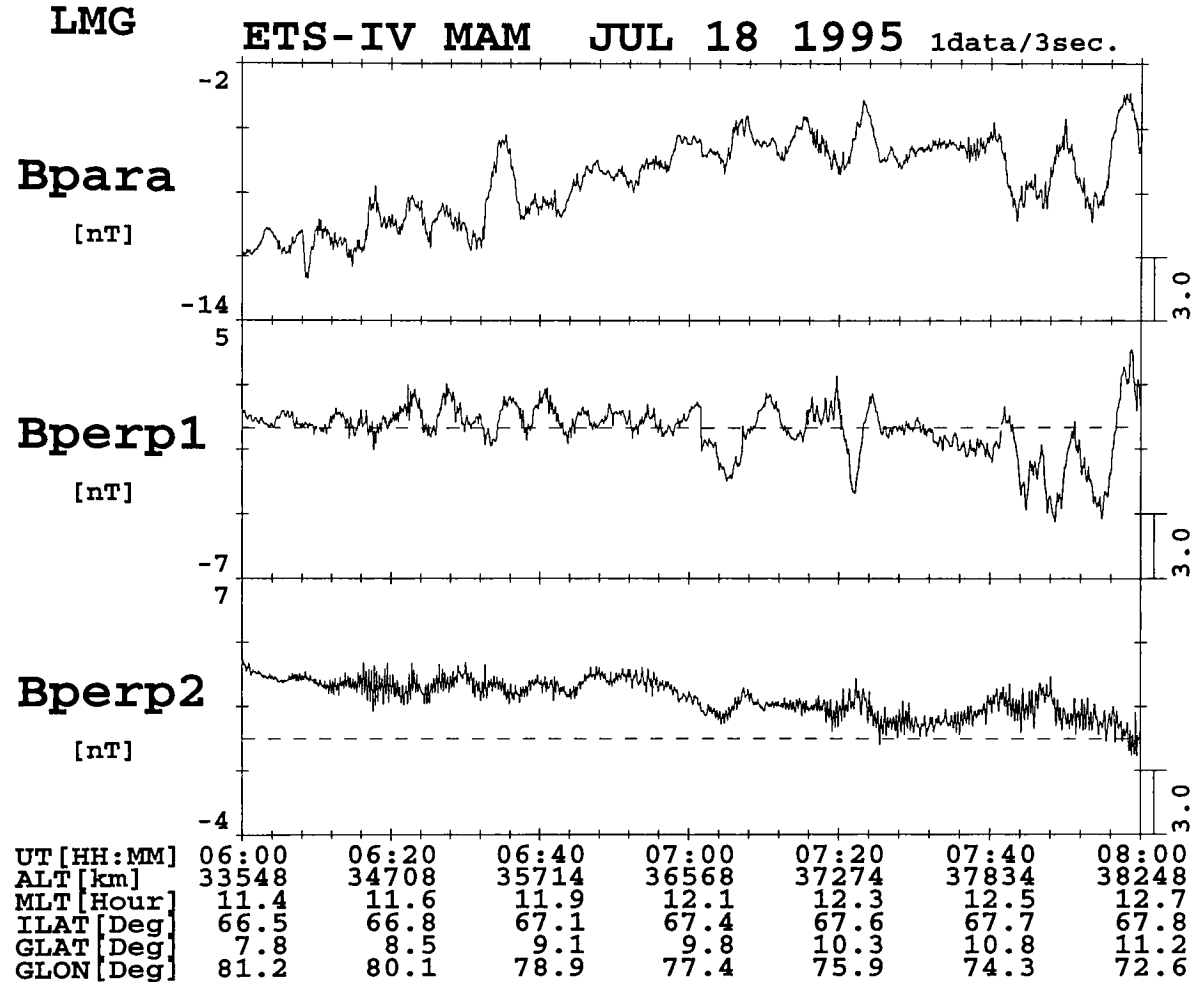
LMG
ETS-IV MAM JUL 18 1995 1data/3sec.
Bpara
[nT]
-2
-14
3.0
Bperp1
[nT]
5
-7
3.0
Bperp2
[nT]
7
-4
3.0
UT[HH:MM] 06:00 06:20 06:40 07:00 07:20 07:40 08:00
ALT[km] 33548 34708 35714 36568 37274 37834 38248
MLT[Hour] 11.4 11.6 11.9 12.1 12.3 12.5 12.7
ILAT[Deg] 66.5 66.8 67.1 67.4 67.6 67.7 67.8
GLAT[Deg] 7.8 8.5 9.1 9.8 10.3 10.8 11.2
GLON[Deg] 81.2 80.1 78.9 77.4 75.9 74.3 72.6

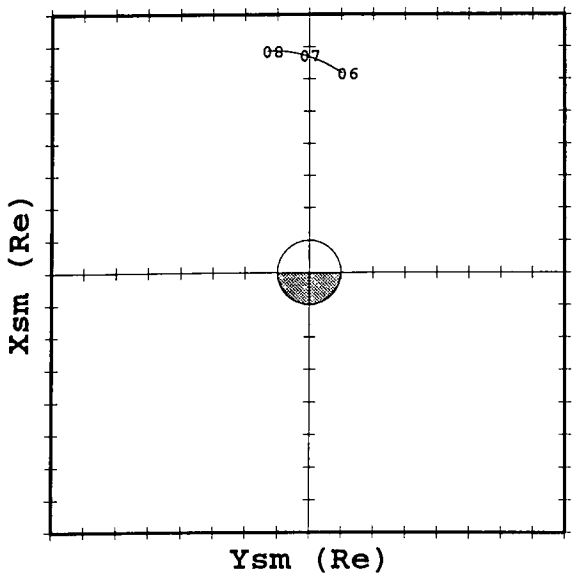
08
07
06
Xsm (Re)
Ysm (Re)

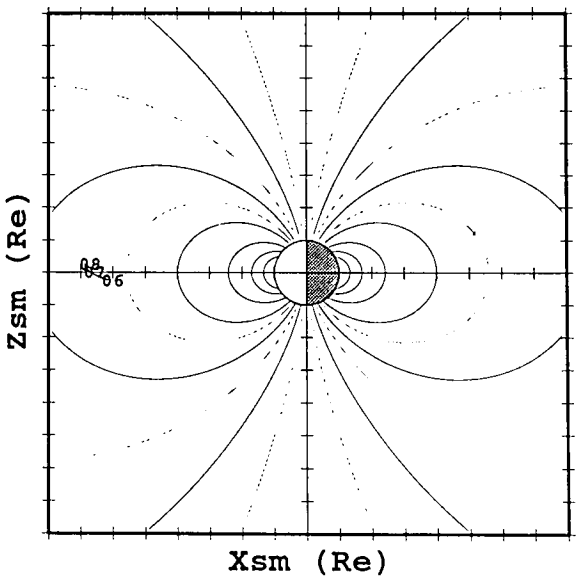
08
06
Zsm (Re)
Xsm (Re)

Figure 3.4

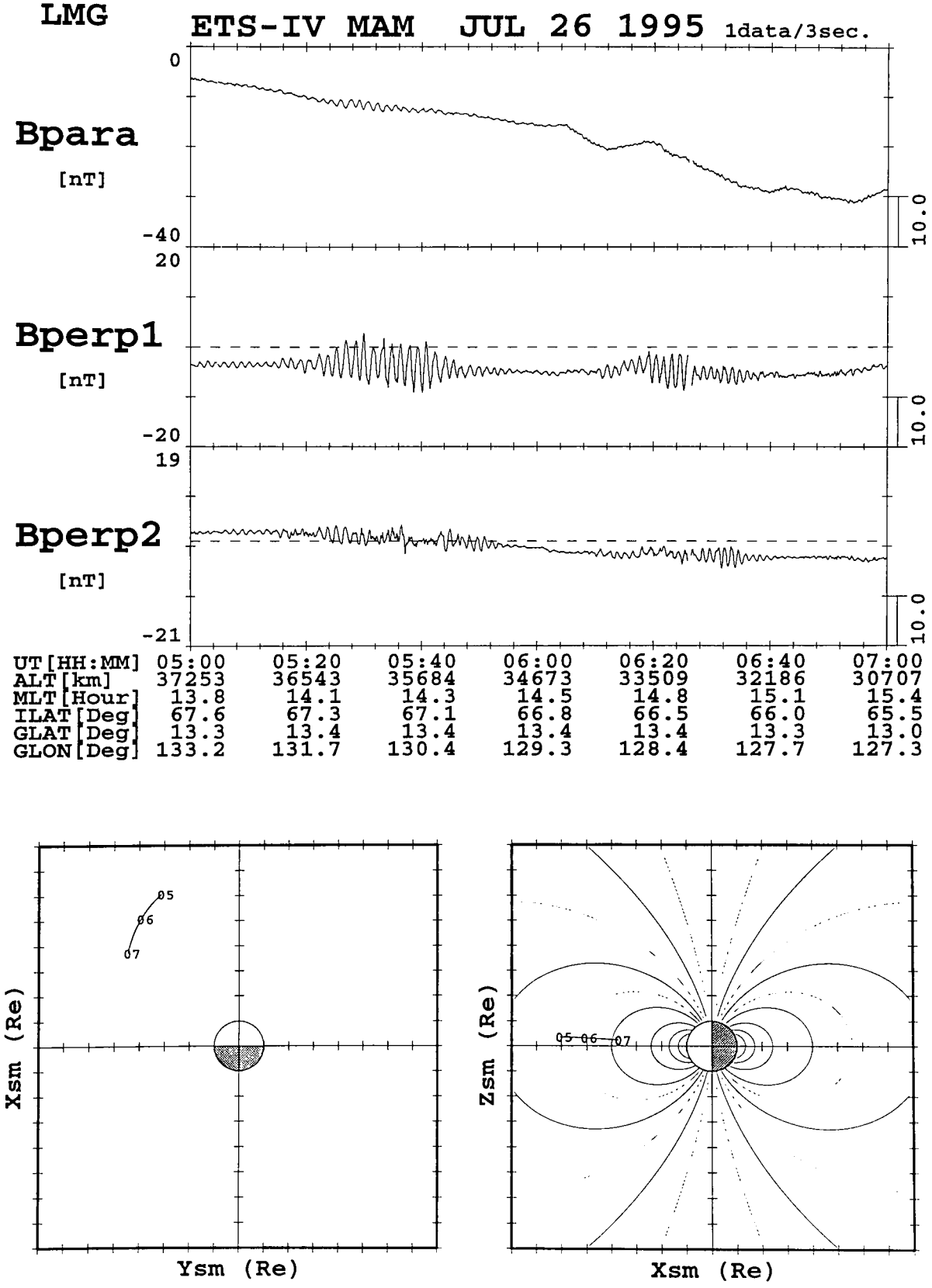
LMG
ETS-IV MAM JUL 26 1995 1data/3sec.
Bpara
[nT]
0
-40
10.0
Bperp1
[nT]
20
-20
10.0
Bperp2
[nT]
19
-21
10.0
UT[HH:MM] 05:00 05:20 05:40 06:00 06:20 06:40 07:00
ALT[km] 37253 36543 35684 34673 33509 32186 30707
MLT[Hour] 13.8 14.1 14.3 14.5 14.8 15.1 15.4
ILAT[Deg] 67.6 67.3 67.1 66.8 66.5 66.0 65.5
GLAT[Deg] 13.3 13.4 13.4 13.4 13.4 13.3 13.0
GLON[Deg] 133.2 131.7 130.4 129.3 128.4 127.7 127.3
05
06
07
Xsm (Re)
Ysm (Re)
05 06 07
Zsm (Re)
Xsm (Re)

Figure 3.5

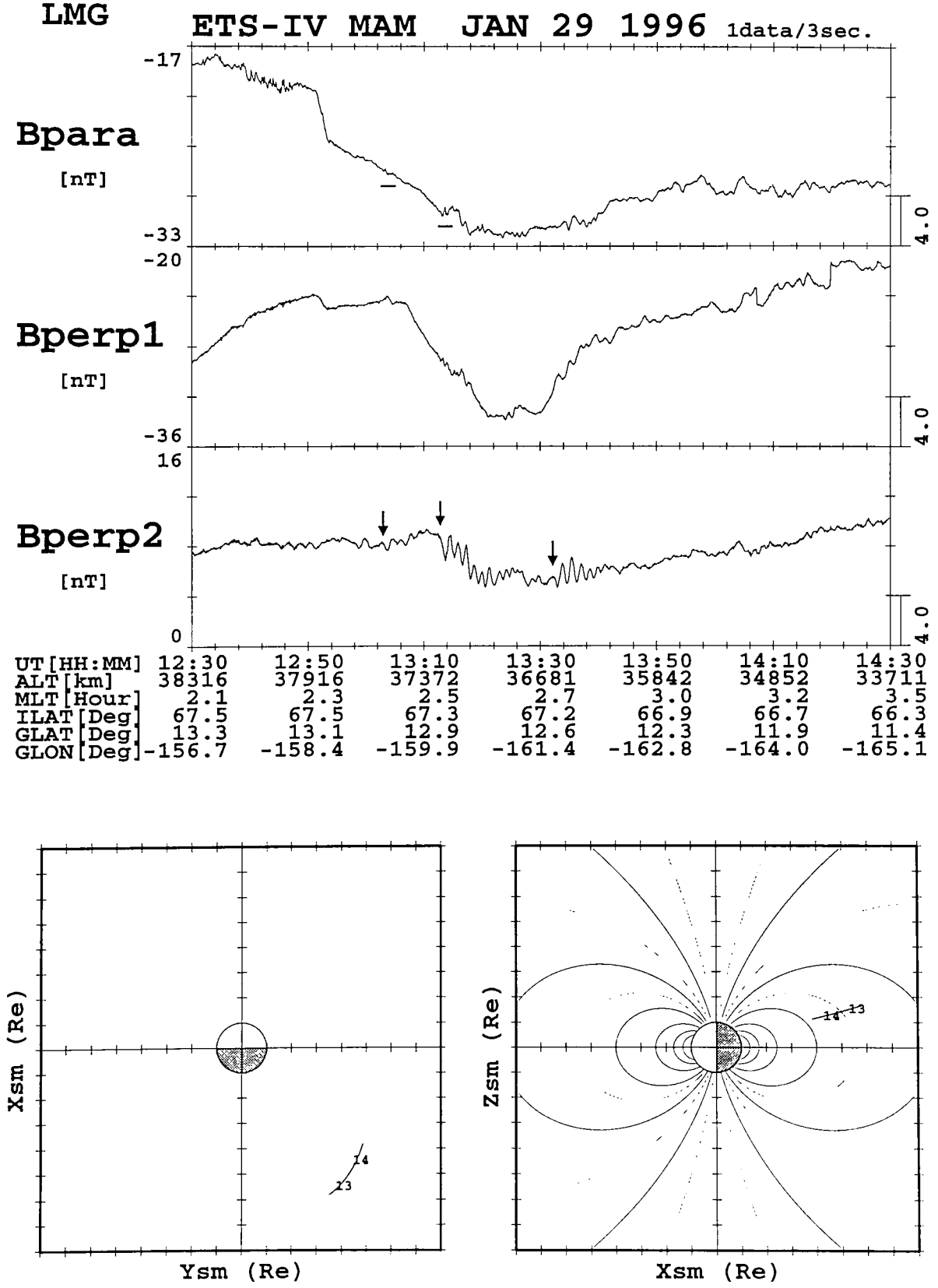
LMG
ETS-IV MAM JAN 29 1996 1data/3sec.
-17
Bpara
[nT]
-33
4.0
-20
Bperp1
[nT]
-36
4.0
16
Bperp2
[nT]
0
4.0
UT[HH:MM] 12:30 12:50 13:10 13:30 13:50 14:10 14:30
ALT[km] 38316 37916 37372 36681 35842 34852 33711
MLT[Hour] 2.1 2.3 2.5 2.7 3.0 3.2 3.5
ILAT[Deg] 67.5 67.5 67.3 67.2 66.9 66.7 66.3
GLAT[Deg] 13.3 13.1 12.9 12.6 12.3 11.9 11.4
GLON[Deg] -156.7 -158.4 -159.9 -161.4 -162.8 -164.0 -165.1
Xsm (Re)
Ysm (Re)
Zsm (Re)
Xsm (Re)

Figure 3.6

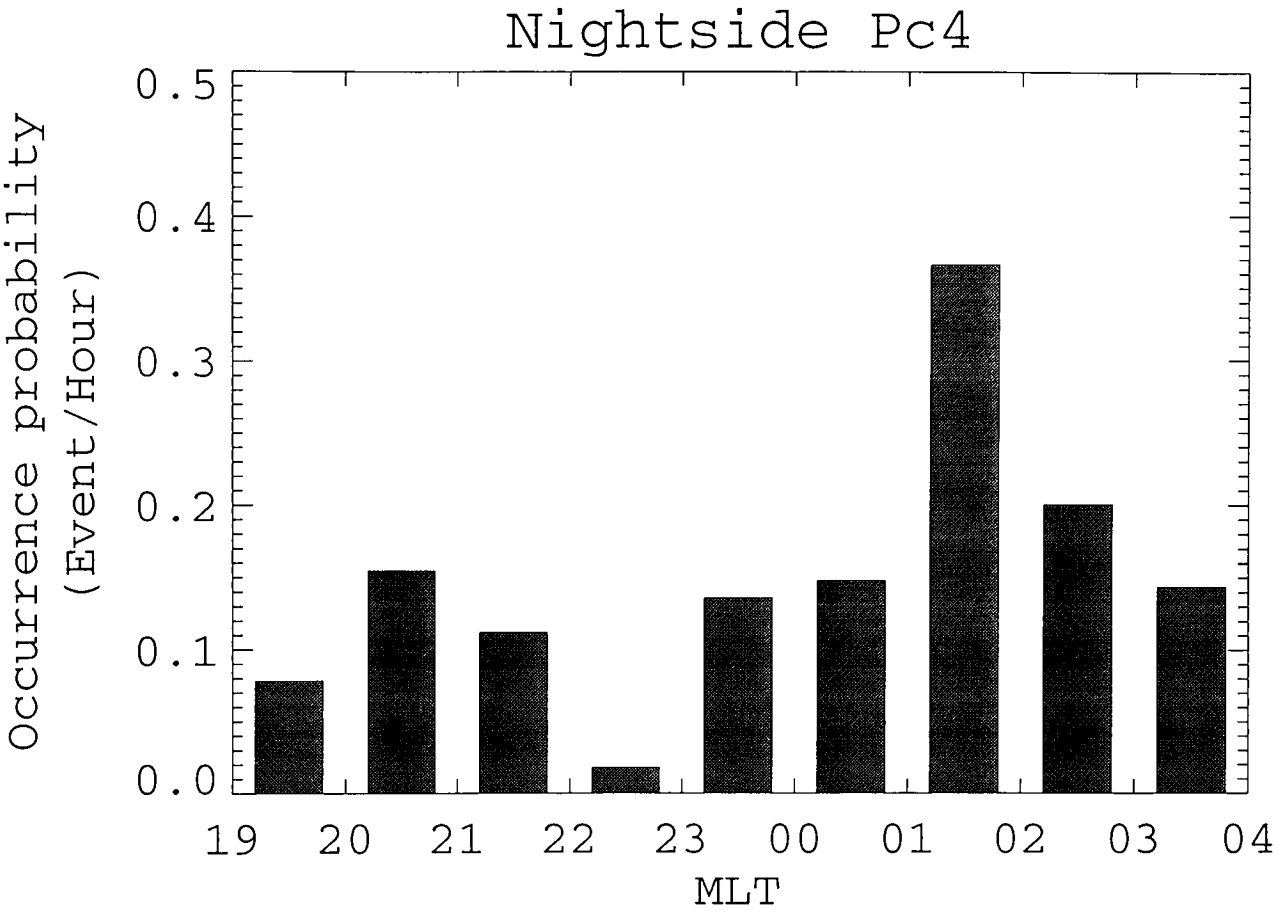
Nightside Pc4
Occurrence probability
(Event/Hour)
0.5
0.4
0.3
0.2
0.1
0.0
19
20
21
22
23
00
01
02
03
04
MLT

Figure 3.7

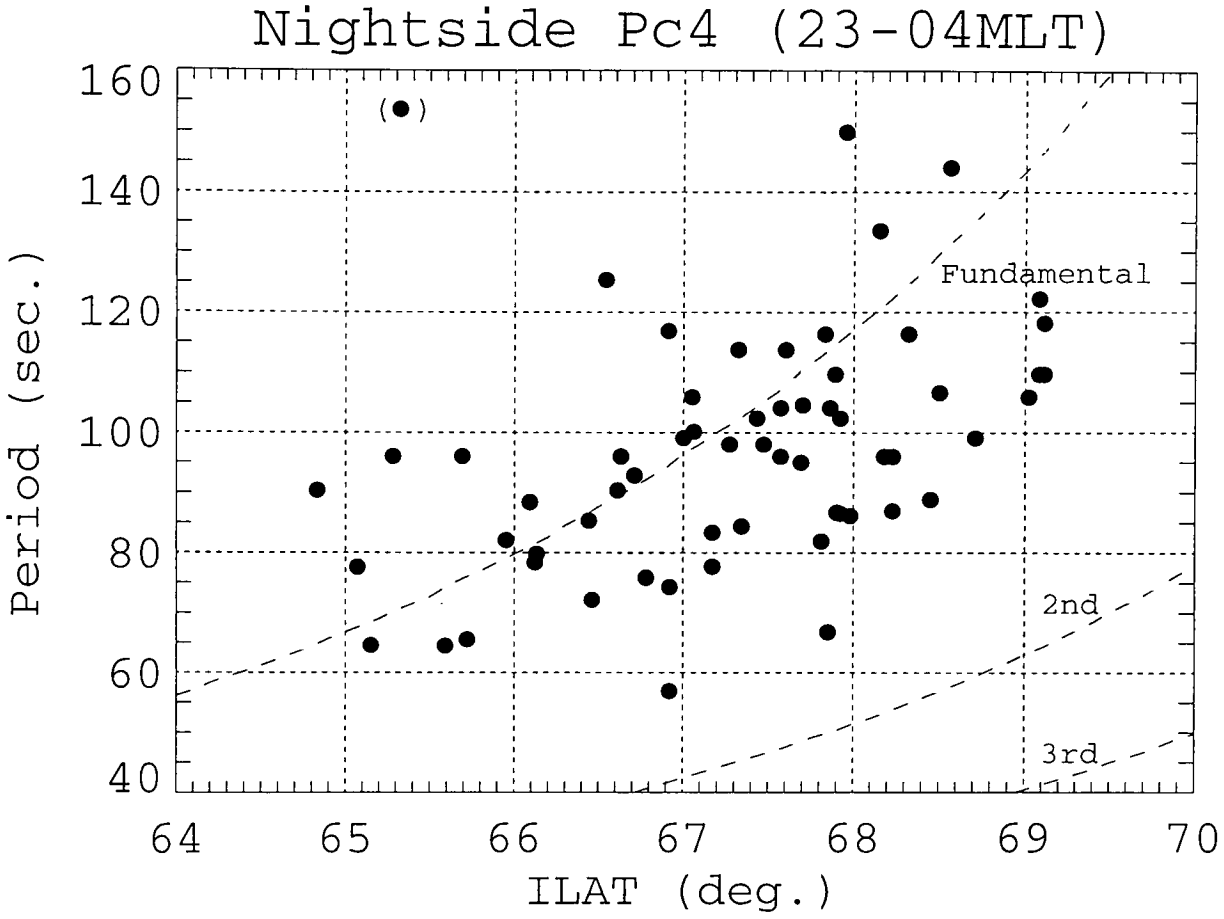
Nightside Pc4 (23-04MLT)
Period (sec.)
ILAT (deg.)
160
140
120
100
80
60
40
64
65
66
67
68
69
70
Fundamental
2nd
3rd

Figure 3.8

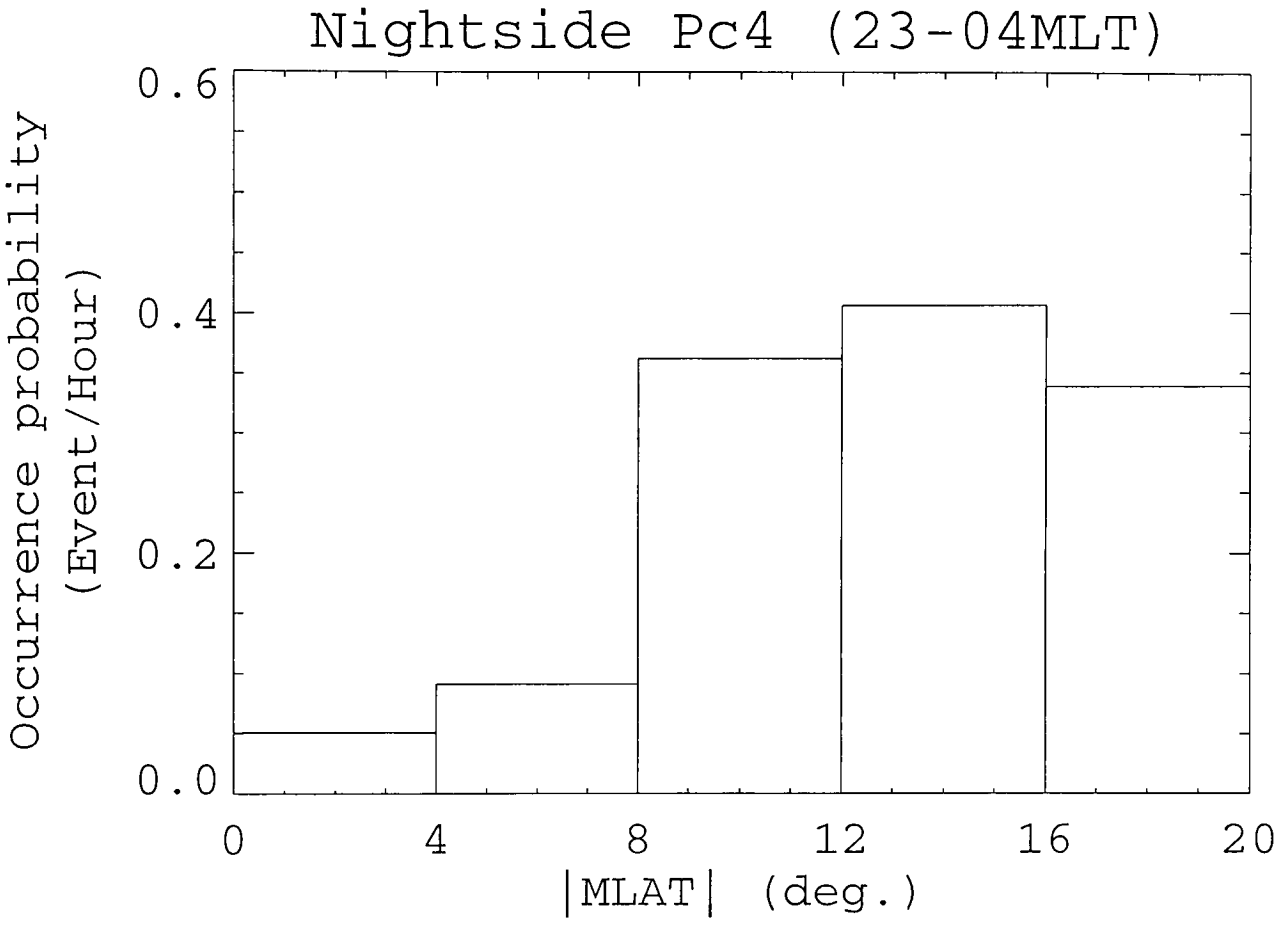
Nightside Pc4 (23-04MLT)
Occurrence probability
(Event/Hour)
0.6
0.4
0.2
0.0
0
4
8
12
16
20
|MLAT| (deg.)

Figure 3.9

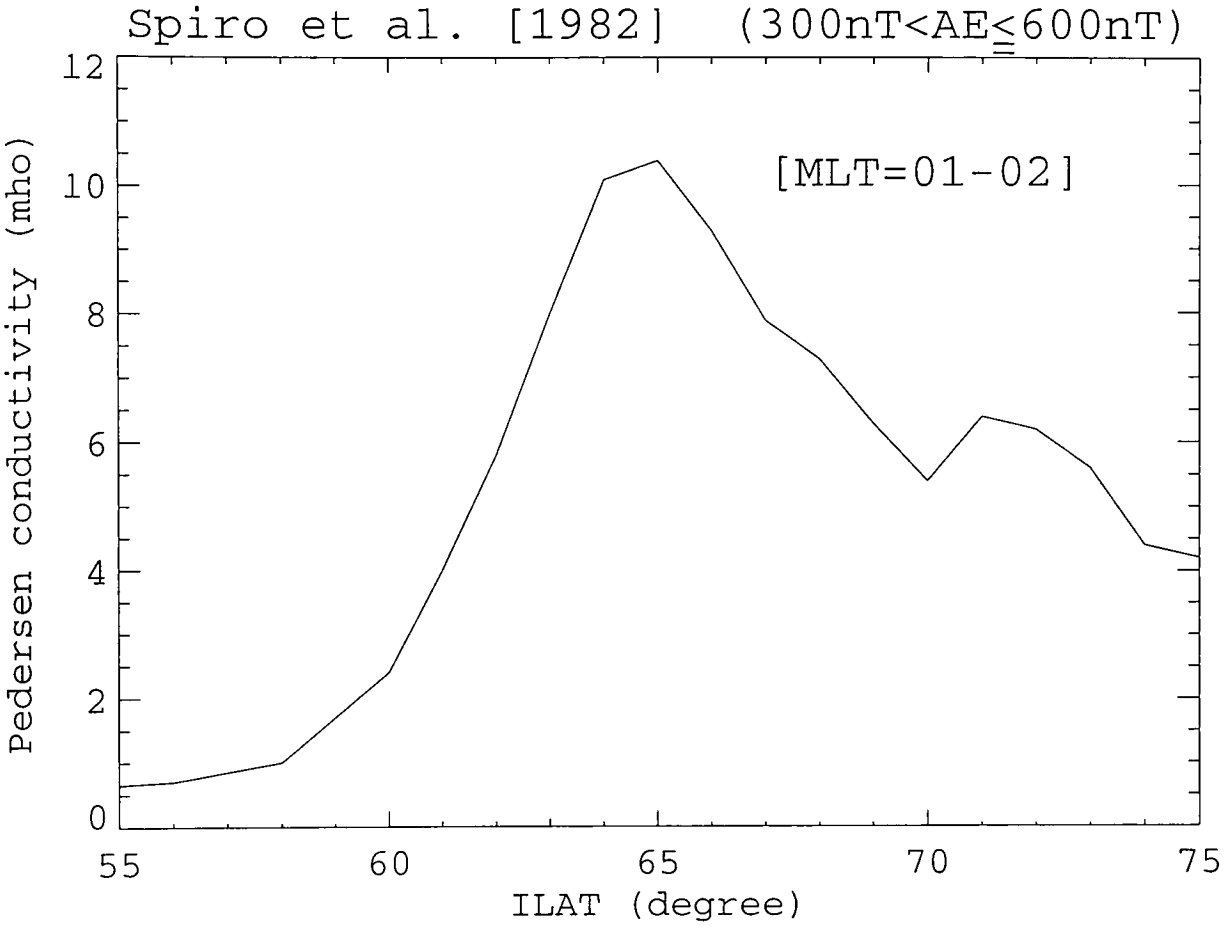
Spiro et al. [1982] (300nT<AE≦600nT)
[MLT=01-02]
Pedersen conductivity (mho)
ILAT (degree)
0
2
4
6
8
10
12
55
60
65
70
75

Figure 3.10

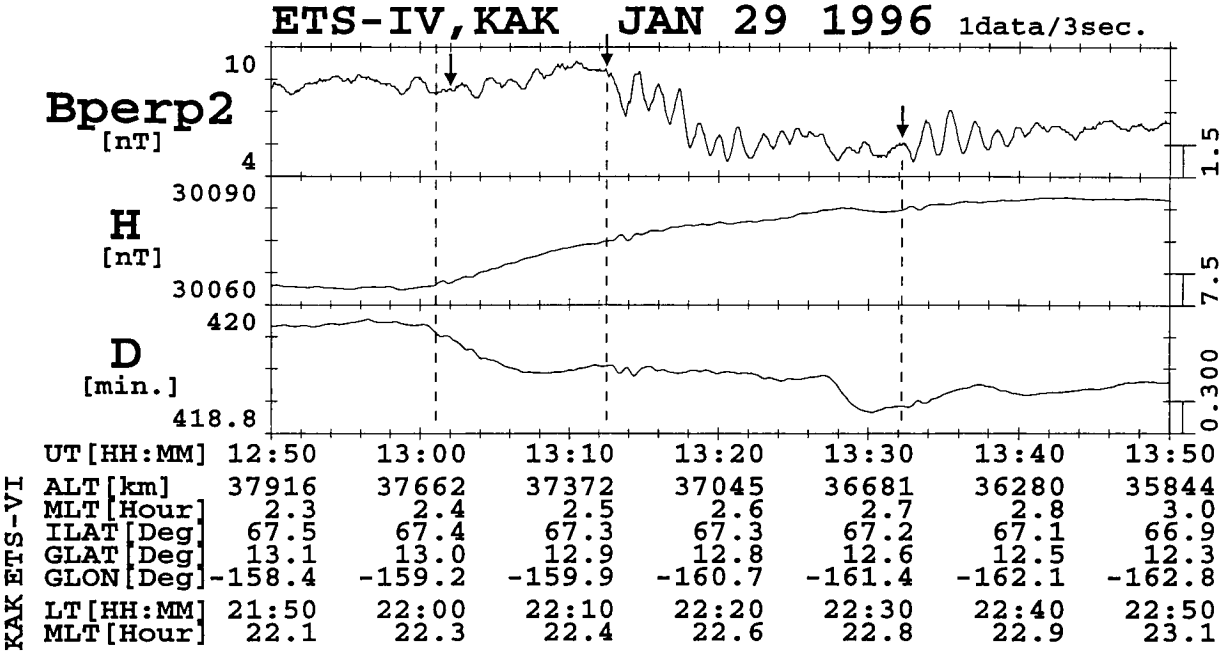
ETS-IV,KAK JAN 29 1996 1data/3sec.
Bperp2
[nT]
10
4
1.5
H
[nT]
30090
30060
7.5
D
[min.]
420
418.8
0.300
UT[HH:MM] 12:50 13:00 13:10 13:20 13:30 13:40 13:50
KAK ETS-VI
ALT[km] 37916 37662 37372 37045 36681 36280 35844
MLT[Hour] 2.3 2.4 2.5 2.6 2.7 2.8 3.0
ILAT[Deg] 67.5 67.4 67.3 67.3 67.2 67.1 66.9
GLAT[Deg] 13.1 13.0 12.9 12.8 12.6 12.5 12.3
GLON[Deg] -158.4 -159.2 -159.9 -160.7 -161.4 -162.1 -162.8
LT[HH:MM] 21:50 22:00 22:10 22:20 22:30 22:40 22:50
MLT[Hour] 22.1 22.3 22.4 22.6 22.8 22.9 23.1

Figure 3.11

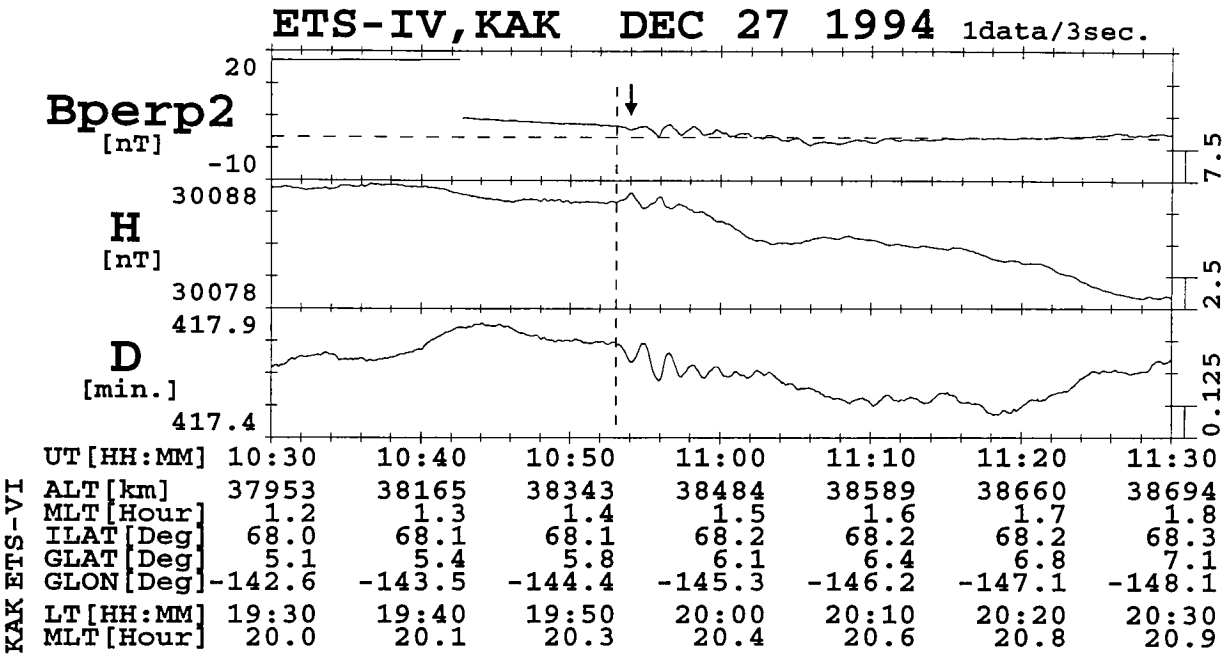
ETS-IV,KAK DEC 27 1994 1data/3sec.
Bperp2
[nT]
20
-10
7.5
H
[nT]
30088
30078
2.5
D
[min.]
417.9
417.4
0.125
UT[HH:MM] 10:30 10:40 10:50 11:00 11:10 11:20 11:30
KAK ETS-VI
ALT[km] 37953 38165 38343 38484 38589 38660 38694
MLT[Hour] 1.2 1.3 1.4 1.5 1.6 1.7 1.8
ILAT[Deg] 68.0 68.1 68.1 68.2 68.2 68.2 68.3
GLAT[Deg] 5.1 5.4 5.8 6.1 6.4 6.8 7.1
GLON[Deg] -142.6 -143.5 -144.4 -145.3 -146.2 -147.1 -148.1
LT[HH:MM] 19:30 19:40 19:50 20:00 20:10 20:20 20:30
MLT[Hour] 20.0 20.1 20.3 20.4 20.6 20.8 20.9

Figure 3.12

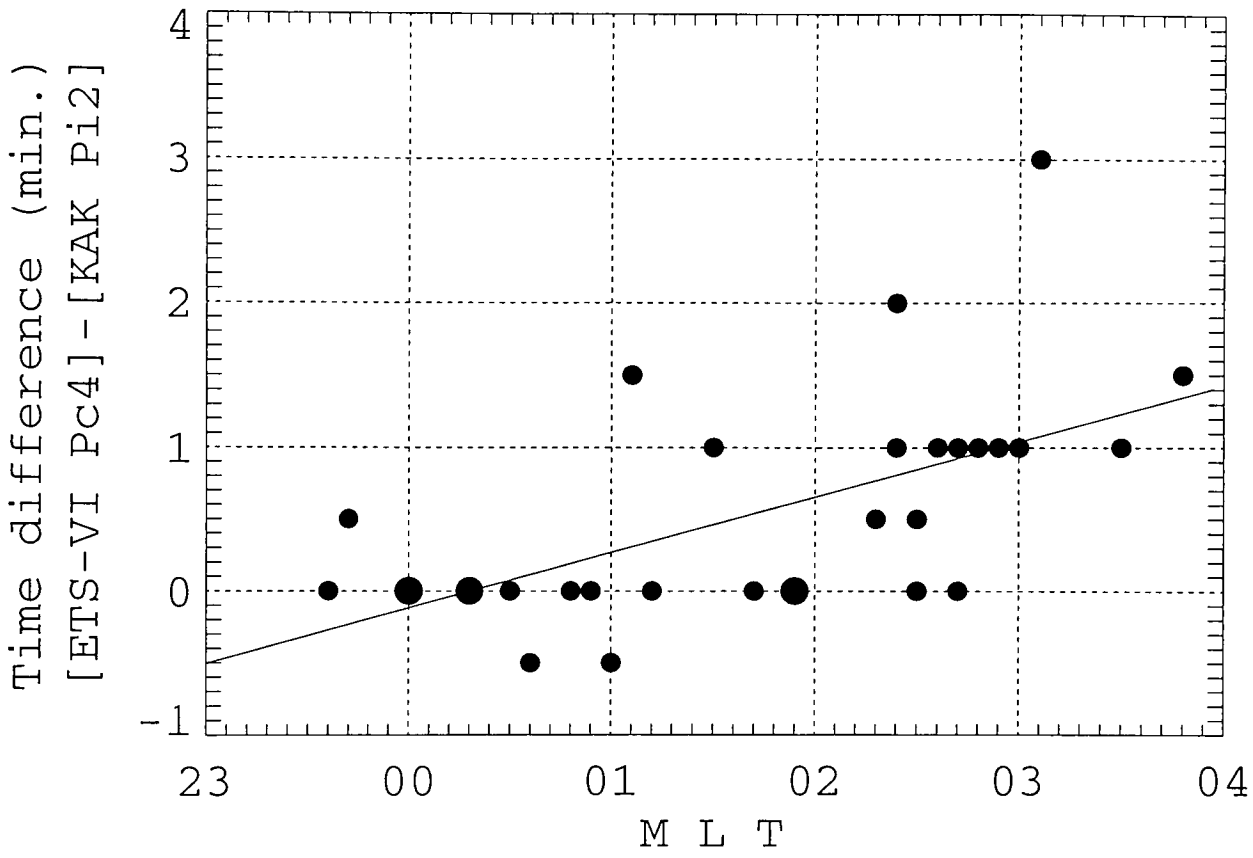
Time difference (min.)
[ETS-VI Pc4]-[KAK Pi2]
4
3
2
1
0
-1
23
00
01
02
03
04
M L T

Figure 3.13

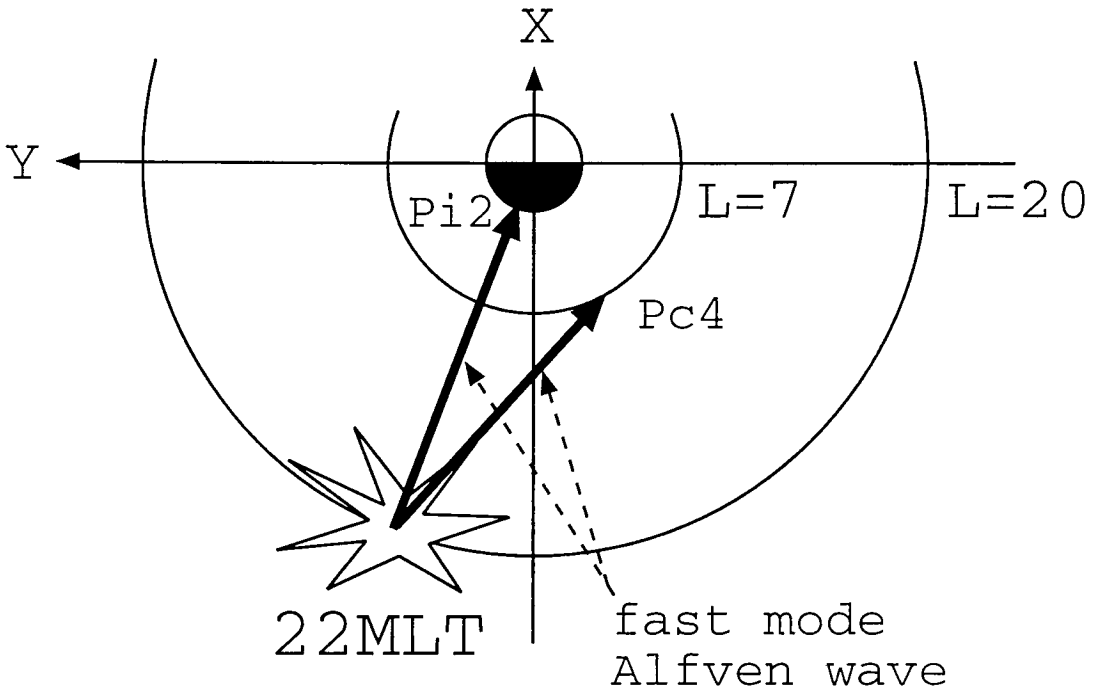

Figure 3.14

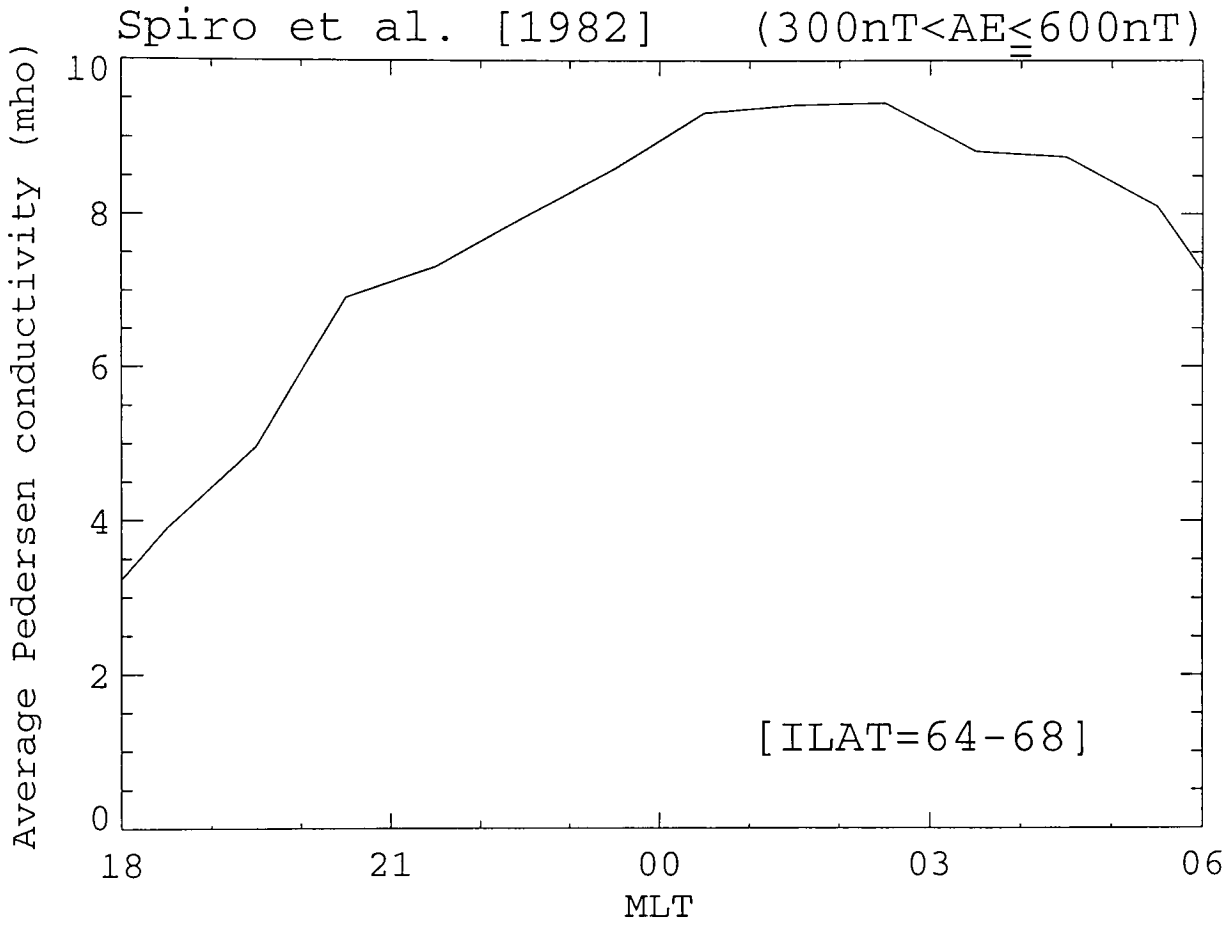
Spiro et al. [1982] (300nT<AE≦600nT)
Average Pedersen conductivity (mho)
10
8
6
4
2
0
18
21
00
03
06
MLT
[ILAT=64-68]

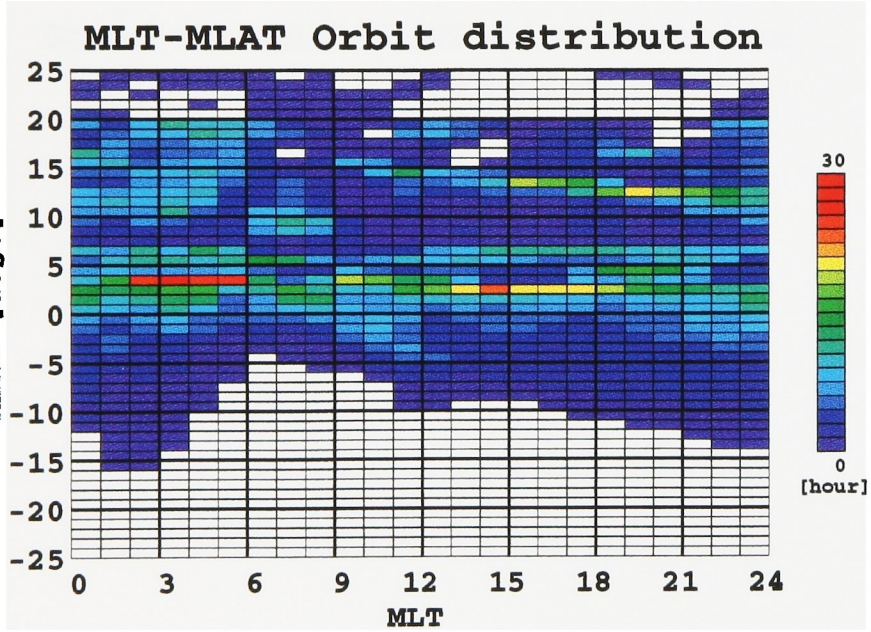
MLT-MLAT Orbit distribution
MLAT [deg.]
25
20
15
10
5
0
-5
-10
-15
-20
-25
0
3
6
9
12
15
18
21
24
MLT
30
0
[hour]

(a)

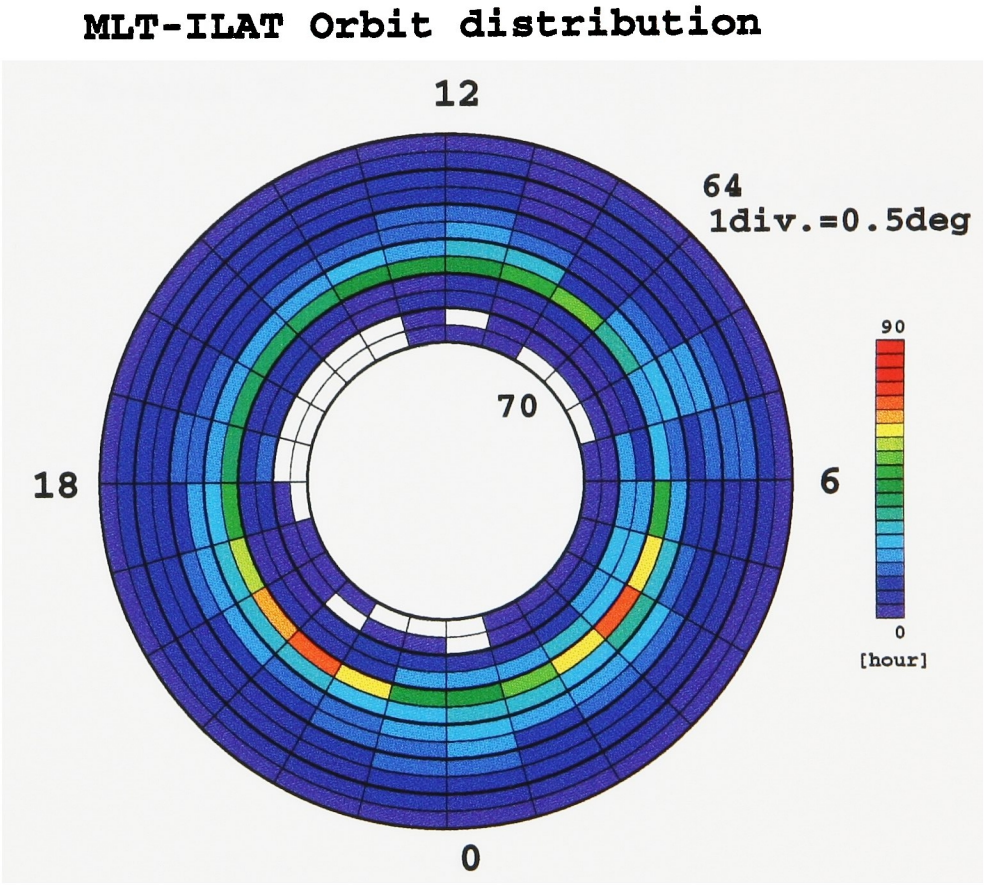
MLT-ILAT Orbit distribution
12
64
1div.=0.5deg
70
18
6
0
90
0
[hour]

(b)

Plate 3.1

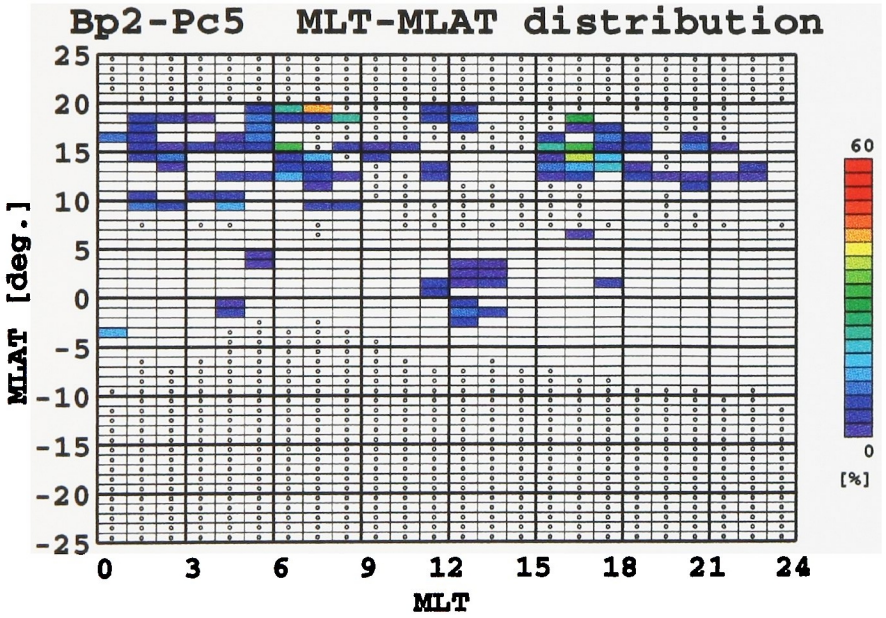
Bp2-Pc5 MLT-MLAT distribution
MLAT [deg.]
25
20
15
10
5
0
-5
-10
-15
-20
-25
0
3
6
9
12
15
18
21
24
MLT
60
0
[%]

(a)

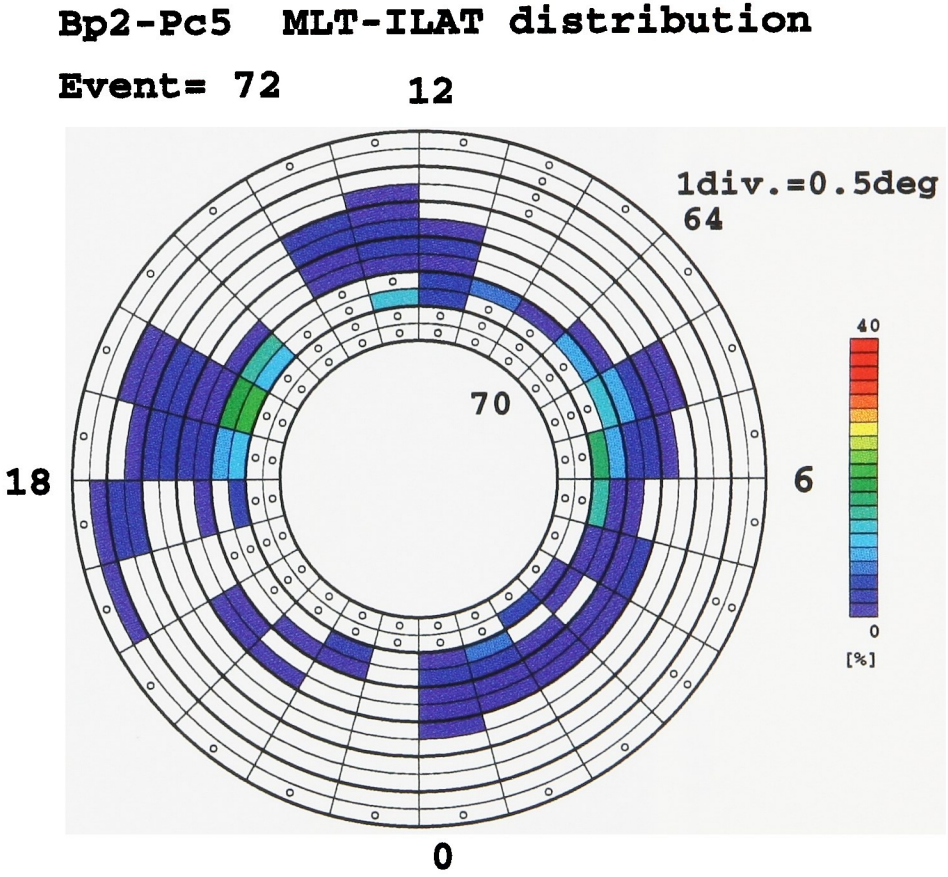
Bp2-Pc5 MLT-ILAT distribution
Event= 72
12
1div.=0.5deg
64
70
18
6
0
40
0
[%]

(b)

Plate 3.2

Plate 3.3

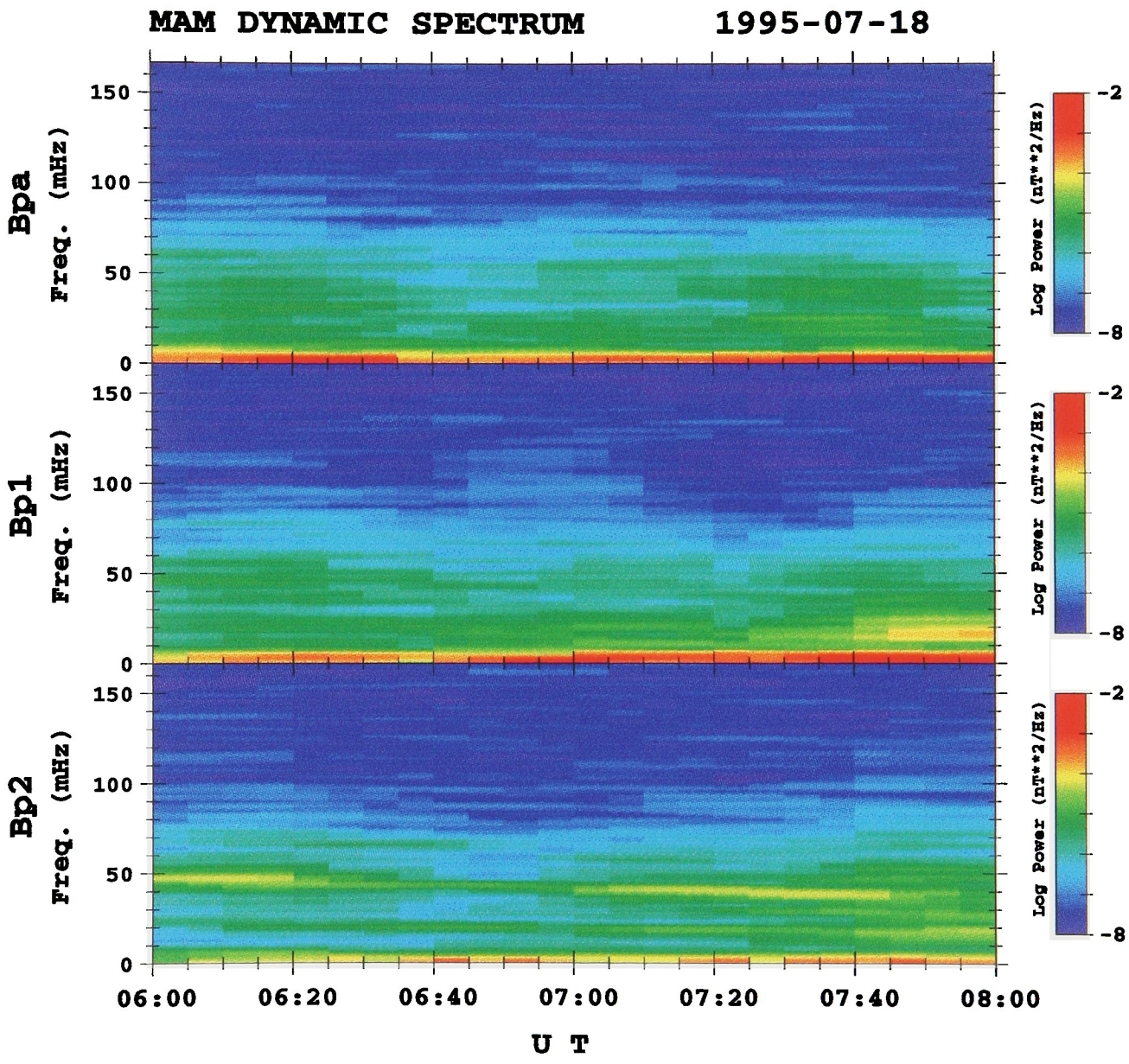
MAM DYNAMIC SPECTRUM
1995-07-18
Bpa
Bp1
Bp2
Freq. (mHz)
150
100
50
0
Log Power (nT**2/Hz)
-2
-8
06:00
06:20
06:40
07:00
07:20
07:40
08:00
U T

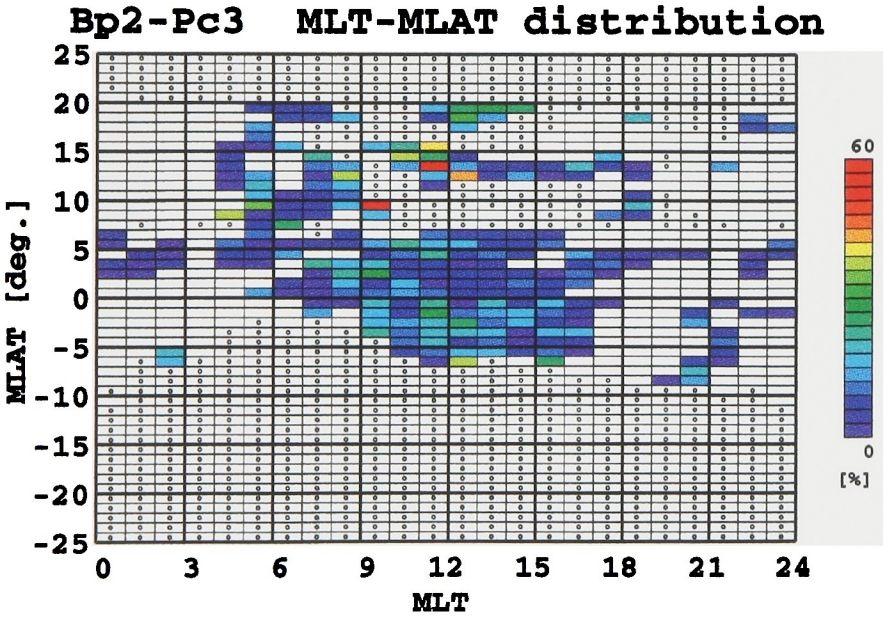
Bp2-Pc3 MLT-MLAT distribution
MLAT [deg.]
25
20
15
10
5
0
-5
-10
-15
-20
-25
0
3
6
9
12
15
18
21
24
MLT
60
0
[%]

(a)

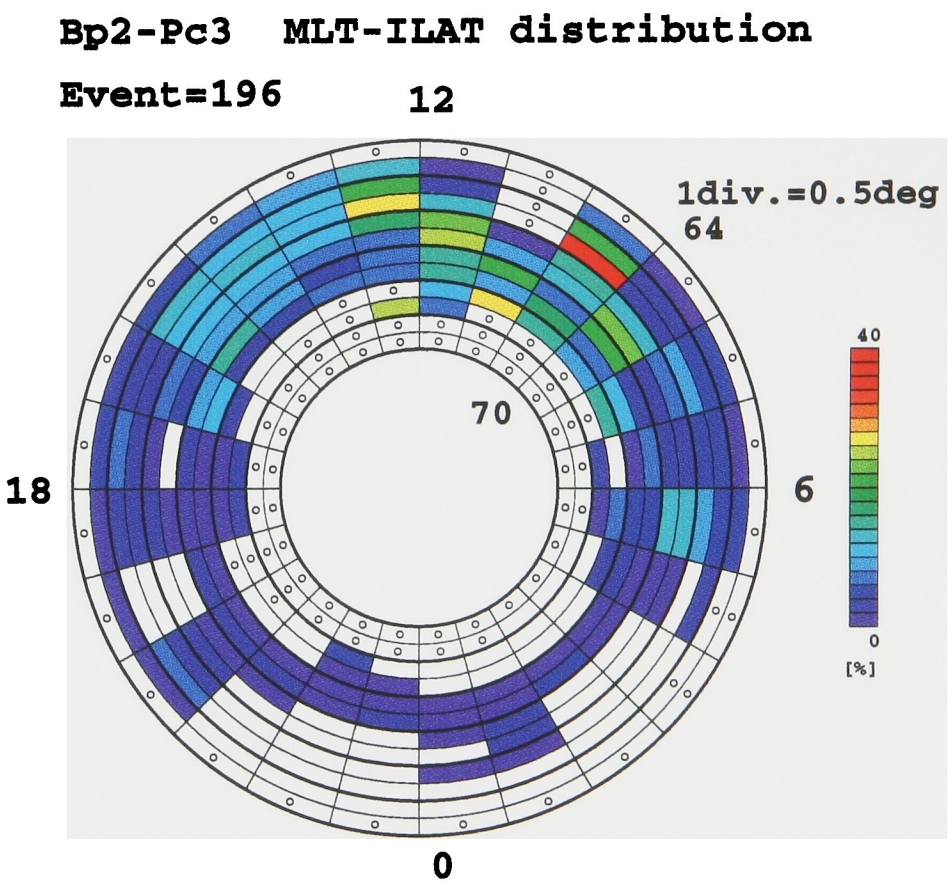
Bp2-Pc3 MLT-ILAT distribution
Event=196
12
1div.=0.5deg
64
70
18
6
0
40
0
[%]

(b)

Plate 3.4

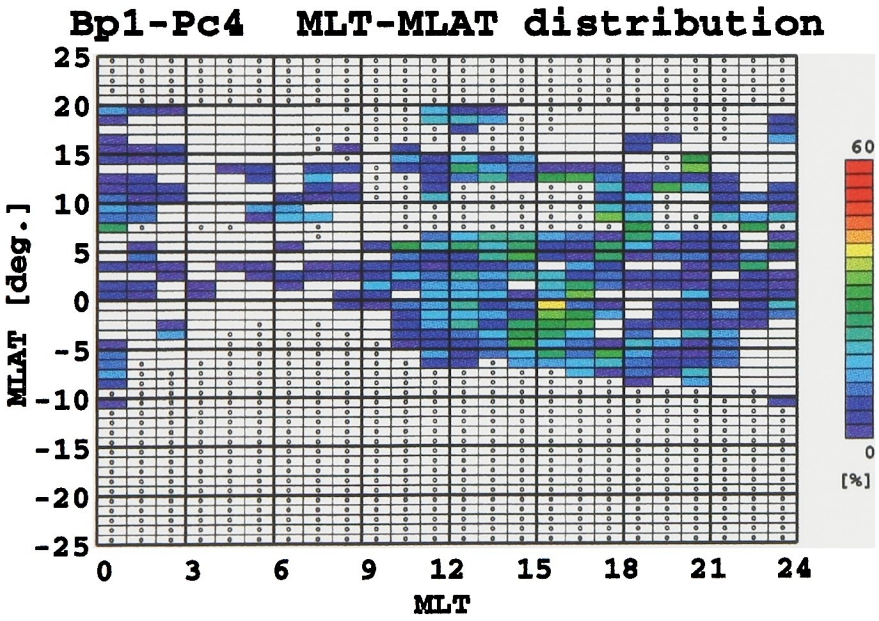
Bp1-Pc4 MLT-MLAT distribution
MLAT [deg.]
25
20
15
10
5
0
-5
-10
-15
-20
-25
0
3
6
9
12
15
18
21
24
MLT
60
0
[%]

(a)

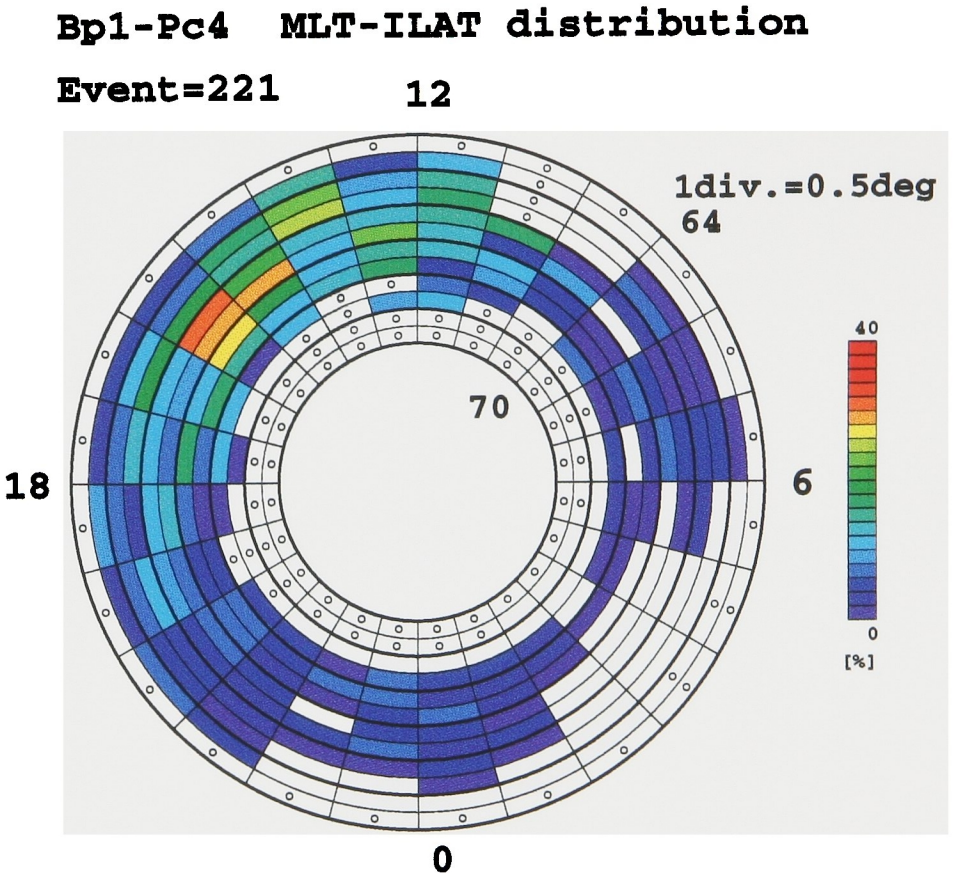
Bp1-Pc4 MLT-ILAT distribution
Event=221
12
1div.=0.5deg
64
70
18
6
0
40
0
[%]

(b)

Plate 3.5

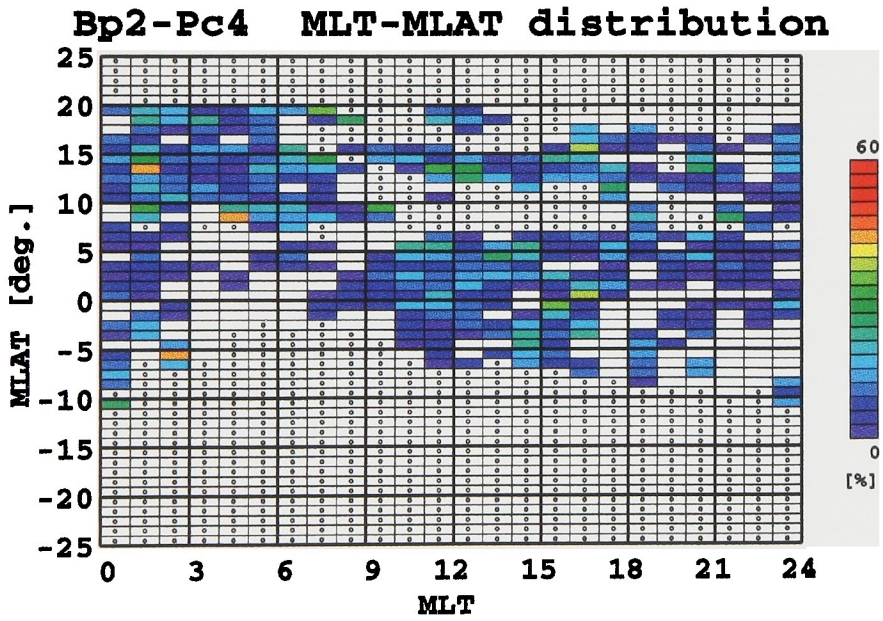
Bp2-Pc4 MLT-MLAT distribution
MLAT [deg.]
25
20
15
10
5
0
-5
-10
-15
-20
-25
0
3
6
9
12
15
18
21
24
MLT
60
0
[%]

(a)

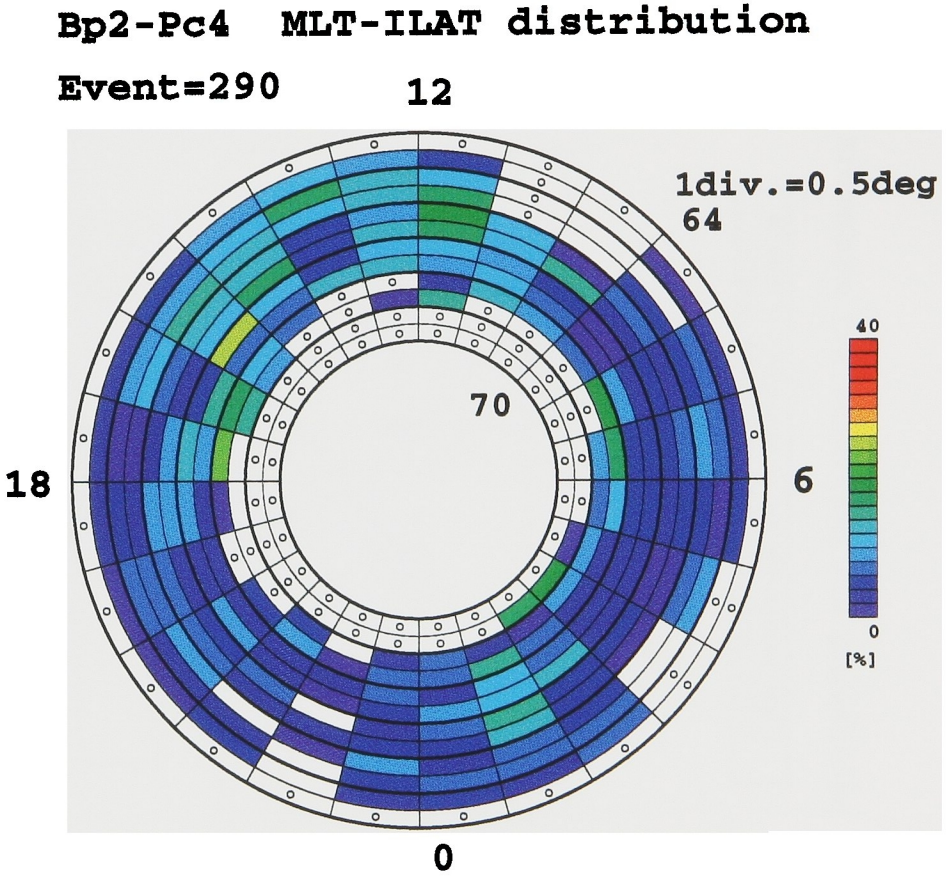
Bp2-Pc4 MLT-ILAT distribution
Event=290
12
1div.=0.5deg
64
70
18
6
0
40
0
[%]

(b)

Plate 3.6

Figure 4.1

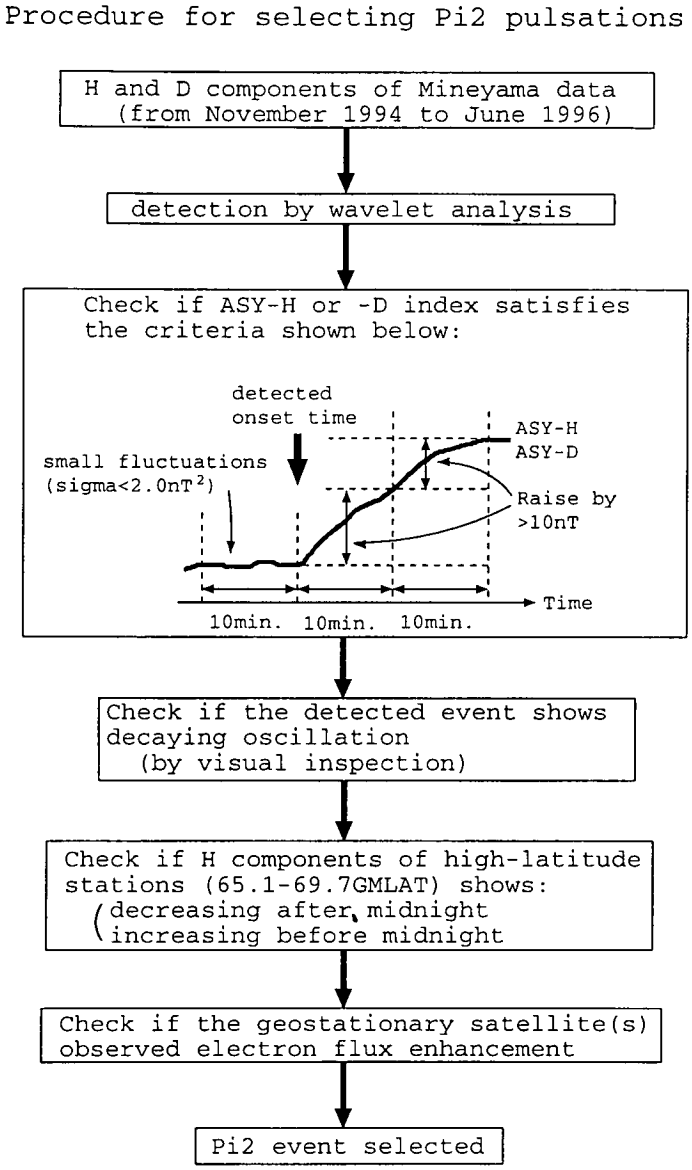
Procedure for selecting Pi2 pulsations
H and D components of Mineyama data (from November 1994 to June 1996)
detection by wavelet analysis
Check if ASY-H or -D index satisfies the criteria shown below:
detected onset time
small fluctuations (sigma<2.0nT²)
ASY-H
ASY-D
Raise by >10nT
Time
10min.
10min.
10min.
Check if the detected event shows decaying oscillation (by visual inspection)
Check if H components of high-latitude stations (65.1-69.7GMLAT) shows:
decreasing after midnight
increasing before midnight
Check if the geostationary satellite(s) observed electron flux enhancement
Pi2 event selected

Figure 4.2

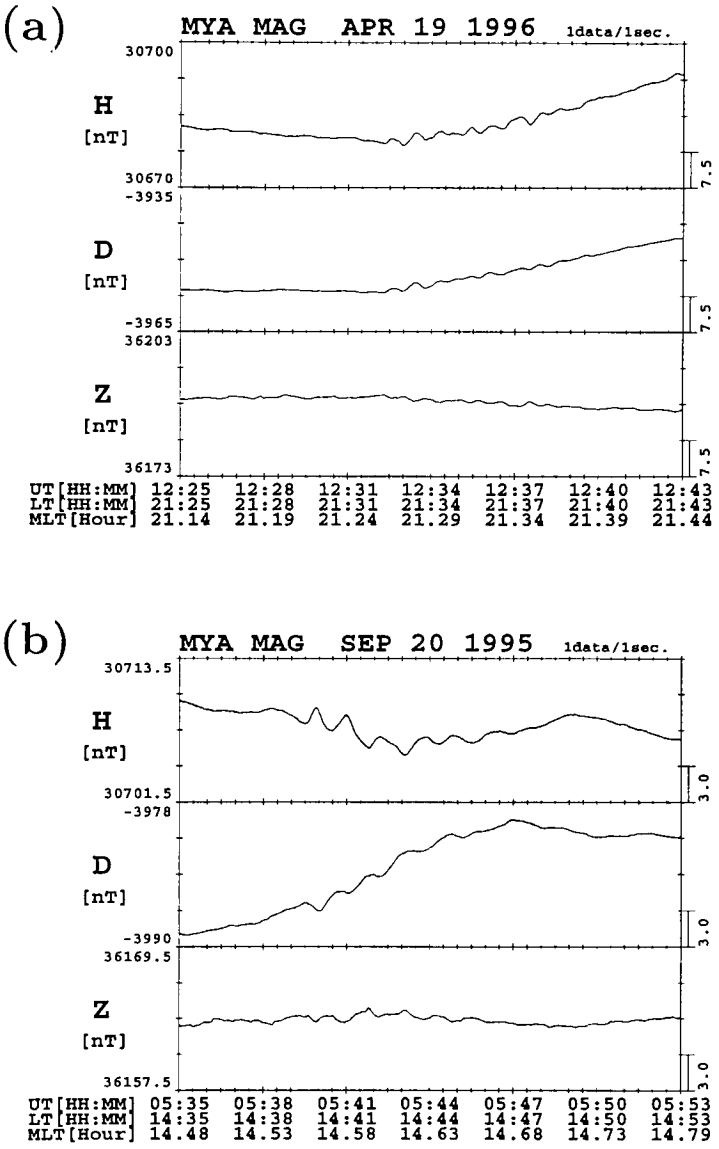
(a)
MYA MAG APR 19 1996 1data/1sec.
30700
H
[nT]
30670
7.5
-3935
D
[nT]
-3965
7.5
36203
Z
[nT]
36173
7.5
UT[HH:MM] 12:25 12:28 12:31 12:34 12:37 12:40 12:43
LT[HH:MM] 21:25 21:28 21:31 21:34 21:37 21:40 21:43
MLT[Hour] 21.14 21.19 21.24 21.29 21.34 21.39 21.44
(b)
MYA MAG SEP 20 1995 1data/1sec.
30713.5
H
[nT]
30701.5
3.0
-3978
D
[nT]
-3990
3.0
36169.5
Z
[nT]
36157.5
3.0
UT[HH:MM] 05:35 05:38 05:41 05:44 05:47 05:50 05:53
LT[HH:MM] 14:35 14:38 14:41 14:44 14:47 14:50 14:53
MLT[Hour] 14.48 14.53 14.58 14.63 14.68 14.73 14.79

Figure 4.3

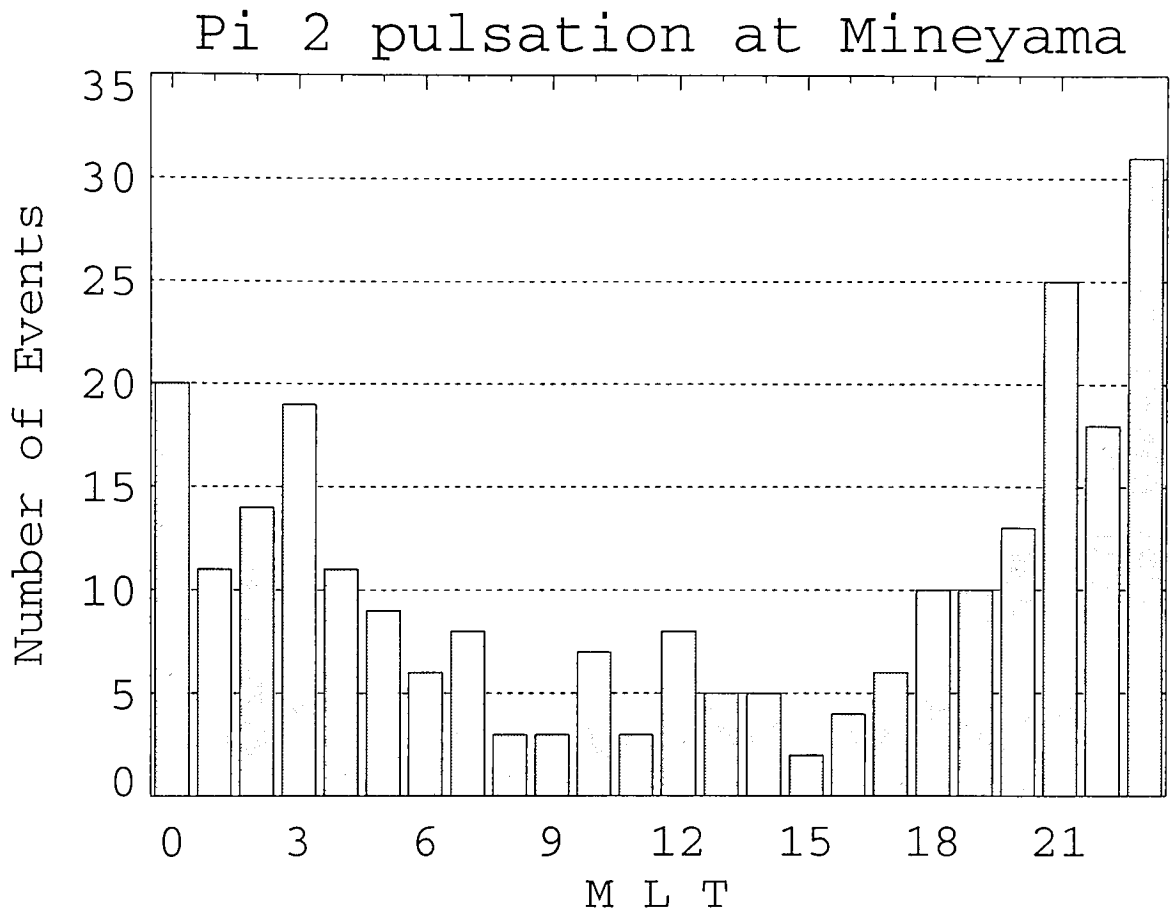
Pi 2 pulsation at Mineyama
Number of Events
0
5
10
15
20
25
30
35
0
3
6
9
12
15
18
21
M L T

Figure 4.4

(a)

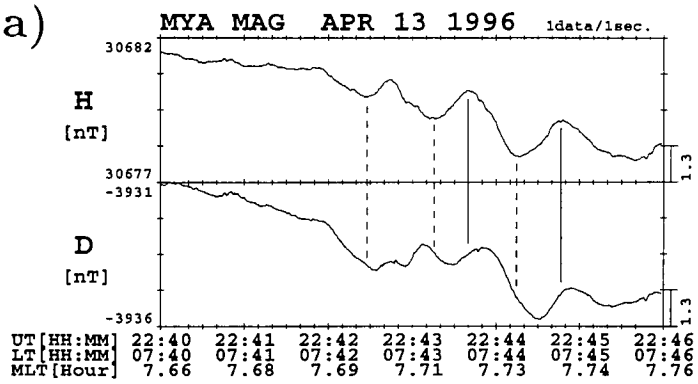
MYA MAG APR 13 1996 1data/1sec.
30682
H
[nT]
30677
-3931
D
[nT]
-3936
1.3
1.3
UT[HH:MM] 22:40 22:41 22:42 22:43 22:44 22:45 22:46
LT[HH:MM] 07:40 07:41 07:42 07:43 07:44 07:45 07:46
MLT[Hour] 7.66 7.68 7.69 7.71 7.73 7.74 7.76

(b)

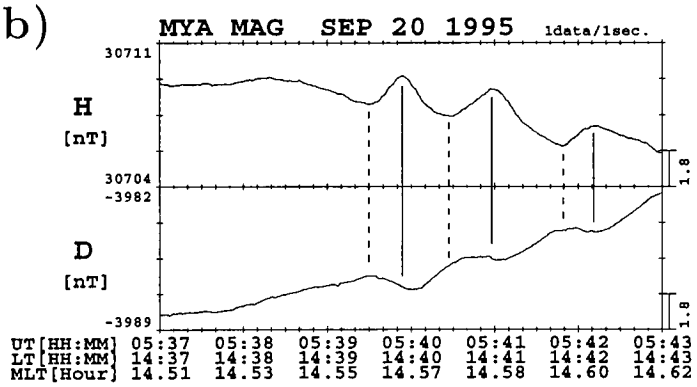
MYA MAG SEP 20 1995 1data/1sec.
30711
H
[nT]
30704
-3982
D
[nT]
-3989
1.8
1.8
UT[HH:MM] 05:37 05:38 05:39 05:40 05:41 05:42 05:43
LT[HH:MM] 14:37 14:38 14:39 14:40 14:41 14:42 14:43
MLT[Hour] 14.51 14.53 14.55 14.57 14.58 14.60 14.62

Figure 4.5

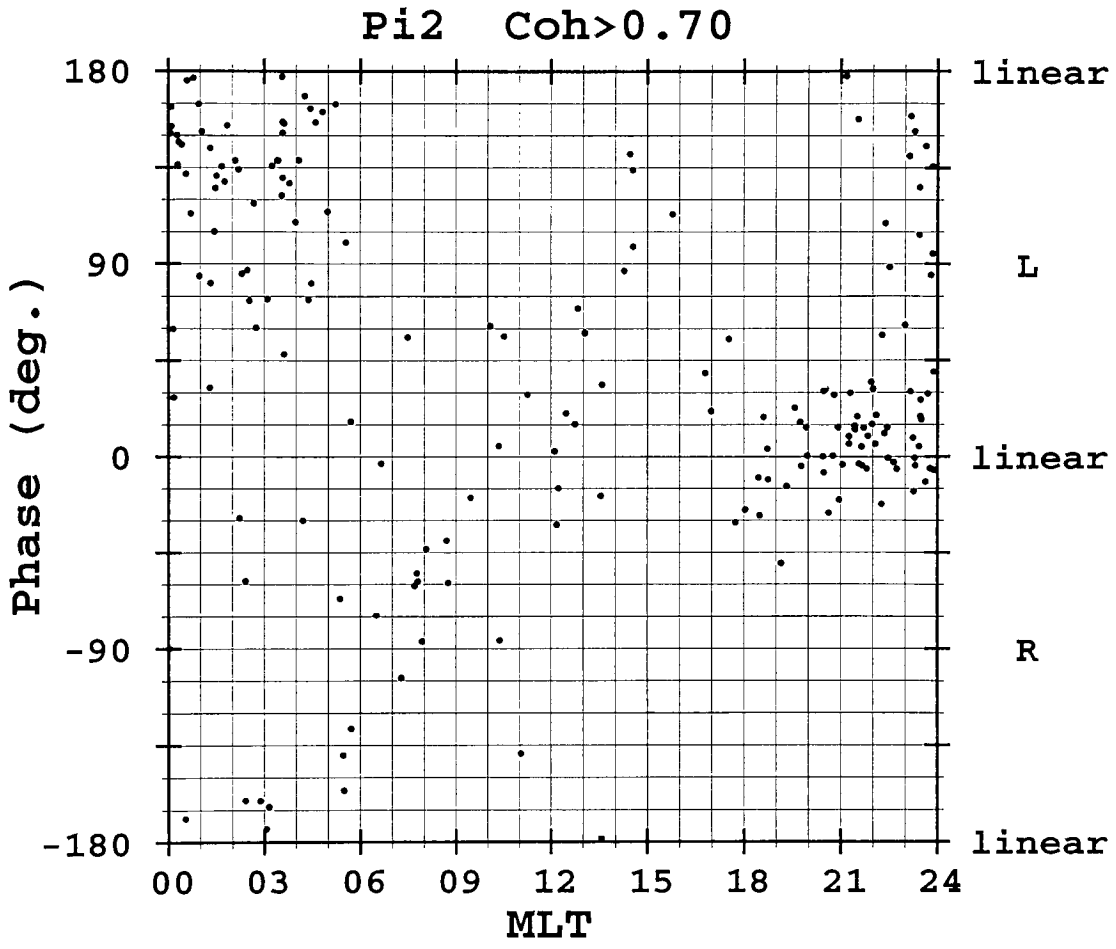
Pi2 Coh>0.70
180
90
0
-90
-180
Phase (deg.)
linear
L
linear
R
linear
00
03
06
09
12
15
18
21
24
MLT

Figure 4.6

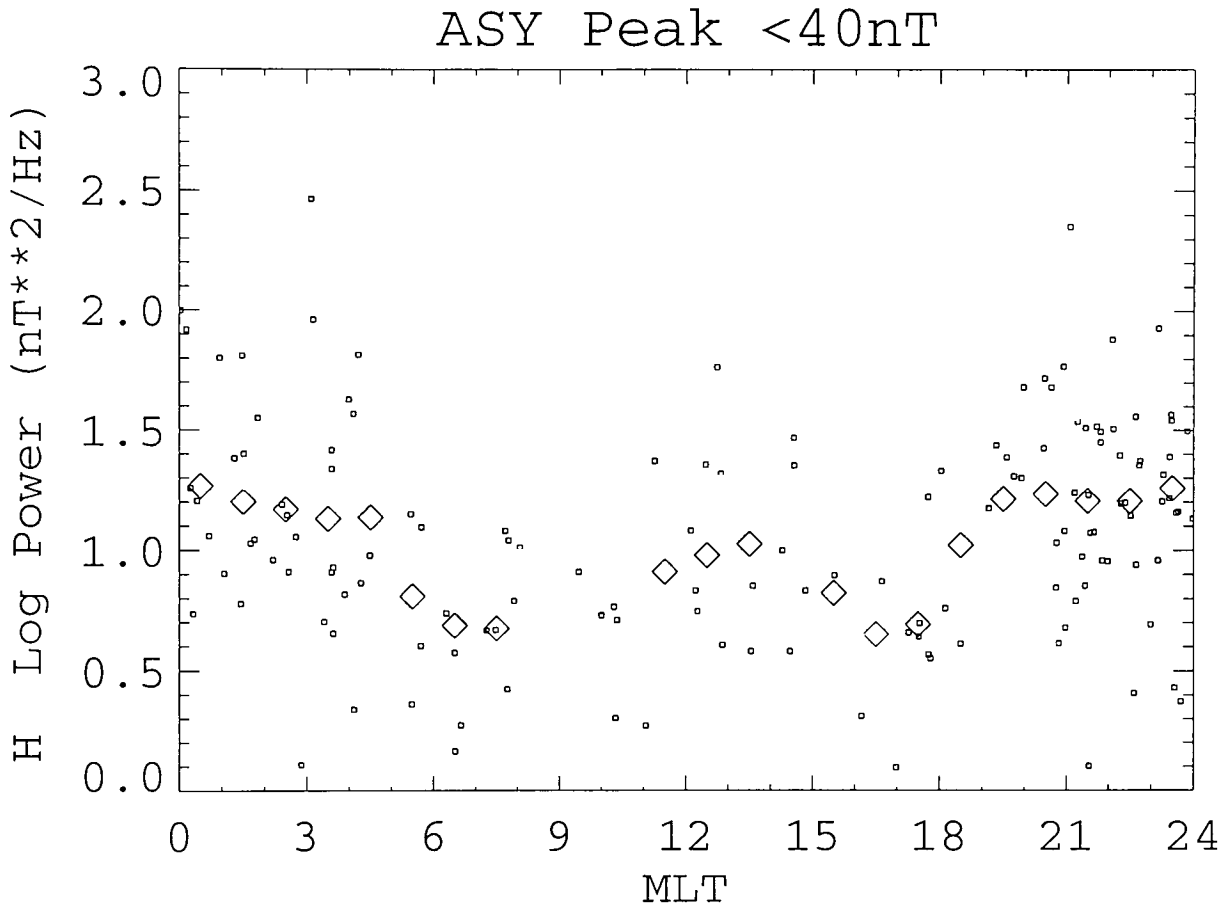
ASY Peak <40nT
H Log Power (nT**2/Hz)
3.0
2.5
2.0
1.5
1.0
0.5
0.0
0
3
6
9
12
15
18
21
24
MLT

Figure 4.7

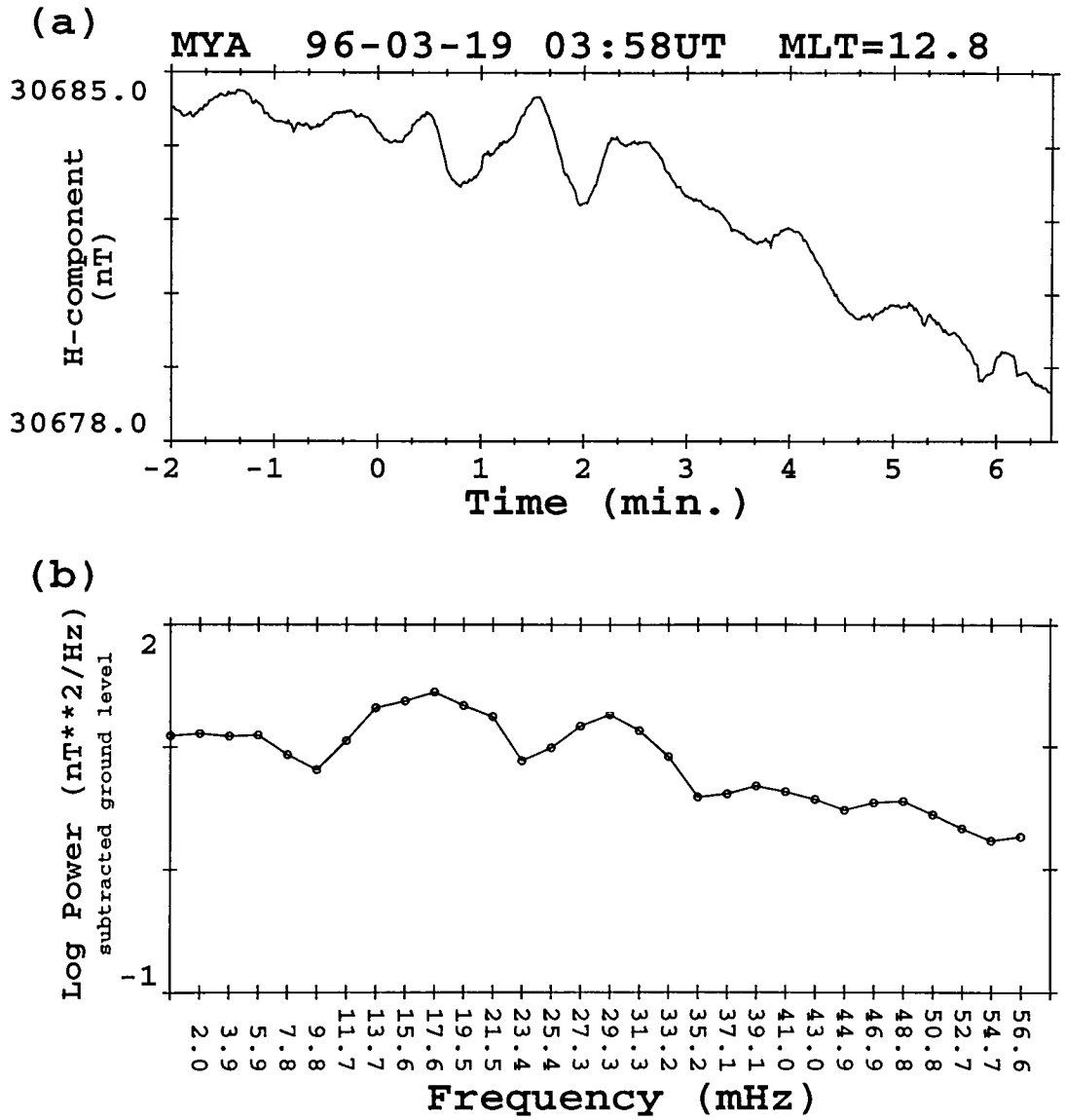
(a)
MYA 96-03-19 03:58UT MLT=12.8
30685.0
30678.0
H-component (nT)
-2
-1
0
1
2
3
4
5
6
Time (min.)
(b)
Log Power (nT**2/Hz)
subtracted ground level
2
-1
2.0
3.9
5.9
7.8
9.8
11.7
13.7
15.6
17.6
19.5
21.5
23.4
25.4
27.3
29.3
31.3
33.2
35.2
37.1
39.1
41.0
43.0
44.9
46.9
48.8
50.8
52.7
54.7
56.6
Frequency (mHz)

Figure 4.8

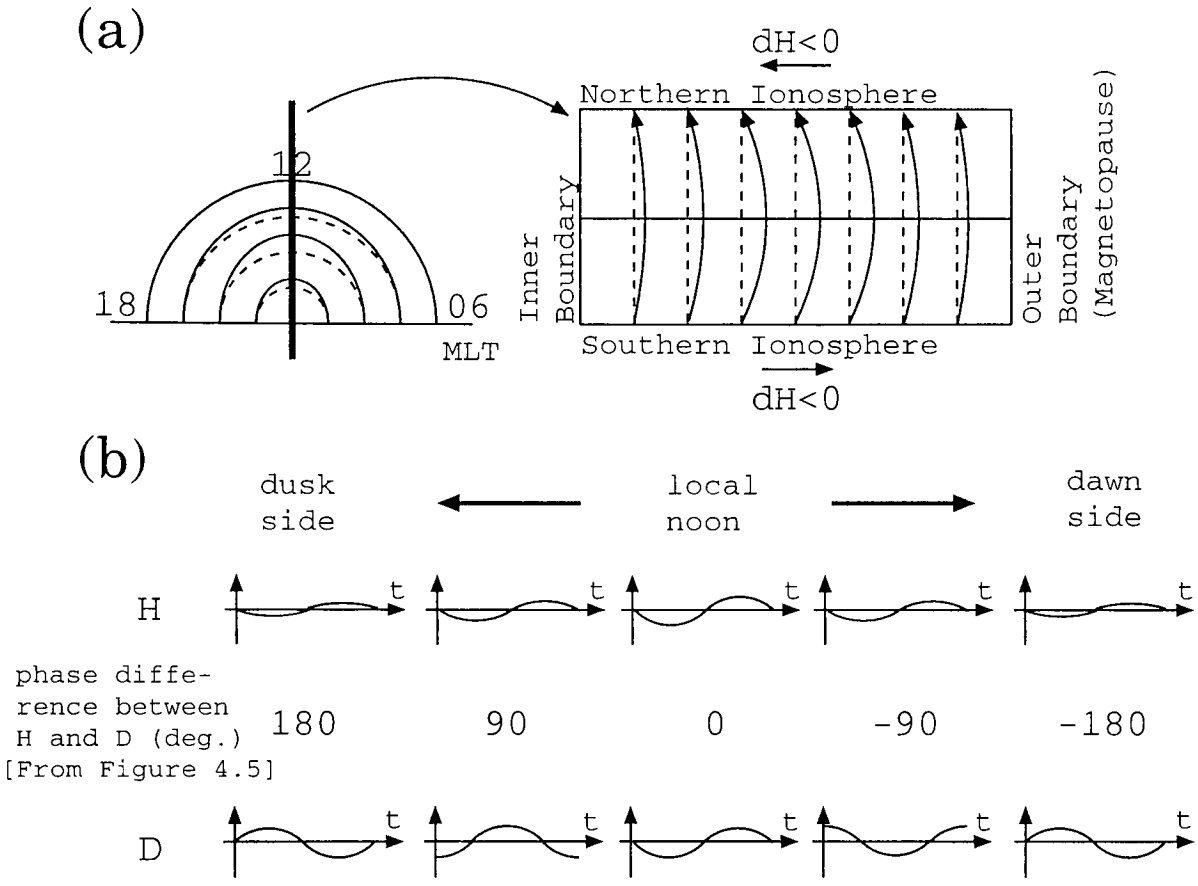
(a)
dH<0
Northern Ionosphere
12
18
06
MLT
Inner Boundary
Outer Boundary (Magnetopause)
Southern Ionosphere
dH<0
(b)
dusk side
local noon
dawn side
H
t
phase difference between H and D (deg.)
[From Figure 4.5]
180
90
0
-90
-180
D

Figure A.1

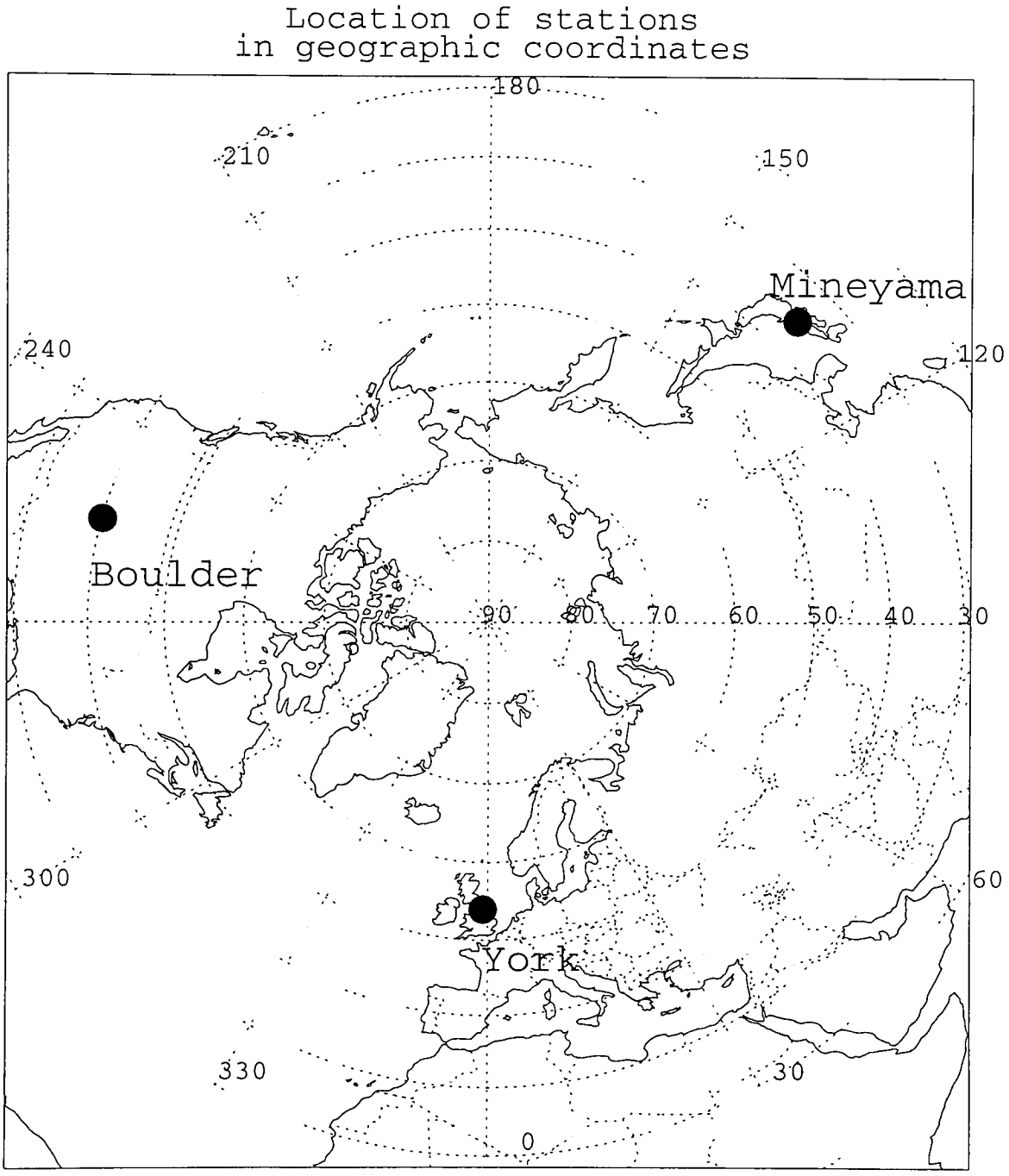
Location of stations
in geographic coordinates
180
210
150
Mineyama
240
120
Boulder
90
80
70
60
50
40
30
300
60
York
330
30
0

Figure A.2

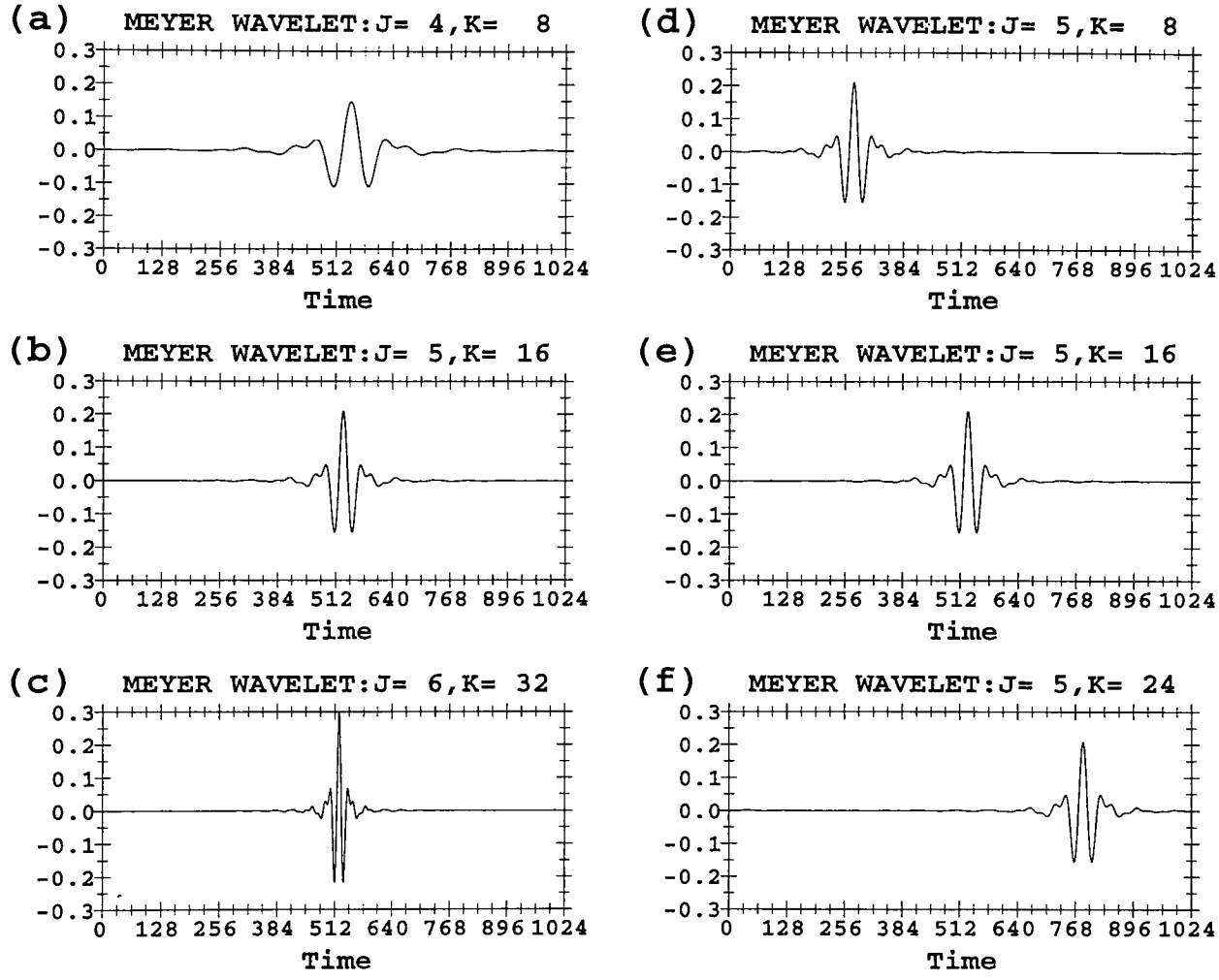
(a) MEYER WAVELET:J= 4,K= 8
(d) MEYER WAVELET:J= 5,K= 8
(b) MEYER WAVELET:J= 5,K= 16
(e) MEYER WAVELET:J= 5,K= 16
(c) MEYER WAVELET:J= 6,K= 32
(f) MEYER WAVELET:J= 5,K= 24
0.3
0.2
0.1
0.0
-0.1
-0.2
-0.3
0 128 256 384 512 640 768 896 1024
Time

Figure A.3

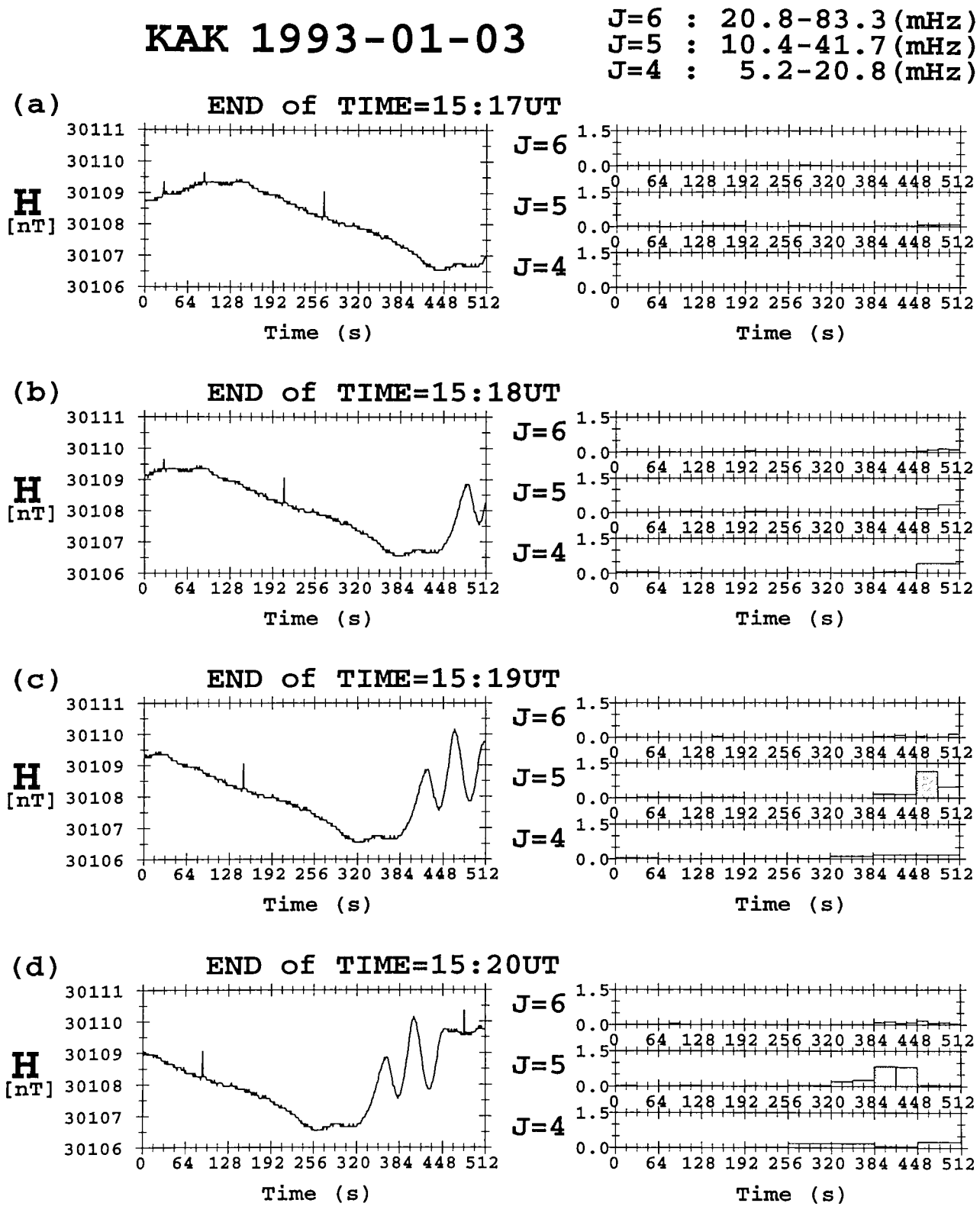
KAK 1993-01-03
J=6 : 20.8-83.3(mHz)
J=5 : 10.4-41.7(mHz)
J=4 : 5.2-20.8(mHz)
(a)
END of TIME=15:17UT
(b)
END of TIME=15:18UT
(c)
END of TIME=15:19UT
(d)
END of TIME=15:20UT
H [nT]
30111
30110
30109
30108
30107
30106
0 64 128 192 256 320 384 448 512
Time (s)
J=6
J=5
J=4
1.5
0.0

Figure A.4

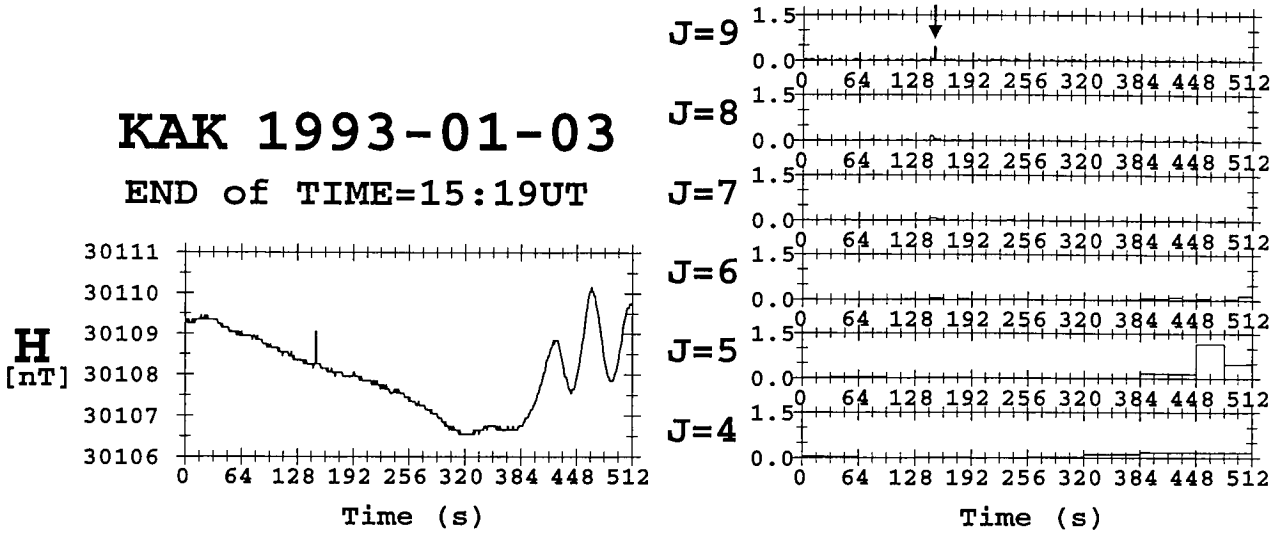
KAK 1993-01-03
END of TIME=15:19UT
H
[nT]
30111
30110
30109
30108
30107
30106
0 64 128 192 256 320 384 448 512
Time (s)
J=9
J=8
J=7
J=6
J=5
J=4
1.5
0.0
0 64 128 192 256 320 384 448 512
Time (s)

Figure A.5

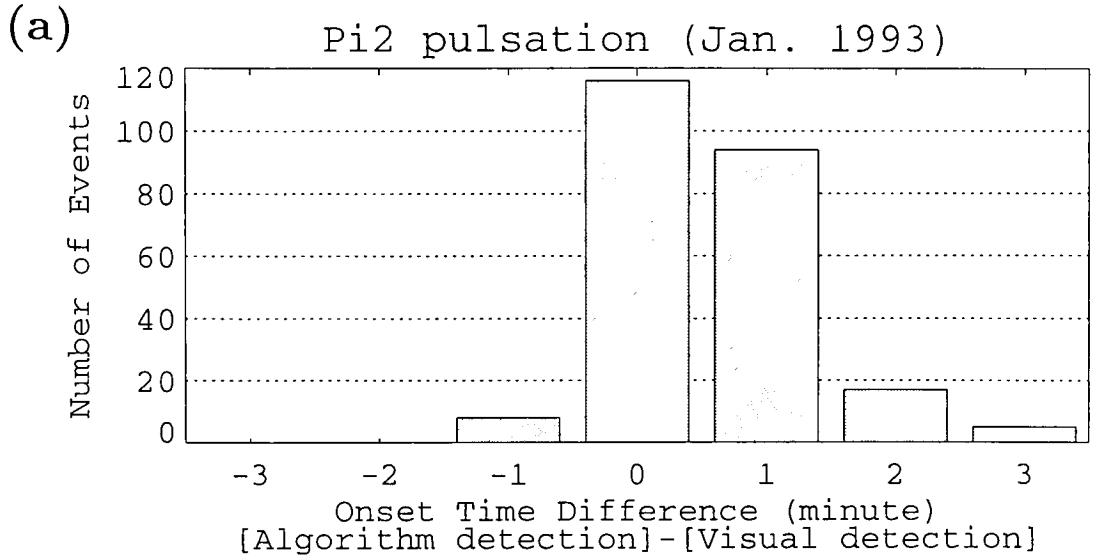
(a)
Pi2 pulsation (Jan. 1993)
Number of Events
120
100
80
60
40
20
0
-3
-2
-1
0
1
2
3
Onset Time Difference (minute)
[Algorithm detection]-[Visual detection]

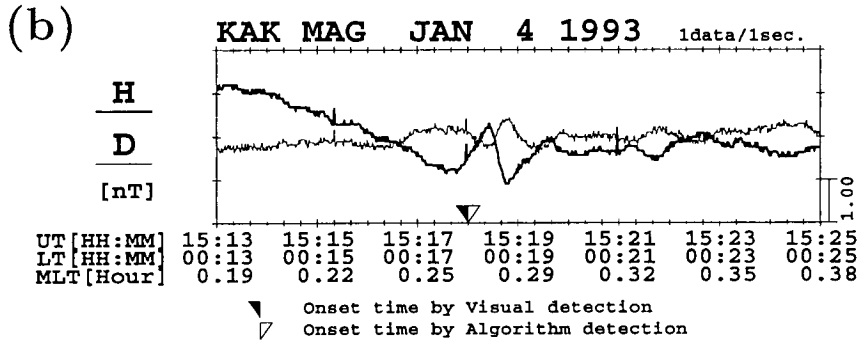
(b)
KAK MAG JAN 4 1993
1data/1sec.
H
D
[nT]
1.00
UT[HH:MM] 15:13 15:15 15:17 15:19 15:21 15:23 15:25
LT[HH:MM] 00:13 00:15 00:17 00:19 00:21 00:23 00:25
MLT[Hour] 0.19 0.22 0.25 0.29 0.32 0.35 0.38
Onset time by Visual detection
Onset time by Algorithm detection

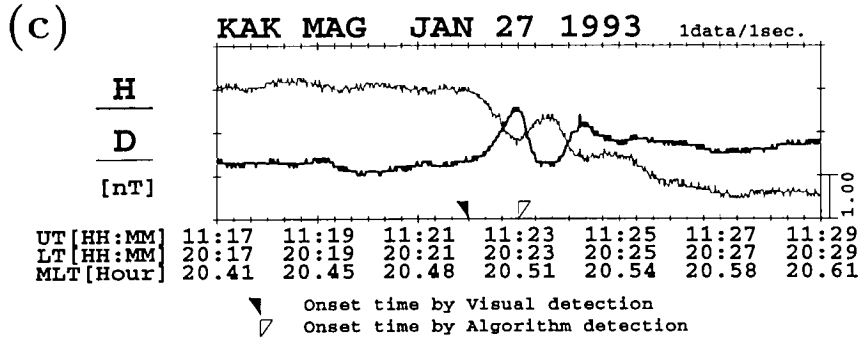
(c)
KAK MAG JAN 27 1993
1data/1sec.
H
D
[nT]
1.00
UT[HH:MM] 11:17 11:19 11:21 11:23 11:25 11:27 11:29
LT[HH:MM] 20:17 20:19 20:21 20:23 20:25 20:27 20:29
MLT[Hour] 20.41 20.45 20.48 20.51 20.54 20.58 20.61
Onset time by Visual detection
Onset time by Algorithm detection

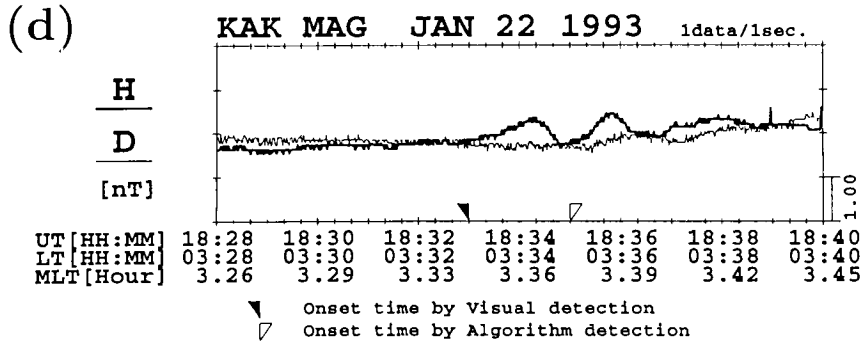
(d)
KAK MAG JAN 22 1993
1data/1sec.
H
D
[nT]
1.00
UT[HH:MM] 18:28 18:30 18:32 18:34 18:36 18:38 18:40
LT[HH:MM] 03:28 03:30 03:32 03:34 03:36 03:38 03:40
MLT[Hour] 3.26 3.29 3.33 3.36 3.39 3.42 3.45
Onset time by Visual detection
Onset time by Algorithm detection

Figure A.6

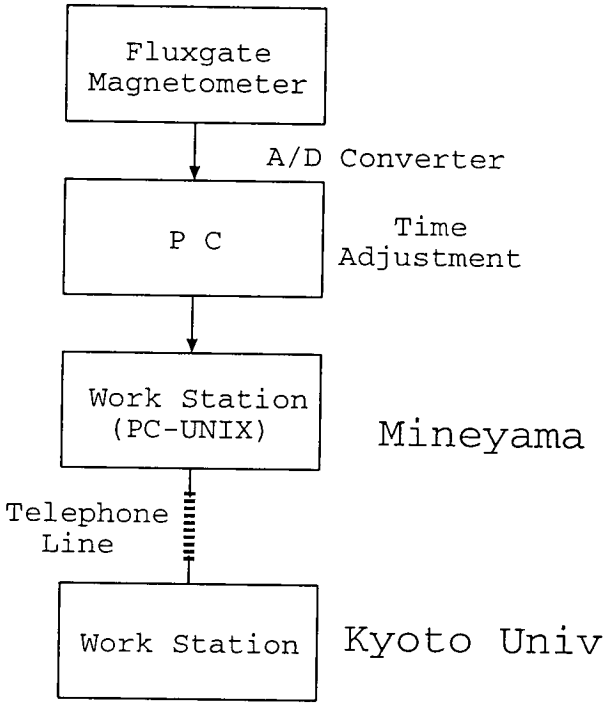
Fluxgate
Magnetometer
A/D Converter
P C
Time
Adjustment
Work Station
(PC-UNIX)
Mineyama
Telephone
Line
Work Station
Kyoto Univ

Figure A.7

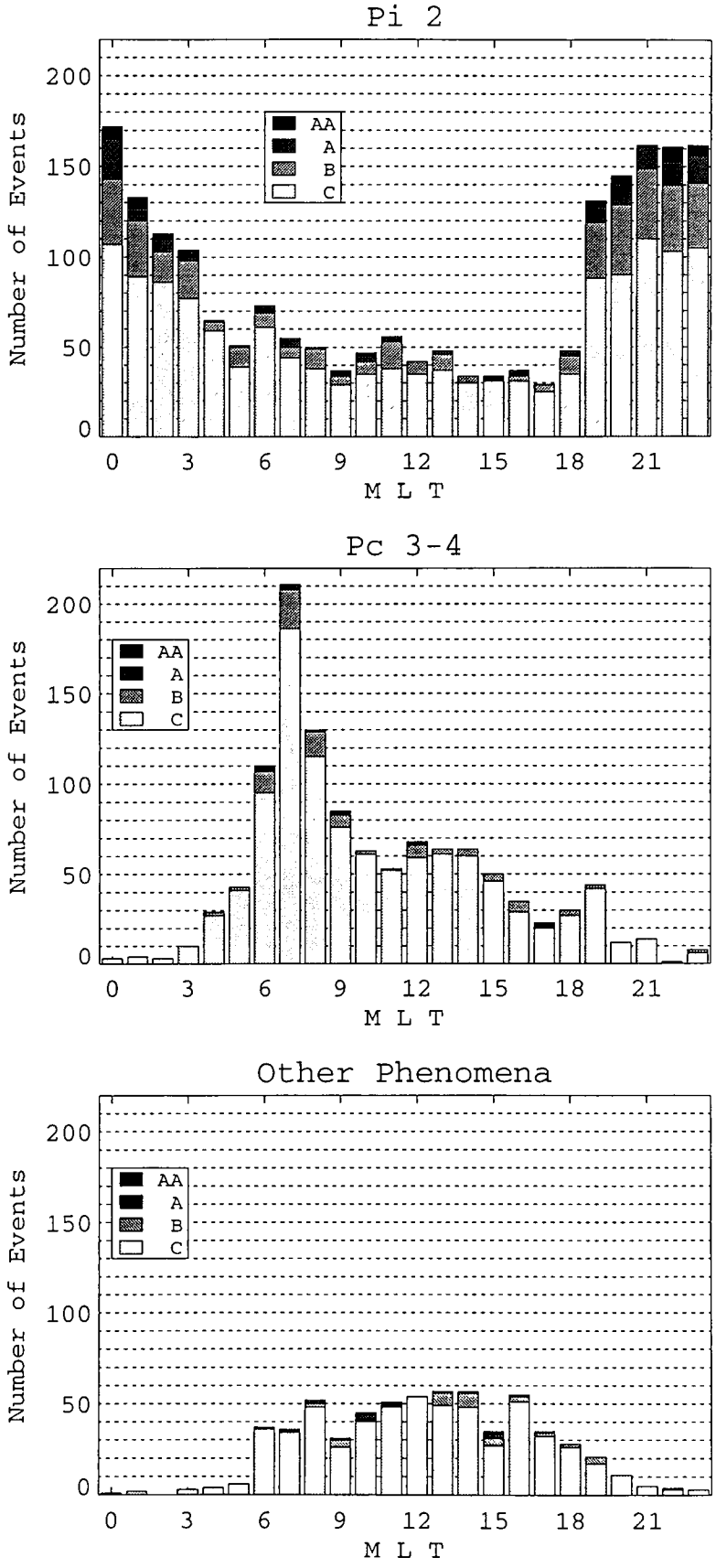
Pi 2
Number of Events
200
150
100
50
0
AA
A
B
C
0
3
6
9
12
15
18
21
M L T
Pc 3-4
Number of Events
200
150
100
50
0
AA
A
B
C
0
3
6
9
12
15
18
21
M L T
Other Phenomena
Number of Events
200
150
100
50
0
AA
A
B
C
0
3
6
9
12
15
18
21
M L T

This thesis consists of the following papers in substance.

1. Electron precipitation accompanying Pc 5 pulsations observed by the DE satellites and at a ground station,
   M. Nosé, T. Iyemori, M. Sugiura, J. A. Slavin, R. A. Hoffman, J. D. Winningham, and N. Sato,
   submitted to *J. Geophys. Res.*.
2. ULF pulsations observed by the ETS-VI satellite: Substorm associated azimuthal Pc 4 pulsations on the nightside,
   M. Nosé, T. Iyemori, S. Nakabe, T. Nagai, H. Matsumoto, and T. Goka,
   Earth, Planets and Space, *50*, 1998, *in press.*
3. Automated detection of Pi 2 pulsations using wavelet analysis: 1. Method and an application for substorm monitoring,
   M. Nosé, T. Iyemori, M. Takeda, T. Kamei, D. K. Milling, D. Orr, H. J. Singer, E. W Worthington, and N. Sumitomo,
   submitted to *Earth, Planets and Space.*
4. Automated detection of Pi 2 pulsations using wavelet analysis: 2. An application for pulsation study,
   M. Nosé,
   submitted to *Earth, Planets and Space.*